
PINNacle: A Comprehensive Benchmark of Physics-Informed Neural Networks for Solving PDEs

Anonymous authors

Abstract

1 While significant progress has been made on Physics-Informed Neural Networks
2 (PINNs), a comprehensive comparison of these methods across a wide range of
3 Partial Differential Equations (PDEs) is still lacking. This study introduces PIN-
4 Nacle, a benchmarking tool designed to fill this gap. PINNacle provides a diverse
5 dataset, comprising over 20 distinct PDEs from various domains, including heat
6 conduction, fluid dynamics, biology, and electromagnetics. These PDEs encapsu-
7 late key challenges inherent to real-world problems, such as complex geometry,
8 multi-scale phenomena, nonlinearity, and high dimensionality. PINNacle also of-
9 fers a user-friendly toolbox, incorporating about 10 state-of-the-art PINN methods
10 for systematic evaluation and comparison. We have conducted extensive experi-
11 ments with these methods, offering insights into their strengths and weaknesses. In
12 addition to providing a standardized means of assessing performance, PINNacle
13 also offers an in-depth analysis to guide future research such as domain decompo-
14 sition methods and loss reweighting for handling multi-scale problems. To the best
15 of our knowledge, it is the largest benchmark with a diverse and comprehensive
16 evaluation that will undoubtedly foster further research in PINNs.

17 1 Introduction

18 Partial Differential Equations (PDEs) are of paramount importance in science and engineering, as
19 they often underpin our understanding of intricate physical systems such as fluid flow, heat transfer,
20 and stress distribution [35]. The computational simulation of PDE systems has been a focal point
21 of research for an extensive period, leading to the development of numerical methods such as finite
22 difference [6], finite element [43], and finite volume methods [12].

23 Recent advancements have led to the use of deep neural networks to solve forward and inverse
24 problems involving PDEs [42, 59, 10, 52]. Among these, Physics-Informed Neural Networks
25 (PINNs) have emerged as a promising alternative to traditional numerical methods in solving such
26 problems [42, 23]. PINNs leverage the underlying physical laws and available data to effectively
27 handle various scientific and engineering applications. The growing interest in this field has spurred
28 the development of numerous PINN variants, each tailored to overcome specific challenges or to
29 enhance the performance of the original framework.

30 While PINN methods have achieved remarkable progress, a comprehensive comparison of these
31 methods across diverse types of PDEs is currently lacking. Establishing such a benchmark is
32 crucial as it could enable researchers to more thoroughly understand existing methods and pinpoint
33 potential challenges. Despite the availability of several studies comparing sampling methods [57] and
34 reweighting methods [2], there has been no concerted effort to develop a rigorous benchmark using
35 challenging datasets from real-world problems. The sheer variety and inherent complexity of PDEs
36 make it difficult to conduct a comprehensive analysis. Moreover, different mathematical properties

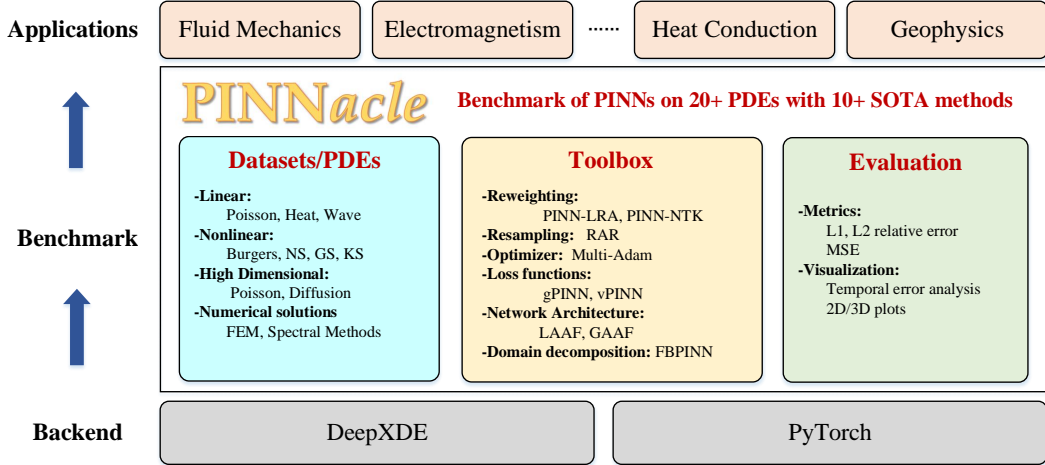


Figure 1: Architecture of PINNacle. It contains a dataset covering more than 20 PDEs, a toolbox that implements about 10 SOTA methods, and an evaluation module. These methods have a wide range of application scenarios like fluid mechanics, electromagnetism, heat conduction, geophysics, and so on.

37 and application scenarios further complicate the task, requiring the benchmark to be adaptable and
 38 exhaustive.

39 To resolve these challenges, we propose PINNacle, a comprehensive benchmark for evaluating and
 40 understanding the performance of PINNs. As shown in Fig. 1, PINNacle consists of three major
 41 components — a diverse dataset, a toolbox, and evaluation modules. The dataset comprises tasks
 42 from over 20 different PDEs from various domains, including heat conduction, fluid dynamics,
 43 biology, and electromagnetics. Each task brings its own set of challenges, such as complex geometry,
 44 multi-scale phenomena, nonlinearity, and high dimensionality, thus providing a rich testing ground
 45 for PINNs. The toolbox incorporates more than 10 state-of-the-art (SOTA) PINN methods, enabling
 46 a systematic comparison of different strategies, including loss reweighting, variational formulation,
 47 adaptive activations, and domain decomposition. These methods can be flexibly applied to the tasks
 48 in the dataset, offering researchers a convenient way to evaluate the performance of PINNs which is
 49 also user-friendly for secondary development. The evaluation modules provide a standardized means
 50 of assessing the performance of different PINN methods across all tasks, ensuring consistency in
 51 comparison and facilitating the identification of strengths and weaknesses in various methods.

52 PINNacle provides a robust, diverse, and comprehensive benchmark suite for PINNs, contributing
 53 significantly to the field’s understanding and application. It represents a major step forward in the
 54 evolution of PINNs which could foster more innovative research and development in this exciting
 55 field. Code and data are publicly available at <https://github.com/i207M/PINNacle>.

56 In a nutshell, our contributions can be summarized as follows:

- 57 • We design a dataset encompassing over 20 challenging PDE problems. These problems
 58 encapsulate several critical challenges faced by PINNs, including handling complex geometries,
 59 multi-scale phenomena, nonlinearity, and high-dimensional problems.
- 60 • We systematically evaluate more than 10 carefully selected representative variants of PINNs.
 61 We conducted thorough experiments and ablation studies to evaluate their performance. To
 62 the best of our knowledge, this is the largest benchmark comparing different PINN variants.
- 63 • We provide an in-depth analysis to guide future research. We show using loss reweighting
 64 and domain decomposition methods could improve the performance on multi-scale and
 65 complex geometry problems. Variational formulation achieves better performance on inverse
 66 problems. However, few methods can adequately address nonlinear problems, indicating a
 67 future direction for exploration and advancement.

68 **2 Related Work**

69 **2.1 Benchmarks and datasets in scientific machine learning**

70 The growing trend of AI in scientific research has stimulated the development of various benchmarks
71 and datasets, which differ greatly in data formats, sizes, and governing principles. For instance, [31]
72 presents a benchmark for comparing neural operators, while [3, 39] benchmarks methods for learning
73 latent Newtonian mechanics. Furthermore, domain-specific datasets and benchmarks exist in fluid
74 mechanics [18], climate science [40, 5], quantum chemistry [1], and biology [4].

75 Beyond these domain-specific datasets and benchmarks, physics-informed machine learning has
76 received considerable attention [16, 8] since the advent of Physics-Informed Neural Networks (PINNs)
77 [42]. These methods successfully incorporate physical laws into model training, demonstrating
78 immense potential across a variety of scientific and engineering domains. Various papers have
79 compared different components within the PINN framework; for instance, [9] and [57] investigate
80 the sampling methods of collocation points in PINNs, and [2] compare reweighting techniques for
81 different loss components. PDEBench [50] and PDEArena [15] design multiple tasks to compare
82 different methods in scientific machine learning such as PINNs, FNO, and U-Net. Nevertheless, a
83 comprehensive comparison of various PINN approaches remains absent in the literature.

84 **2.2 Softwares and Toolboxes**

85 A plethora of software solutions have been developed for solving PDEs with neural networks. These
86 include SimNet [17], NeuralPDE [41], TorchDiffEq [7], and PyDEns [27]. More recently, DeepXDE
87 [32] has been introduced as a fundamental library for implementing PINNs across different backends.
88 However, there remains a void for a toolbox that provides a unified implementation for advanced PINN
89 variants. Our PINNacle fills this gap by offering a flexible interface that facilitates the implementation
90 and evaluation of diverse PINN variants. We furnish clear and concise code for researchers to execute
91 benchmarks across all problems and methods.

92 **2.3 Variants of Physics-informed neural networks**

93 The PINNs have received much attention due to their remarkable performance in solving both forward
94 and inverse PDE problems. However, vanilla PINNs have many limitations. Researchers have
95 proposed numerous PINN variants to address challenges associated with high-dimensionality, non-
96 linearity, multi-scale issues, and complex geometries [16, 8, 23, 28]. Broadly speaking, these variants
97 can be categorized into: loss reweighting/resampling [54, 55, 51, 57, 38], innovative optimizers
98 [58], novel loss functions such as variational formulations [59, 24, 25, 26] or regularization terms
99 [60, 48], and novel architectures like domain decomposition [19, 29, 36, 22] and adaptive activations
100 [21, 20]. These variants have enhanced PINN’s performance across various problems. Here we
101 select representative methods from each category and conduct a comprehensive analysis using our
102 benchmark dataset to evaluate these variants.

103 **3 PINNacle: A Hierarchical Benchmark for PINNs**

104 In this section, we first introduce the preliminaries of PINNs. Then we introduce the details of
105 datasets (tasks), PINN methods, the toolbox framework, and the evaluation metrics.

106 **3.1 Preliminaries of Physics-informed Neural Networks**

107 Physics-informed neural networks are neural network-based methods for solving PDEs as well as
108 inverse problems of PDEs, which have received much attention recently. Specifically, let’s consider a
109 general Partial Differential Equation (PDE) system defined on Ω , which can be represented as:

$$\mathcal{F}(u(x); x) = 0, \quad x \in \Omega, \quad (1)$$

$$\mathcal{B}(u(x); x) = 0, \quad x \in \partial\Omega. \quad (2)$$

110 where \mathcal{F} is a differential operator and \mathcal{B} is the boundary/initial condition. PINN uses a neural network
 111 $u_\theta(x)$ with parameters θ to approximate $u(x)$. The objective of PINN is to minimize the following
 112 loss function:

$$\mathcal{L}(\theta) = \frac{w_c}{N_c} \sum_{i=1}^{N_c} \|\mathcal{F}(u_\theta(x_c^i); x_c^i)\|^2 + \frac{w_b}{N_b} \sum_{i=1}^{N_b} \|\mathcal{B}(u_\theta(x_b^i); x_b^i)\|^2 + \frac{w_d}{N_d} \sum_{i=1}^{N_d} \|u_\theta(x_d^i) - u(x_d^i)\|^2. \quad (3)$$

113 where w_c, w_b, w_d are weights. The first two terms enforce the PDE constraints on $\{x_c^i\}_{1\dots N_c}$ and
 114 boundary conditions on $\{x_b^i\}_{1\dots N_b}$. The last term is data loss, which is optional when there is data
 115 available. However, PINNs have several inherent drawbacks. First, PINNs optimize a mixture of
 116 imbalance loss terms which might hinder its convergence as illustrated in [54]. Second, nonlinear or
 117 stiff PDEs might lead to unstable optimization [55]. Third, the vanilla MLPs might have difficulty
 118 in representing multi-scale or high-dimensional functions. For example, [28] shows that vanilla
 119 PINNs only work for a small parameter range, even in a simple convection problem. To resolve these
 120 challenges, numerous variants of PINNs are proposed. However, a comprehensive comparison of
 121 these methods is lacking, and thus it is imperative to develop a benchmark.

122 3.2 Datasets

123 To effectively compare PINN variants, we've curated a set of PDE problems (datasets) representing
 124 a wide range of challenges. We chose PDEs from diverse domains, reflecting their importance in
 125 science and engineering. Our dataset includes 22 unique cases, with further details in Appendix B.

- 126 • The **Burgers' Equation**, fundamental to fluid mechanics, considering both one and two-
 127 dimensional problems.
- 128 • The **Poisson's Equation**, widely used in math and physics, with four different cases.
- 129 • The **Heat Equation**, a time-dependent PDE that describes diffusion or heat conduction,
 130 demonstrated in four unique cases.
- 131 • The **Navier-Stokes Equation**, describing the motion of viscous fluid substances, showcased
 132 in three scenarios: a lid-driven flow (NS2d-C), a geometrically complex backward step flow
 133 (NS2d-CG), and a time-dependent problem (NS2d-LT).
- 134 • The **Wave Equation**, modeling wave behavior, exhibited in three cases.
- 135 • **Chaotic PDEs**, featuring two popular examples: the Gray-Scott (GS) and Kuramoto-
 136 Sivashinsky (KS) equations.
- 137 • **High Dimensional PDEs**, including the high-dimensional Poisson equation (PNd) and the
 138 high-dimensional diffusion or heat equation (HNd).
- 139 • **Inverse Problems**, focusing on the reconstruction of the coefficient field from noisy data
 140 for the Poisson equation (PInv) and the diffusion equation (HInv).

141 It is important to note that we have chosen PDEs encompassing a wide range of mathematical
 142 properties. This ensures that the benchmarks do not favor a specific type of PDE. The selected PDE
 143 problems introduce several core challenges, which include:

- 144 • **Complex Geometry**: Many PDE problems involve complex or irregular geometry, such as
 145 heat conduction or wave propagation around obstacles. These complexities pose significant
 146 challenges for PINNs in terms of accurate boundary behavior representation.
- 147 • **Multi-Scale Phenomena**: Multi-scale phenomena, where the solution varies significantly
 148 over different scales, are prevalent in situations such as turbulent fluid flow. Achieving a
 149 balanced representation across all scales is a challenge for PINNs in multi-scale scenarios.
- 150 • **Nonlinear Behavior**: Many PDEs exhibit nonlinear or even chaotic behavior, where mi-
 151 nor variations in initial conditions can lead to substantial divergence in outcomes. The
 152 optimization of PINNs becomes intriguing on nonlinear PDEs.

153 • **High Dimensionality:** High-dimensional PDE problems, frequently encountered in quantum
 154 mechanics, present significant challenges for PINNs due to the “curse of dimensionality”.
 155 This term refers to the increase in computational complexity with the addition of each
 156 dimension, accompanied by statistical issues like data sparsity in high-dimensional space.

157 These challenges are selected due to their frequent occurrence in numerous real-world applications.
 158 As such, a method’s performance in addressing these challenges serves as a reliable indicator of
 159 its overall practical utility. Table 1 presents a detailed overview of the dataset, the PDEs, and
 160 the challenges associated with these problems. We generate data using FEM solver provided by
 161 COMSOL 6.0 [37] for problems with complex geometry and spectral method provided by Chebfun
 162 [11] for chaotic problems. More details can be found in Appendix B.

Dataset	Complex geometry	Multi-scale	Nonlinearity	High dim
Burgers ^{1~2}	×	×	√	×
Poisson ^{3~6}	×/√	×/√	×	×
Heat ^{7~10}	×/√	×/√	×	×
NS ^{11~13}	×/√	×/√	√	×
Wave ^{14~16}	×/√	×/√	×	×
Chaotic ^{17~18}	×	√	√	×
High dim ^{19~20}	×	×	×	√
Inverse ^{21~22}	×	×	√	×

Table 1: Overview of our datasets along with their challenges. We chose 22 cases in total to evaluate the methods of PINNs. The left picture shows the visualization of cases with these four challenges, i.e., complex geometry, multi-scale, nonlinearity, and high dimension.

163 3.3 Methods and Toolbox

164 After conducting an extensive literature review, we present an overview of diverse PINNs approaches
 165 for comparison. Then we present the high-level structure of our PINNacle.

166 3.3.1 Methods

167 As mentioned above, variants of PINNs are mainly based on loss functions, architecture, and
 168 optimizer [16]. The modifications to loss functions can be divided into reweighting existing losses
 169 and developing novel loss functions like regularization and variational formulation. Variants of
 170 architectures include using domain decomposition and adaptive activations.

171 The methods discussed are directly correlated with the challenges highlighted in Table 1. For example,
 172 domain decomposition methods are particularly effective for problems involving complex geometries
 173 and multi-scale phenomena. Meanwhile, loss reweighting strategies are adept at addressing imbal-
 174 ances in problems with multiple losses. We have chosen variants from these categories based on their
 175 significant contributions to the field.

176 Here, we list the primary categories and representative methods as summarized in Table 2:

- 177 • **Loss reweighting/Resampling (2~4):** PINNs are trained with a mixed loss of PDE residuals,
 178 boundary conditions, and available data losses shown in Eq 3. Various methods [54, 56, 2,
 179 33, 45] propose different strategies to adjust these weights w_c , w_b and w_d at different epochs
 180 or resample collocation points $\{x_c^i\}$ and $\{x_b^i\}$ in Eq 3, which indirectly adjust the weights
 181 [57, 38]. We choose three famous examples, i.e., reweighting using gradient norms (PINN-
 182 LRA) [54], using neural tangent kernel (PINN-NTK) [56], and residual-based resampling
 183 (RAR)[32, 57].
- 184 • **Novel optimizer (5):** To handle the problem of multi-scale objectives, some new optimizers
 185 [30, 58] are proposed. We chose MultiAdam, which is resistant to domain scale changes.

	Complex Geometry	Multi-scale	Nonlinearity	High dim
Vanilla PINN ¹	×	×	×	×
Reweighting/Resampling ^{2~4}	√	√	×	×
Novel Optimizer ⁷	×	√	×	×
Novel Loss Functions ^{5~6}	×	×	×	×
Novel Architecture ^{8~10}	√	√	×	×

Table 2: Overview of methods in our PINNacle. √ denotes the method is potentially designed to solve or show empirical improvements for problems encountering the challenge and vice versa.

- 186 • **Novel loss functions (6~7)**: Some works introduce novel loss functions like variational
187 formulation [47, 26, 25] and regularization terms to improve training. We choose hp-VPINN
188 [25] and gPINN [60, 48], which are representative examples from these two categories.
- 189 • **Novel activation architectures (8~10)**: Some works propose various network architectures,
190 such as using CNN and LSTM [61, 13, 44], custom activation functions [20, 21], and domain
191 decomposition [19, 46, 22, 36]. Among adaptive activations for PINNs, we choose LAAF
192 [20] and GAAF [21]. Domain decomposition is a method that divides the whole domain
193 into multiple subdomains and trains subnetworks on these subdomains. It is helpful for
194 solving multi-scale problems, but multiple subnetworks increase the difficulty of training.
195 XPINNs, cPINNs, and FBPINNs [19, 22, 36] are three representative examples. We choose
196 FBPINNs which is the state-of-the-art domain decomposition that applies domain-specific
197 normalization to stabilize training.

198 3.3.2 Structure of Toolbox

199 We provide a user-friendly and concise toolbox for implementing, training, and evaluating diverse
200 PINN variants. Specifically, our codebase is based on DeepXDE and provides a series of encapsulated
201 classes and functions to facilitate high-level training and custom PDEs. These utilities allow for a
202 standardized and streamlined approach to the implementation of various PINN variants and PDEs.
203 Moreover, we provided many auxiliary functions, including computing different metrics, visualizing
204 predictions, and recording results.

205 Despite the unified implementation of diverse PINNs, we also design an adaptive multi-GPU parallel
206 training framework To enhance the efficiency of systematic evaluations of PINN methods. It addresses
207 the parallelization phase of training on multiple tasks, effectively balancing the computational loads
208 of multiple GPUs. It allows for the execution of larger and more complex tasks. In a nutshell, we
209 provide an example code for training and evaluating PINNs on two Poisson equations using our
210 PINNacle framework in Appendix D.

211 3.4 Evaluation

212 To comprehensively analyze the discrepancy between the PINN solutions and the true solutions,
213 we adopt multiple metrics to evaluate the performance of the PINN variants. Generally, we choose
214 several metrics that are commonly used in literature that apply to all methods and problems. We
215 suppose that $\mathbf{y} = (y_i)_{i=1}^n$ is the prediction and $\mathbf{y}' = (y'_i)_{i=1}^n$ to is ground truth, where n is the number
216 of testing examples. Specifically, we use ℓ_2 relative error (L2RE), and ℓ_1 relative error (L1RE)
217 which are two most commonly used metrics to measure the global quality of the solution,

$$\text{L2RE} = \sqrt{\frac{\sum_{i=1}^n (y_i - y'_i)^2}{\sum_{i=1}^n y_i'^2}}, \text{L1RE} = \frac{\sum_{i=1}^n |y_i - y'_i|}{\sum_{i=1}^n |y'_i|}. \quad (4)$$

218 We also compute max error (mERR in short), mean square error (MSE), and Fourier error (fMSE) for
219 a detailed analysis of the prediction. These three metrics are computed as follows:

$$\text{MSE} = \frac{1}{n} \sum_{i=1}^n (y_i - y'_i)^2, \text{mERR} = \max_i |y_i - y'_i|, \text{fMSE} = \frac{\sqrt{\sum_{k_{\min}}^{k_{\max}} |\mathcal{F}(\mathbf{y}) - \mathcal{F}(\mathbf{y}')|^2}}{k_{\max} - k_{\min} + 1}, \quad (5)$$

L2RE	Name	Vanilla			Loss Reweighting/Sampling			Optimizer	Loss functions		Architecture		
		PINN	PINN-w	LBFSGS	LRA	NTK	RAR	MultiAdam	gPINN	vPINN	LAAF	GAAF	FBPINN
Burgers	1d-C	1.45E-2	2.63E-2	1.33E-2	2.61E-2	1.84E-2	3.32E-2	4.85E-2	2.16E-1	3.47E-1	1.43E-2	5.20E-2	2.32E-1
	2d-C	3.24E-1	2.70E-1	4.65E-1	2.60E-1	2.75E-1	3.45E-1	3.33E-1	3.27E-1	6.38E-1	2.77E-1	2.95E-1	-
Poisson	2d-C	6.94E-1	3.49E-2	NaN	1.17E-1	1.23E-2	6.99E-1	2.63E-2	6.87E-1	4.91E-1	7.68E-1	6.04E-1	4.49E-2
	2d-CG	6.36E-1	6.08E-2	2.96E-1	4.34E-2	1.43E-2	6.48E-1	2.76E-1	7.92E-1	2.86E-1	4.80E-1	8.71E-1	2.90E-2
	3d-CG	5.60E-1	3.74E-1	7.05E-1	1.02E-1	9.47E-1	5.76E-1	3.63E-1	4.85E-1	7.38E-1	5.79E-1	5.02E-1	7.39E-1
	2d-MS	6.30E-1	7.60E-1	1.45E+0	7.94E-1	7.48E-1	6.44E-1	5.90E-1	6.16E-1	9.72E-1	5.93E-1	9.31E-1	1.04E+0
Heat	2d-VC	1.01E+0	2.35E-1	2.32E-1	2.12E-1	2.14E-1	9.66E-1	4.75E-1	2.12E+0	9.40E-1	6.42E-1	8.49E-1	9.52E-1
	2d-MS	6.21E-2	2.42E-1	1.73E-2	8.79E-2	4.40E-2	7.49E-2	2.18E-1	1.13E-1	9.30E-1	7.40E-2	9.85E-1	8.20E-2
	2d-CG	3.64E-2	1.45E-1	8.57E-1	1.25E-1	1.16E-1	2.72E-2	7.12E-2	9.38E-2	-	2.39E-2	4.61E-1	9.16E-2
	2d-LT	9.99E-1	9.99E-1	1.00E+0	9.99E-1	1.00E+0	9.99E-1	1.00E+0	1.00E+0	1.00E+0	9.99E-1	9.99E-1	1.01E+0
NS	2d-C	4.70E-2	1.45E-1	2.14E-1	NaN	1.98E-1	4.69E-1	7.27E-1	7.70E-2	2.92E-1	3.60E-2	3.79E-2	8.45E-2
	2d-CG	1.19E-1	3.26E-1	NaN	3.32E-1	2.93E-1	3.34E-1	4.31E-1	1.54E-1	9.94E-1	8.24E-2	1.74E-1	8.27E+0
	2d-LT	9.96E-1	1.00E+0	9.70E-1	1.00E+0	9.99E-1	1.00E+0	1.00E+0	9.95E-1	1.73E+0	9.98E-1	9.99E-1	1.00E+0
Wave	1d-C	5.88E-1	2.85E-1	NaN	3.61E-1	9.79E-2	5.39E-1	1.21E-1	5.56E-1	8.39E-1	4.54E-1	6.77E-1	5.91E-1
	2d-CG	1.84E+0	1.66E+0	1.33E+0	1.48E+0	2.16E+0	1.15E+0	1.09E+0	8.14E-1	7.99E-1	8.19E-1	7.94E-1	1.06E+0
	2d-MS	1.34E+0	1.02E+0	1.37E+0	1.02E+0	1.04E+0	1.35E+0	1.01E+0	1.02E+0	9.82E-1	1.06E+0	1.06E+0	1.03E+0
Chaotic	GS	3.19E-1	1.58E-1	NaN	9.37E-2	2.16E-1	9.46E-2	9.37E-2	2.48E-1	1.16E+0	9.47E-2	9.46E-2	7.99E-2
	KS	1.01E+0	9.86E-1	NaN	9.57E-1	9.64E-1	1.01E+0	9.61E-1	9.94E-1	9.72E-1	1.01E+0	1.00E+0	1.02E+0
High dim	Pnd	3.04E-3	2.58E-3	4.67E-4	4.58E-4	4.64E-3	3.59E-3	3.98E-3	5.05E-3	-	4.14E-3	7.75E-3	-
	HNd	3.61E-1	4.59E-1	1.19E-4	3.94E-1	3.97E-1	3.57E-1	3.02E-1	3.17E-1	-	5.22E-1	5.21E-1	-
Inverse	Pinv	9.42E-2	1.66E-1	NaN	1.54E-1	1.93E-1	9.35E-2	1.30E-1	8.03E-2	2.45E-2	1.30E-1	2.54E-1	8.44E-1
	HInv	1.57E+0	5.26E-2	NaN	5.09E-2	7.52E-2	1.52E+0	8.04E-2	4.84E+0	4.56E-1	5.59E-1	2.12E-1	9.27E-1

Table 3: Mean L2RE of different PINN variants on our benchmark. Best results are highlighted in blue and second-places in lightblue. We do not bold any result if errors of all methods are about 100%. “NaN” means the method does not converge and “-” means the method is not suitable for the problem.

where \mathcal{F} denotes Fourier transform of \mathbf{y} and k_{\min}, k_{\max} are chosen similar to PDEBench [50]. Besides, for time-dependent problems, investigating the quality of the solution with time is important. Therefore we compute the L2RE error varying with time in Appendix E.2.

We assess the performance of PINNs against the reference from numerical solvers. Experimental results utilizing the ℓ_2 relative error (L2RE) metric are incorporated within the main text, while a more exhaustive set of results, based on the aforementioned metrics, is available in the Appendix E.1.

4 Experiments

4.1 Main Results

We now present experimental results. Except for the ablation study in Sec 4.3 and Appendix E.2, we use a learning rate of 0.001 and train all models with 20,000 epochs. We repeat all experiments three times and record the mean and std. Table 3 presents the main results for all methods on our tasks and shows their average ℓ_2 relative errors (with standard deviation results available in Appendix E.1).

PINN. We use PINN-w to denote training PINNs with larger boundary weights. The vanilla PINNs struggle to accurately solve complex physics systems, indicating substantial room for improvement. Using an ℓ_2 relative error (L2RE) of 10% as a threshold for a successful solution, we find that vanilla PINN only solves 10 out of 22 tasks, most of which involve simpler equations (e.g., 1.45% on Burgers-1d-C). They encounter significant difficulties when faced with physics systems characterized by complex geometries, multi-scale phenomena, nonlinearity, and longer time spans. This shows that directly optimizing an average of the PDE losses and initial/boundary condition losses leads to critical issues such as loss imbalance, suboptimal convergence, and limited expressiveness.

PINN variants. PINN variants offer approaches to addressing some of these challenges to varying degrees. Methods involving loss reweighting and resampling have shown improved performance in some cases involving complex geometries and multi-scale phenomena (e.g., 1.43% on Poisson-2d-CG). This is due to the configuration of loss weights and sampled collocation points, which adaptively place more weight on more challenging domains during the training process. However, these methods still struggle with Wave equations, Navier-Stokes equations, and other cases with higher dimensions

L2RE	Name	Vanilla	Loss Reweighting/Sampling			Optimizer	Loss functions		Architecture		
		PINN	LRA	NTK	RAR	MultiAdam	gPINN	vPINN	LAAF	GAAF	FBPINN
Burgers-P	2d-C	4.74E-01	4.36E-01	4.13E-01	4.71E-01	4.93E-01	4.91E-01	2.82E+0	4.37E-01	4.34E-01	-
Poisson-P	2d-C	2.24E-01	7.07E-02	1.66E-02	2.33E-01	8.24E-02	4.03E-01	5.51E-1	1.84E-01	2.97E-01	2.87E-2
Heat-P	2d-MS	1.73E-01	1.23E-01	1.50E-01	1.53E-01	4.00E-01	4.59E-01	5.12E-1	6.27E-02	1.89E-01	2.46E-1
NS-P	2d-C	3.89E-01	-	4.52E-01	3.91E-01	9.33E-01	7.19E-01	3.76E-1	3.63E-01	4.85E-01	3.99E-1
Wave-P	1d-C	5.22E-01	3.44E-01	2.69E-01	5.05E-01	6.89E-01	7.66E-01	3.58E-1	4.03E-01	9.00E-01	1.15E+0
High dim-P	HNd	7.66E-03	6.53E-03	9.04E-03	8.07E-03	2.22E-03	7.87E-03	-	6.97E-03	1.94E-01	-

Table 4: Results of different PINN variants on parametric PDEs. We report average L2RE on all examples within a class of PDE. We **bold** the best results across all methods.

246 or longer time spans. MultiAdam, a representative of novel optimizers, solves several simple cases
247 and the chaotic GS equation (9.37%), but does not significantly outperform other methods. The new
248 loss term of variational form demonstrates significant superiority in solving inverse problems (*e.g.*,
249 1.19% on HInv for vPINN), but no clear improvement in fitting error over standard PINN in forward
250 cases. Changes in architecture can enhance expressiveness and flexibility for cases with complex
251 geometries and multi-scale systems. For example, FBPINN achieves the smallest error on the chaotic
252 GS equation (7.99%), while LAAF delivers the best fitting result on Heat-2d-CG (2.39%).

253 **Discussion.** For challenges related to complex geometries and multi-scale phenomena, some methods
254 can mitigate these issues by implementing mechanisms like loss reweighting, novel optimizers, and
255 better capacity through adaptive activation. This holds true for the 2D cases of Heat and Poisson
256 equations, which are classic linear equations. However, when systems have higher dimensions
257 (Poisson3d-CG) or longer time spans (Heat2d-LT), all methods fail to solve, highlighting the difficul-
258 ties associated with complex geometries and multi-scale systems.

259 In contrast, nonlinear, long-time PDEs like 2D Burgers, NS, and KS pose challenges for most
260 methods. These equations are sensitive to initial conditions, resulting in complicated solution
261 spaces and more local minima for PINNs [49]. The Wave equation, featuring a second-order time
262 derivative and periodic behavior, is particularly hard for PINNs, which often become unstable and
263 may violate conservation laws [22, 53]. Although all methods perform well on Poisson-Nd, only
264 PINN with LBFSGS solves Heat-Nd, indicating the potential of a second-order optimizer for solving
265 high dimensional PDEs[51].

266 4.2 Parameterized PDE Experiments

267 The performance of PINNs is also highly influenced by parameters in PDEs [28]. To investigate
268 whether PINNs could handle a class of PDEs, we design this experiment to solve the same PDEs
269 with different parameters. We choose 6 PDEs, *i.e.*, Burgers2d-C, Poisson2d-C, Heat2d-MS, NS-C,
270 Wave1d-C, and Heat-Nd (HNd), with each case containing five parameterized examples. Details
271 of the parameterized PDEs are shown in Appendix B. Here we report the average L2RE metric on
272 these parameterized PDEs for every case, and results are shown in the following Table 4. First,
273 we see that compared with the corresponding cases in Table E.1, the mean L2RE of parameterized
274 PDEs is usually higher. We suggest that this is because there are some difficult cases under certain
275 parameters for these PDEs with very high errors. Secondly, we find that PINN-NTK works well on
276 parameterized PDE tasks which achieve three best results among all six experiments. We speculate
277 that solving PDEs with different parameters requires different weights for loss terms, and PINN-NTK
278 is a powerful method for automatically balancing these weights.

279 4.3 Hyperparameter Analysis

280 The performance of PINNs is strongly affected by hyperparameters, with each variant introducing its
281 own unique set. The results are shown in Figure 2. We focus on a set of problems, *i.e.*, Burgers1d,
282 GS, Heat2d-CG, and Poisson2d-C. Detailed results and additional findings are in Appendix E.2.

283 **Batch size and training epochs.** Figure 18 presents the effects of varying batch sizes and training
284 epochs. Larger batch sizes generally yield better outcomes due to more accurate gradient estimations,
285 though saturation is observed beyond a batch size of 2048 for the GS and Poisson2d-C problems.

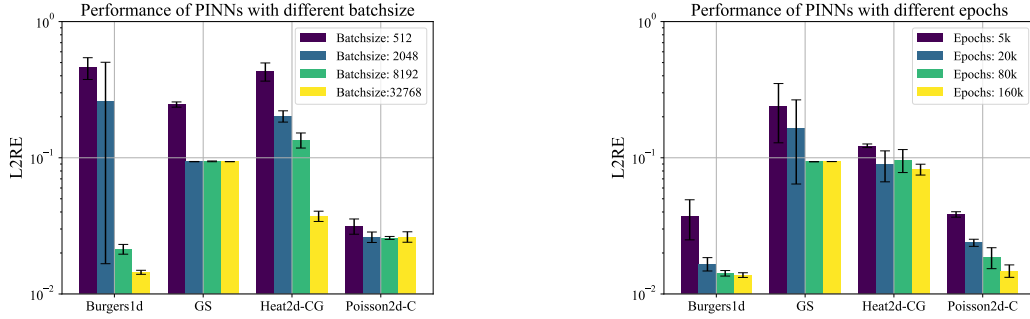


Figure 2: Performance of vanilla PINNs under different batch sizes (number of collocation points), which is shown in the left figure; and number of training epochs, which is shown in the right figure.

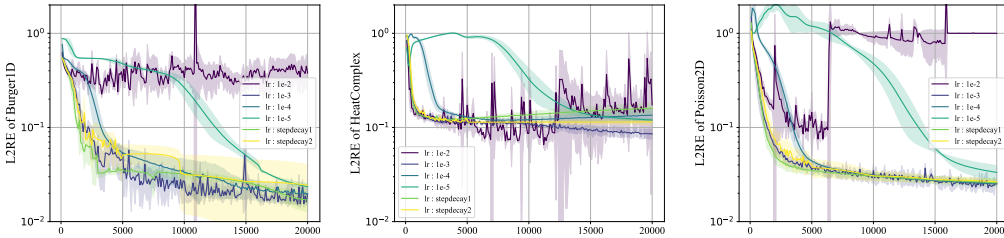


Figure 3: Convergence curve of PINNs with different learning rate schedules on Burgers1d, Heat2d-CG, and Poisson2d-C.

286 Similarly, increasing the number of training epochs reduces the L2RE, indicating an improvement in
 287 model accuracy. However, this benefit plateaus around 20k to 80k epochs, where further increases in
 288 epochs do not significantly reduce the error.

289 **Learning Rates.** The performance of standard PINNs under various learning rates and learning rate
 290 schedules is shown in Figure 3. We observe that the influence of the learning rate on performance is
 291 intricate, with optimal learning rates varying across problems. Furthermore, PINN training tends to
 292 be unstable. High learning rates, such as 10^{-2} , often lead to error spikes, while low learning rates,
 293 like 10^{-5} , result in slow convergence. Our findings suggest that a moderate learning rate, such as
 294 10^{-3} or 10^{-4} , or a step decay learning rate schedule, tends to yield more stable performance.

295 5 Conclusion

296 In this work, we introduced PINNacle, a comprehensive benchmark offering a user-friendly toolbox
 297 that encompasses over 10 PINN methods. We evaluated these methods against more than 20 chal-
 298 lenging PDE problems, conducting extensive experiments and ablation studies for hyperparameters.
 299 Looking forward, we plan to expand the benchmark by integrating additional state-of-the-art methods
 300 and incorporating more practical problem scenarios.

301 Our analysis of the experimental results yields several key insights. First, domain decomposition is
 302 beneficial for addressing problems characterized by complex geometries, and PINN-NTK is a strong
 303 method for balancing loss weights as experiments show. Second, the choice of hyperparameters
 304 is crucial to the performance of PINNs. Selecting a larger batch size and appropriately weighting
 305 losses or betas in Adam may significantly reduce the error. However, the best hyperparameters
 306 usually vary with PDEs. Third, we identify high-dimensional and nonlinear problems as a pressing
 307 challenge. The overall performance of PINNs is not yet on par with traditional numerical methods
 308 [14]. Fourth, from a theoretical standpoint, the exploration of PINNs’ loss landscape during the
 309 training of high-dimensional or nonlinear problems remains largely unexplored. Finally, from an
 310 algorithmic perspective, integrating the strengths of neural networks with numerical methods like
 311 preconditioning, weak formulation, and multigrid may present a promising avenue toward overcoming
 312 the challenges identified herein [34].

313 References

- 314 [1] Simon Axelrod and Rafael Gomez-Bombarelli. Geom, energy-annotated molecular conforma-
315 tions for property prediction and molecular generation. *Scientific Data*, 9(1):185, 2022.
- 316 [2] Rafael Bischof and Michael Kraus. Multi-objective loss balancing for physics-informed deep
317 learning. *arXiv preprint arXiv:2110.09813*, 2021.
- 318 [3] Aleksandar Botev, Andrew Jaegle, Peter Wirnsberger, Daniel Hennes, and Irina Higgins.
319 Which priors matter? benchmarking models for learning latent dynamics. *arXiv preprint*
320 *arXiv:2111.05458*, 2021.
- 321 [4] Emmanuel Boutet, Damien Lieberherr, Michael Tognolli, Michel Schneider, Parit Bansal, Alan J
322 Bridge, Sylvain Poux, Lydie Bougueleret, and Ioannis Xenarios. Uniprotkb/swiss-prot, the
323 manually annotated section of the uniprot knowledgebase: how to use the entry view. *Plant*
324 *bioinformatics: methods and protocols*, pages 23–54, 2016.
- 325 [5] Salva Rühling Cachay, Venkatesh Ramesh, Jason NS Cole, Howard Barker, and David Rolnick.
326 Climart: A benchmark dataset for emulating atmospheric radiative transfer in weather and
327 climate models. *arXiv preprint arXiv:2111.14671*, 2021.
- 328 [6] DM Causon and CG Mingham. *Introductory finite difference methods for PDEs*. Bookboon,
329 2010.
- 330 [7] Feiyu Chen, David Sondak, Pavlos Protopapas, Marios Mattheakis, Shuheng Liu, Devansh
331 Agarwal, and Marco Di Giovanni. Neurodiffeq: A python package for solving differential
332 equations with neural networks. *Journal of Open Source Software*, 5(46):1931, 2020.
- 333 [8] Salvatore Cuomo, Vincenzo Schiano Di Cola, Fabio Giampaolo, Gianluigi Rozza, Maziar
334 Raissi, and Francesco Piccialli. Scientific machine learning through physics-informed neural
335 networks: where we are and what’s next. *Journal of Scientific Computing*, 92(3):88, 2022.
- 336 [9] Sourav Das and Solomon Tesfamariam. State-of-the-art review of design of experiments for
337 physics-informed deep learning. *arXiv preprint arXiv:2202.06416*, 2022.
- 338 [10] Arka Daw, Anuj Karpatne, William Watkins, Jordan Read, and Vipin Kumar. Physics-
339 guided neural networks (pgnn): An application in lake temperature modeling. *arXiv preprint*
340 *arXiv:1710.11431*, 2017.
- 341 [11] Tobin A Driscoll, Nicholas Hale, and Lloyd N Trefethen. *Chebfun guide*, 2014.
- 342 [12] Robert Eymard, Thierry Gallouët, and Raphaële Herbin. Finite volume methods. *Handbook of*
343 *numerical analysis*, 7:713–1018, 2000.
- 344 [13] Han Gao, Luning Sun, and Jian-Xun Wang. Phygeonet: Physics-informed geometry-adaptive
345 convolutional neural networks for solving parameterized steady-state pdes on irregular domain.
346 *Journal of Computational Physics*, 428:110079, 2021.
- 347 [14] Tamara G Grossmann, Urszula Julia Komorowska, Jonas Latz, and Carola-Bibiane Schön-
348 lieb. Can physics-informed neural networks beat the finite element method? *arXiv preprint*
349 *arXiv:2302.04107*, 2023.
- 350 [15] Jayesh K Gupta and Johannes Brandstetter. Towards multi-spatiotemporal-scale generalized
351 pde modeling. *arXiv preprint arXiv:2209.15616*, 2022.
- 352 [16] Zhongkai Hao, Songming Liu, Yichi Zhang, Chengyang Ying, Yao Feng, Hang Su, and Jun
353 Zhu. Physics-informed machine learning: A survey on problems, methods and applications.
354 *arXiv preprint arXiv:2211.08064*, 2022.

- 355 [17] Oliver Hennigh, Susheela Narasimhan, Mohammad Amin Nabian, Akshay Subramaniam,
356 Kaustubh Tangsali, Zhiwei Fang, Max Rietmann, Wonmin Byeon, and Sanjay Choudhry.
357 Nvidia simnet™: An ai-accelerated multi-physics simulation framework. In *International*
358 *Conference on Computational Science*, pages 447–461. Springer, 2021.
- 359 [18] Zizhou Huang, Teseo Schneider, Minchen Li, Chenfanfu Jiang, Denis Zorin, and Daniele
360 Panozzo. A large-scale benchmark for the incompressible navier-stokes equations. *arXiv*
361 *preprint arXiv:2112.05309*, 2021.
- 362 [19] Ameya D Jagtap and George E Karniadakis. Extended physics-informed neural networks
363 (xpinns): A generalized space-time domain decomposition based deep learning framework for
364 nonlinear partial differential equations. In *AAAI Spring Symposium: MLPS*, 2021.
- 365 [20] Ameya D Jagtap, Kenji Kawaguchi, and George Em Karniadakis. Locally adaptive activation
366 functions with slope recovery for deep and physics-informed neural networks. *Proceedings of*
367 *the Royal Society A*, 476(2239):20200334, 2020.
- 368 [21] Ameya D Jagtap, Kenji Kawaguchi, and George Em Karniadakis. Adaptive activation functions
369 accelerate convergence in deep and physics-informed neural networks. *Journal of Computational*
370 *Physics*, 404:109136, 2020.
- 371 [22] Ameya D Jagtap, Ehsan Kharazmi, and George Em Karniadakis. Conservative physics-informed
372 neural networks on discrete domains for conservation laws: Applications to forward and inverse
373 problems. *Computer Methods in Applied Mechanics and Engineering*, 365:113028, 2020.
- 374 [23] George Em Karniadakis, Ioannis G Kevrekidis, Lu Lu, Paris Perdikaris, Sifan Wang, and Liu
375 Yang. Physics-informed machine learning. *Nature Reviews Physics*, 3(6):422–440, 2021.
- 376 [24] Ehsan Kharazmi, Zhongqiang Zhang, and George Em Karniadakis. Variational physics-informed
377 neural networks for solving partial differential equations. *arXiv preprint arXiv:1912.00873*,
378 2019.
- 379 [25] Ehsan Kharazmi, Zhongqiang Zhang, and George Em Karniadakis. hp-vpinns: Variational
380 physics-informed neural networks with domain decomposition. *Computer Methods in Applied*
381 *Mechanics and Engineering*, 374:113547, 2021.
- 382 [26] Reza Khodayi-Mehr and Michael Zavlanos. Varnet: Variational neural networks for the solution
383 of partial differential equations. In *Learning for Dynamics and Control*, pages 298–307. PMLR,
384 2020.
- 385 [27] R Khudorozhkov, S Tsimfer, and A Koryagin. Pydens framework for solving differential
386 equations with deep learning. *arXiv preprint arXiv:1909.11544*, 2019.
- 387 [28] Aditi Krishnapriyan, Amir Gholami, Shandian Zhe, Robert Kirby, and Michael W Mahoney.
388 Characterizing possible failure modes in physics-informed neural networks. *Advances in Neural*
389 *Information Processing Systems*, 34:26548–26560, 2021.
- 390 [29] Ke Li, Kejun Tang, Tianfan Wu, and Qifeng Liao. D3m: A deep domain decomposition method
391 for partial differential equations. *IEEE Access*, 8:5283–5294, 2019.
- 392 [30] Yuhao Liu, Xiaojian Li, and Zhengxian Liu. An improved physics-informed neural network
393 based on a new adaptive gradient descent algorithm for solving partial differential equations of
394 nonlinear systems. 2022.
- 395 [31] Lu Lu, Xuhui Meng, Shengze Cai, Zhiping Mao, Somdatta Goswami, Zhongqiang Zhang,
396 and George Em Karniadakis. A comprehensive and fair comparison of two neural operators
397 (with practical extensions) based on fair data. *Computer Methods in Applied Mechanics and*
398 *Engineering*, 393:114778, 2022.

- 399 [32] Lu Lu, Xuhui Meng, Zhiping Mao, and George Em Karniadakis. Deepxde: A deep learning
400 library for solving differential equations. *SIAM review*, 63(1):208–228, 2021.
- 401 [33] Suryanarayana Maddu, Dominik Sturm, Christian L Müller, and Ivo F Sbalzarini. Inverse
402 dirichlet weighting enables reliable training of physics informed neural networks. *Machine*
403 *Learning: Science and Technology*, 3(1):015026, 2022.
- 404 [34] Stefano Markidis. The old and the new: Can physics-informed deep-learning replace traditional
405 linear solvers? *Frontiers in big Data*, 4:669097, 2021.
- 406 [35] Keith W Morton and David Francis Mayers. *Numerical solution of partial differential equations:
407 an introduction*. Cambridge university press, 2005.
- 408 [36] Ben Moseley, Andrew Markham, and Tarje Nissen-Meyer. Finite basis physics-informed
409 neural networks (fbpinns): a scalable domain decomposition approach for solving differential
410 equations. *arXiv preprint arXiv:2107.07871*, 2021.
- 411 [37] COMSOL Multiphysics. Introduction to comsol multiphysics®. *COMSOL Multiphysics,
412 Burlington, MA, accessed Feb, 9:2018*, 1998.
- 413 [38] Mohammad Amin Nabian, Rini Jasmine Gladstone, and Hadi Meidani. Efficient training
414 of physics-informed neural networks via importance sampling. *Computer-Aided Civil and*
415 *Infrastructure Engineering*, 36(8):962–977, 2021.
- 416 [39] Karl Otness, Arvi Gjoka, Joan Bruna, Daniele Panozzo, Benjamin Peherstorfer, Teseo Schneider,
417 and Denis Zorin. An extensible benchmark suite for learning to simulate physical systems.
418 *arXiv preprint arXiv:2108.07799*, 2021.
- 419 [40] Evan Racah, Christopher Beckham, Tegan Maharaj, Samira Ebrahimi Kahou, Mr Prabhat,
420 and Chris Pal. Extremeweather: A large-scale climate dataset for semi-supervised detection,
421 localization, and understanding of extreme weather events. *Advances in neural information*
422 *processing systems*, 30, 2017.
- 423 [41] Christopher Rackauckas and Qing Nie. Differentialequations.jl—a performant and feature-rich
424 ecosystem for solving differential equations in julia. *Journal of open research software*, 5(1),
425 2017.
- 426 [42] Maziar Raissi, Paris Perdikaris, and George E Karniadakis. Physics-informed neural networks:
427 A deep learning framework for solving forward and inverse problems involving nonlinear partial
428 differential equations. *Journal of Computational physics*, 378:686–707, 2019.
- 429 [43] Junuthula Narasimha Reddy. *Introduction to the finite element method*. McGraw-Hill Education,
430 2019.
- 431 [44] Pu Ren, Chengping Rao, Yang Liu, Jian-Xun Wang, and Hao Sun. Phycrnet: Physics-informed
432 convolutional-recurrent network for solving spatiotemporal pdes. *Computer Methods in Applied*
433 *Mechanics and Engineering*, 389:114399, 2022.
- 434 [45] Franz M Rohrhofer, Stefan Posch, and Bernhard C Geiger. On the pareto front of physics-
435 informed neural networks. *arXiv preprint arXiv:2105.00862*, 2021.
- 436 [46] Khemraj Shukla, Ameya D Jagtap, and George Em Karniadakis. Parallel physics-informed
437 neural networks via domain decomposition. *Journal of Computational Physics*, 447:110683,
438 2021.
- 439 [47] Justin Sirignano and Konstantinos Spiliopoulos. Dgm: A deep learning algorithm for solving
440 partial differential equations. *Journal of computational physics*, 375:1339–1364, 2018.
- 441 [48] Hwijae Son, Jin Woo Jang, Woo Jin Han, and Hyung Ju Hwang. Sobolev training for the neural
442 network solutions of pdes. 2021.

- 443 [49] Sophie Steger, Franz M Rohrhofer, and Bernhard C Geiger. How pinns cheat: Predicting chaotic
444 motion of a double pendulum. In *The Symbiosis of Deep Learning and Differential Equations*
445 *II*, 2022.
- 446 [50] Makoto Takamoto, Timothy Praditia, Raphael Leiteritz, Daniel MacKinlay, Francesco Alesiani,
447 Dirk Pflüger, and Mathias Niepert. Pdebench: An extensive benchmark for scientific machine
448 learning. *Advances in Neural Information Processing Systems*, 35:1596–1611, 2022.
- 449 [51] Kejun Tang, Xiaoliang Wan, and Chao Yang. Das: A deep adaptive sampling method for solving
450 partial differential equations. *arXiv preprint arXiv:2112.14038*, 2021.
- 451 [52] Nanzhe Wang, Dongxiao Zhang, Haibin Chang, and Heng Li. Deep learning of subsurface flow
452 via theory-guided neural network. *Journal of Hydrology*, 584:124700, 2020.
- 453 [53] Sifan Wang, Shyam Sankaran, and Paris Perdikaris. Respecting causality is all you need for
454 training physics-informed neural networks. *arXiv preprint arXiv:2203.07404*, 2022.
- 455 [54] Sifan Wang, Yujun Teng, and Paris Perdikaris. Understanding and mitigating gradient flow
456 pathologies in physics-informed neural networks. *SIAM Journal on Scientific Computing*,
457 43(5):A3055–A3081, 2021.
- 458 [55] Sifan Wang, Hanwen Wang, and Paris Perdikaris. On the eigenvector bias of fourier feature
459 networks: From regression to solving multi-scale pdes with physics-informed neural networks.
460 *Computer Methods in Applied Mechanics and Engineering*, 384:113938, 2021.
- 461 [56] Sifan Wang, Xinling Yu, and Paris Perdikaris. When and why pinns fail to train: A neural
462 tangent kernel perspective. *Journal of Computational Physics*, 449:110768, 2022.
- 463 [57] Chenxi Wu, Min Zhu, Qinyang Tan, Yadhu Kartha, and Lu Lu. A comprehensive study of non-
464 adaptive and residual-based adaptive sampling for physics-informed neural networks. *Computer*
465 *Methods in Applied Mechanics and Engineering*, 403:115671, 2023.
- 466 [58] Jiachen Yao, Chang Su, Zhongkai Hao, Songming Liu, Hang Su, and Jun Zhu. Multiadam:
467 Parameter-wise scale-invariant optimizer for multiscale training of physics-informed neural
468 networks. *arXiv preprint arXiv:2306.02816*, 2023.
- 469 [59] Bing Yu et al. The deep ritz method: a deep learning-based numerical algorithm for solving
470 variational problems. *Communications in Mathematics and Statistics*, 6(1):1–12, 2018.
- 471 [60] Jeremy Yu, Lu Lu, Xuhui Meng, and George Em Karniadakis. Gradient-enhanced physics-
472 informed neural networks for forward and inverse pde problems. *Computer Methods in Applied*
473 *Mechanics and Engineering*, 393:114823, 2022.
- 474 [61] Ruiyang Zhang, Yang Liu, and Hao Sun. Physics-informed multi-lstm networks for meta-
475 modeling of nonlinear structures. *Computer Methods in Applied Mechanics and Engineering*,
476 369:113226, 2020.

477 **6 Limitations**

478 While PINNacle incorporates a wide range of problems and compares numerous PINN variants, it
479 still has many limitations and might lead to both positive and negative broad impacts. Real-world
480 problems often exhibit much more additional complexity, like giant geometric domains and chaotic
481 behaviors. Good performance on this benchmark does not assume it applies to practical problems.
482 Second, the issues of explainability and stability in the PINN methods pose potential roadblocks,
483 especially for risk-sensitive applications. Possible ideas to address these limitations include,

- 484 • Exploring larger-scale PINN training methods and more efficient domain decomposition
485 methods, which might be beneficial for handling real-world multi-physics field coupling
486 problems.

- 487 • Developing theoretical convergence for PINN, especially the stability and convergence
488 analysis of the training process. A theoretically guaranteed PINN is more likely to be used
489 in risk-sensitive areas.

490 Checklist

491 The checklist follows the references. Please read the checklist guidelines carefully for information on
492 how to answer these questions. For each question, change the default **[TODO]** to **[Yes]**, **[No]**, or
493 **[N/A]**. You are strongly encouraged to include a **justification to your answer**, either by referencing
494 the appropriate section of your paper or providing a brief inline description. For example:

- 495 • Did you include the license to the code and datasets? **[Yes]** See Section 1.

496 Please do not modify the questions and only use the provided macros for your answers. Note that the
497 Checklist section does not count towards the page limit. In your paper, please delete this instructions
498 block and only keep the Checklist section heading above along with the questions/answers below.

499 1. For all authors...

- 500 (a) Do the main claims made in the abstract and introduction accurately reflect the paper’s
501 contributions and scope? **[Yes]**
- 502 (b) Did you describe the limitations of your work? **[Yes]**
- 503 (c) Did you discuss any potential negative societal impacts of your work? **[Yes]**
- 504 (d) Have you read the ethics review guidelines and ensured that your paper conforms to
505 them? **[Yes]**

506 2. If you are including theoretical results...

- 507 (a) Did you state the full set of assumptions of all theoretical results? **[N/A]**
- 508 (b) Did you include complete proofs of all theoretical results? **[N/A]**

509 3. If you ran experiments (e.g. for benchmarks)...

- 510 (a) Did you include the code, data, and instructions needed to reproduce the main experi-
511 mental results (either in the supplemental material or as a URL)? **[Yes]**
- 512 (b) Did you specify all the training details (e.g., data splits, hyperparameters, how they
513 were chosen)? **[Yes]**
- 514 (c) Did you report error bars (e.g., with respect to the random seed after running experi-
515 ments multiple times)? **[Yes]**
- 516 (d) Did you include the total amount of compute and the type of resources used (e.g., type
517 of GPUs, internal cluster, or cloud provider)? **[Yes]**

518 4. If you are using existing assets (e.g., code, data, models) or curating/releasing new assets...

- 519 (a) If your work uses existing assets, did you cite the creators? **[Yes]**
- 520 (b) Did you mention the license of the assets? **[Yes]**
- 521 (c) Did you include any new assets either in the supplemental material or as a URL? **[Yes]**
- 522 (d) Did you discuss whether and how consent was obtained from people whose data you’re
523 using/curating? **[Yes]**
- 524 (e) Did you discuss whether the data you are using/curating contains personally identifiable
525 information or offensive content? **[N/A]**

526 5. If you used crowdsourcing or conducted research with human subjects...

- 527 (a) Did you include the full text of instructions given to participants and screenshots, if
528 applicable? **[N/A]**
- 529 (b) Did you describe any potential participant risks, with links to Institutional Review
530 Board (IRB) approvals, if applicable? **[N/A]**
- 531 (c) Did you include the estimated hourly wage paid to participants and the total amount
532 spent on participant compensation? **[N/A]**

533 A Overview of Appendices

534 We provide supplementary details about problems and experiments for the main text in the Appendix.
535 In Appendix B, we provide mathematical descriptions and visualization for all PDEs in this paper.
536 In Appendix C, we list the detailed hyperparameters and training/testing settings. In Appendix D,
537 we provide a high-level overview of the codebase of the toolbox. In Appendix E, the results for the
538 main experiments, i.e., the performance of L2RE, L1RE, MSE, and runtime for all methods on all
539 PDEs are displayed. In Appendix F, we show the visualization results for several methods on some
540 problems.

541 B Details of PDEs and Methods

542 Here provide details of PDE tasks used for evaluating different variants of PINNs. Denote u to be the
543 function to solve and x, t to be spatial and temporal variables.

544 B.1 Definitions for PDEs in main experiments

545 1. One-dimensional Burgers Equation (Burgers1d)

546 The Burgers 1D equation is given by

$$u_t + uu_x = \nu u_{xx}. \quad (6)$$

547 The domain is defined as

$$(x, t) \in \Omega = [-1, 1] \times [0, 1]. \quad (7)$$

548 The initial and boundary conditions are

$$u(x, 0) = -\sin \pi x, \quad (8)$$

$$u(-1, t) = u(1, t) = 0. \quad (9)$$

549 The parameter is

$$\nu = \frac{0.01}{\pi}. \quad (10)$$

550 2. 2D Coupled Burgers equation (Burgers 2d)

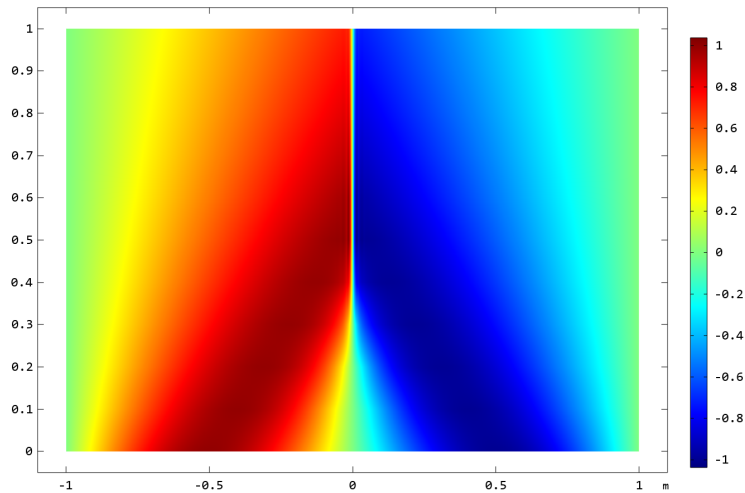


Figure 4: Reference solution of Burgers1d using FEM solver.

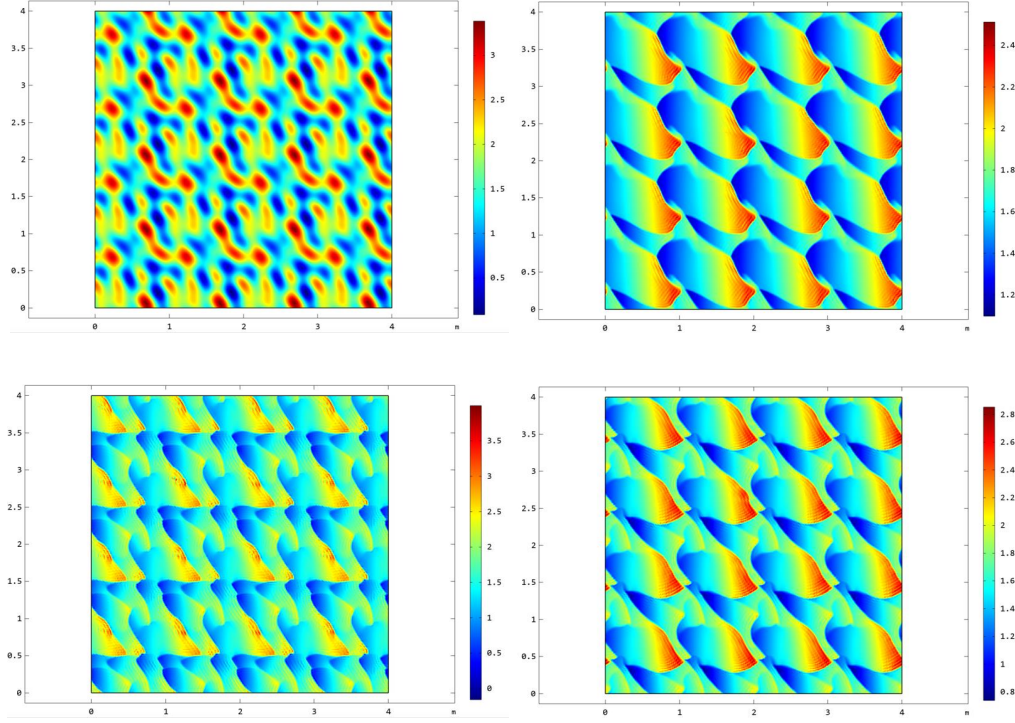


Figure 5: Reference solution of Burgers2d at timesteps $t = 0, 0.2, 0.4, 1.0$ using FEM solver.

551 The 2D Coupled Burgers equation is given by

$$\mathbf{u}_t + \mathbf{u} \cdot \nabla \mathbf{u} - \nu \Delta \mathbf{u} = 0, \quad (11)$$

$$\mathbf{u}(0, y, t) = \mathbf{u}(L, y, t), \quad \mathbf{u}(x, 0, t) = \mathbf{u}(x, L, t), \quad (12)$$

$$\{x, y\} \in [0, L], \quad t \in [0, T], \quad (13)$$

552 The domain is defined as

$$(x, y, t) \in \Omega = [0, L]^2 \times [0, 1]. \quad (14)$$

553 The initial conditions are given by

$$\mathbf{w}(x, y) = \sum_{i=-L}^L \sum_{j=-L}^L \mathbf{a}_{ij} \sin(2\pi(ix + jy)) + \mathbf{b}_{ij} \cos(2\pi(ix + jy)), \quad (15)$$

$$\mathbf{u}(x, y, 0) = 2\mathbf{w}(x, y) + \mathbf{c} \quad (16)$$

554 where $a, b, c \sim N(0, 1)$. The parameters are

$$L = 4, \quad T = 1, \quad \nu = 0.001. \quad (17)$$

555

556 3. Poisson 2D Classic (Poisson2d-C)

557 The Poisson 2D equation is given by

$$-\Delta u = 0. \quad (18)$$

558 The domain is a rectangle minus four circles $\Omega = \Omega_{rec} \setminus R_i$ where $\Omega_{rec} = [-0.5, 0.5]^2$ is the
 559 rectangle and R_i denotes four circle areas:

$$R_1 = \{(x, y) : (x - 0.3)^2 + (y - 0.3)^2 \leq 0.1^2\}, \quad (19)$$

$$R_2 = \{(x, y) : (x + 0.3)^2 + (y - 0.3)^2 \leq 0.1^2\}, \quad (20)$$

$$R_3 = \{(x, y) : (x - 0.3)^2 + (y + 0.3)^2 \leq 0.1^2\}, \quad (21)$$

$$R_4 = \{(x, y) : (x + 0.3)^2 + (y + 0.3)^2 \leq 0.1^2\}. \quad (22)$$

560 The boundary condition is

$$u = 0, x \in \partial R_i, \quad (23)$$

$$u = 1, x \in \partial \Omega_{rec}. \quad (24)$$

561 4. Poisson-Boltzmann (Helmholtz) 2D Irregular Geometry (Poisson2d-CG)

562 The Poisson-Boltzmann (Helmholtz) 2D equation is given by

$$-\Delta u + k^2 u = f(x, y). \quad (25)$$

563 The function $f(x)$ is defined as

$$f(x) = A \cdot \left(\sum_i \mu_i^2 + x_i^2 \right) \sin(\mu_1 \pi x_1) \sin(\mu_2 \pi x_2). \quad (26)$$

564 The domain is $[-1, 1]^2$ and the boundary conditions are

$$u = 0.2, \quad x \in \partial \Omega_{rec}, \quad (27)$$

$$u = 1, \quad x \in \partial \Omega_{circle}. \quad (28)$$

565 Parameter references are

$$\mu_1 = 1, \quad \mu_2 = 4, \quad k = 8, \quad A = 10. \quad (29)$$

566 The domain is $[-1, 1]^2$ with several circles removed. The circles $\Omega_{circle} = \cup_{i=1}^4 R_i$ are

$$R_1 = \{(x, y) : (x - 0.5)^2 + (y - 0.5)^2 \leq 0.2^2\} \quad (30)$$

$$R_2 = \{(x, y) : (x - 0.4)^2 + (y + 0.4)^2 \leq 0.4^2\} \quad (31)$$

$$R_3 = \{(x, y) : (x + 0.2)^2 + (y + 0.7)^2 \leq 0.1^2\} \quad (32)$$

$$R_4 = \{(x, y) : (x + 0.6)^2 + (y - 0.5)^2 \leq 0.3^2\} \quad (33)$$

567 5. Poisson 3D Complex Geometry with Two Domains (Poisson3d-CG)

568 The Poisson 3D equation with two domains is given by

$$-\mu_i \Delta u + k_i^2 u = f(x, y, z), \quad i = 1, 2. \quad (34)$$

569 The function $f(x, y, z)$ is defined as

$$f(x, y, z) = A_1 \frac{\exp(\sin m_1 \pi x + \sin m_2 \pi y + \sin m_3 \pi z)}{x^2 + y^2 + z^2 + 1} (x^2 + y^2 + z^2 - 1) \\ + A_2 \sin(m_1 \pi x) \sin(m_2 \pi y) \sin(m_3 \pi z). \quad (35)$$

570 The coefficients are defined as $\begin{cases} \mu = \mu_1, & k = k_1, & x \in \Omega_1, \\ \mu = \mu_2, & k = k_2, & x \in \Omega_2. \end{cases}$

571 The boundary condition is

$$\frac{\partial u}{\partial n} = 0, \quad x \in \partial \Omega. \quad (36)$$

572 The domains and other parameters are defined as follows:

$$\Omega_1 = [0, 1] \times [0, 1] \times [0, 0.5] / \cup_{i=1}^4 R_i, \quad (37)$$

$$\Omega_2 = [0, 1] \times [0, 1] \times [0.5, 1] / \cup_{i=1}^4 R_i. \quad (38)$$

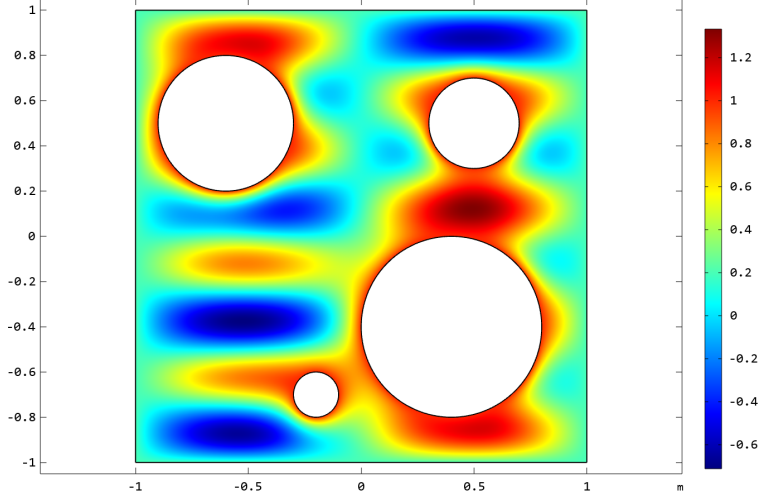


Figure 6: Reference solution of Poisson2d-CG by FEM solver.

573 The circular regions R_i are

$$R_1 = \{(x, y, z) : (x - 0.4)^2 + (y - 0.3)^2 + (z - 0.6)^2 \leq 0.2^2\} \quad (39)$$

$$R_1 = \{(x, y, z) : (x - 0.6)^2 + (y - 0.7)^2 + (z - 0.6)^2 \leq 0.2^2\} \quad (40)$$

$$R_1 = \{(x, y, z) : (x - 0.2)^2 + (y - 0.8)^2 + (z - 0.7)^2 \leq 0.1^2\} \quad (41)$$

$$R_1 = \{(x, y, z) : (x - 0.6)^2 + (y - 0.2)^2 + (z - 0.3)^2 \leq 0.1^2\} \quad (42)$$

$$(43)$$

574 Other parameters are

$$m_1 = 1, m_2 = 10, m_3 = 5, \mu_1 = 1, \mu_2 = 1, k_1 = 8, k_2 = 10, A_1 = 20, A_2 = 100. \quad (44)$$

575 6. 2D Poisson equation with many subdomains (Poisson2d-MS)

576 The PDE and boundary condition is given by

$$-\nabla(a(x)\nabla u) = f(x, y), \quad x \in \Omega \quad (45)$$

$$\frac{\partial u}{\partial n} + u = 0, \quad x \in \partial\Omega. \quad (46)$$

577 Here the domain is $(x, y) \in \Omega = [-10, 10]^2$. We divide the whole domain into many small squares,
578 and $a(x)$ is a piecewise linear function in each square. We store the $a(x)$ in a file in practical
579 implementation.

580 7. 2D Heat with Varying Coefficients (Heat2d-VC)

581 The 2D heat equation with a varying source is given by

$$\frac{\partial u}{\partial t} - \nabla(a(x)\nabla u) = f(x, t). \quad (47)$$

582 The domain is $\Omega \times T = [0, 1]^2 \times [0, 5]$. The function $a(x)$ is chosen similarly to Darcy flow but with
583 an exponential GRF. The function $f(x, t)$ is defined as

$$f(x, t) = A \sin(m_1 \pi x) \sin(m_2 \pi y) \sin(m_3 \pi t). \quad (48)$$

584 with $A = 200, m_1 = 1, m_2 = 5, m_3 = 1$. The initial and boundary conditions are

$$u(x, y, 0) = 0, \quad x \in \Omega \quad (49)$$

$$u(x, y, t) = 0, \quad x \in \partial\Omega. \quad (50)$$

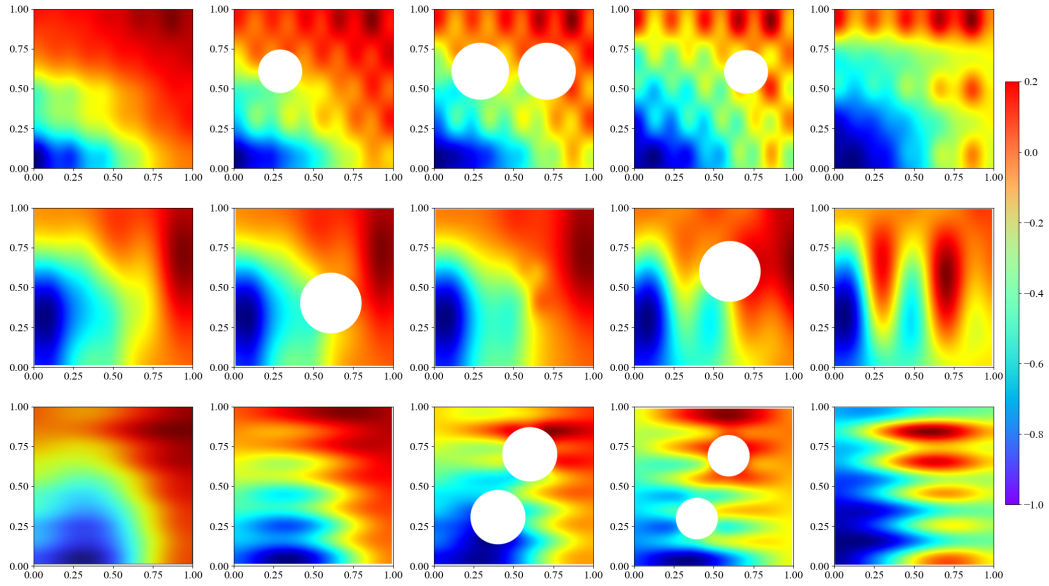


Figure 7: Reference solution of Poisson3d-CG by FEM solver. The top row displays the solution at 5 YZ planes with $x = 0, 0.25, 0.5, 0.75, 1.0$. The medium row displays it at XZ planes with $y = 0.0, 0.25, 0.5, 0.75, 1.0$. The bottom row displays it at XY planes with $z = 0.0, 0.25, 0.5, 0.75, 1.0$.

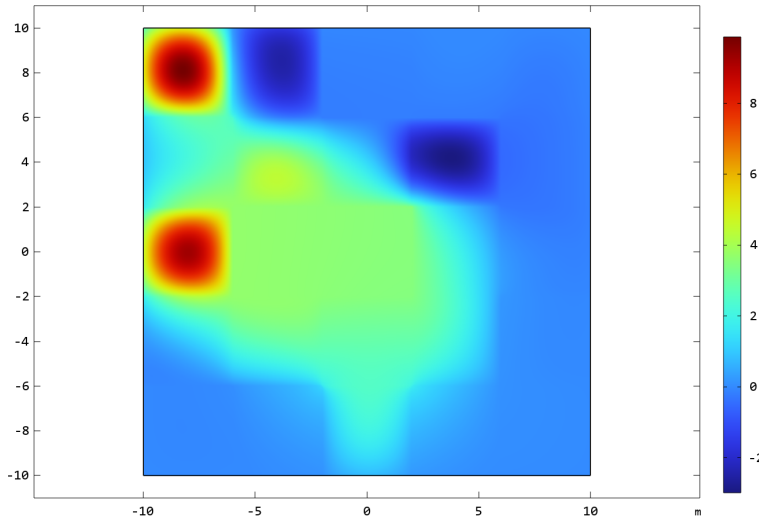


Figure 8: Reference solution of Poisson2d-MS by FEM solver.

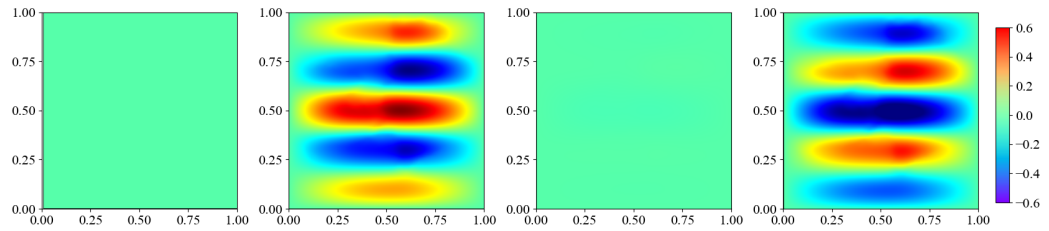


Figure 9: Reference solution of Heat2d-VC by FEM solver at timesteps $t = 0, 0.5, 2.0, 3.5$.

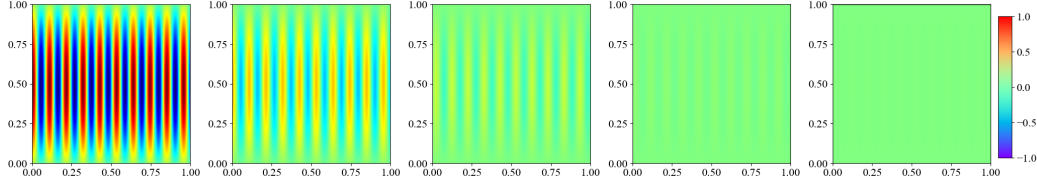


Figure 10: Reference solution of Heat2d-MS by FEM solver.

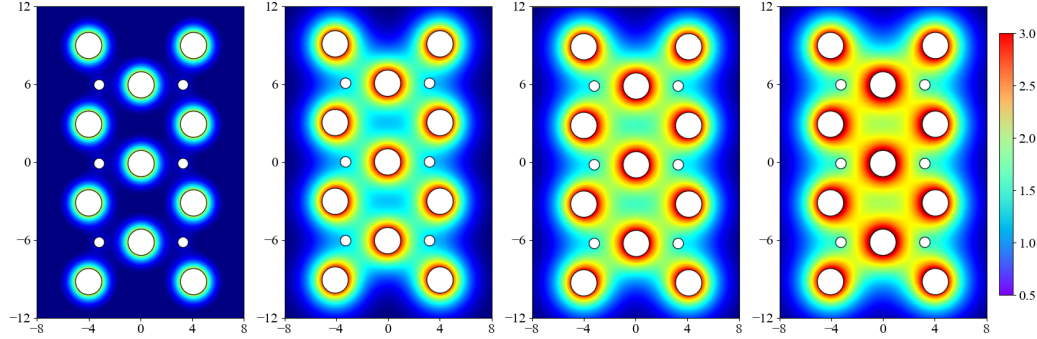


Figure 11: reference solution of Heat2d-CG by FEM solver at timesteps $t = 0.5, 2.0, 2, 5, 3.0$.

585 **8. 2D Heat Multi-Scale (Heat2d-MS)**

586 The 2D heat multi-scale equation is given by

$$\frac{\partial u}{\partial t} - \frac{1}{(500\pi)^2} u_{xx} - \frac{1}{\pi^2} u_{yy} = 0, \quad (51)$$

587 with domain $\Omega \times T = [0, 1]^2 \times [0, 5]$.

588 The initial and boundary conditions are

$$u(x, y, 0) = \sin(20\pi x) \sin(\pi y), \quad x \in \Omega, \quad (52)$$

$$u(x, y, t) = 0, \quad x \in \partial\Omega. \quad (53)$$

589 **9. 2D Heat Complex Geometry (Heat Exchanger, Heat2d-CG)**

590 The 2D heat equation for a complex geometry is given by

$$\frac{\partial u}{\partial t} - \Delta u = 0. \quad (54)$$

591 The domain is defined as $\Omega \times T = ([-8, 8] \times [-12, 12] \setminus \cup_i R_i) \times [0, 3]$.

592 The boundary condition is

$$-n \cdot (-c\nabla u) = g - qu. \quad (55)$$

593 Here we choose $c = 1$. The positions of large circles are

$$(\pm 4, \pm 3), \quad (\pm 4, \pm 9), \quad (0, 0), \quad (0, \pm 6), \quad r = 1 \quad (56)$$

594 with $g = 5$ and $q = 1$. The positions of small circles are

$$(\pm 3.2, \pm 6), \quad (\pm 3.2, 0), \quad r = 0.4 \quad (57)$$

595 with $g = 1$ and $q = 1$. For the rectangular boundary conditions, $g = 0.1$ and $q = 1$.

596 **10. 2D Heat Long Time (Heat2d-LT)**

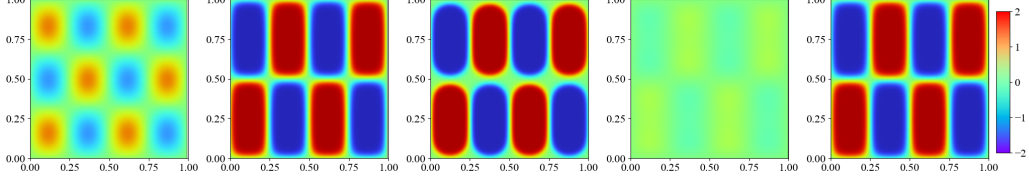


Figure 12: reference solution of Heat2d-LT by FEM solver at timesteps $t = 0, 20, 50, 80, 100$.

597 The governing PDE is

$$\frac{\partial u}{\partial t} = 0.001\Delta u + 5 \sin(ku^2) \left(1 + 2 \sin\left(\frac{\pi t}{4}\right) \right) \sin(m_1\pi x) \sin(m_2\pi y) \quad (58)$$

598 with domain $\Omega \times T = [0, 1]^2 \times [0, 100]$, $m_1 = 4$, $m_2 = 2$, and $k = 1$.

599 The initial and boundary conditions are given by

$$u(x, y, 0) = \sin(4\pi x) \sin(3\pi y), x \in \Omega \quad (59)$$

$$u(x, y, t) = 0, x \in \partial\Omega. \quad (60)$$

600 11. 2D NS lid-driven flow (NS2d-C).

601 The PDE is given by

$$\mathbf{u} \cdot \nabla \mathbf{u} + \nabla p - \frac{1}{Re} \Delta \mathbf{u} = 0, x \in \Omega \quad (61)$$

$$\nabla \cdot \mathbf{u} = 0, x \in \Omega \quad (62)$$

602 The domain is $\Omega = [0, 1]^2$, the top boundary is Γ_1 , the left, right and bottom boundary is Γ_2 .

603 The boundary conditions are

$$\mathbf{u}(\mathbf{x}) = (4x(1-x), 0), x \in \Gamma_1 \quad (63)$$

$$\mathbf{u}(\mathbf{x}) = (0, 0), x \in \Gamma_2 \quad (64)$$

$$p = 0, x = (0, 0). \quad (65)$$

604 The Reynolds number $Re = 100$.

605 12. 2D Back Step Flow (NS-CG)

606 The equations and boundary conditions are given by

$$\mathbf{u} \cdot \nabla \mathbf{u} + \nabla p - \frac{1}{Re} \Delta \mathbf{u} = 0, \quad (66)$$

$$\nabla \cdot \mathbf{u} = 0. \quad (67)$$

607 The domain is defined as $\Omega = [0, 4] \times [0, 2] \setminus ([0, 2] \times [1, 2] \cup R_i)$ (excluding the top-left quarter).

608 The inlet velocity is given by $u_{in} = 4y(1-y)$, the outlet pressure is $p = 0$, and the boundary
609 condition is no-slip: $\mathbf{u} = 0$. The Reynolds number of $Re = 100$.

610 13. 2D NS Long Time (NS2d-LT)

611 The PDE of this case is given by

$$\frac{\partial u}{\partial t} + \mathbf{u} \cdot \nabla \mathbf{u} + \nabla p - \frac{1}{Re} \Delta \mathbf{u} = f(x, y, t), \quad (68)$$

$$\nabla \cdot \mathbf{u} = 0. \quad (69)$$

612 The domain is $\Omega \times T = ([0, 2] \times [0, 1]) \times [0, 5]$, and the forcing term $f(x, y, t)$ can be given as

$$f(x, y, t) = (0, -\sin(\pi x) \sin(\pi y) \sin(\pi t)). \quad (70)$$

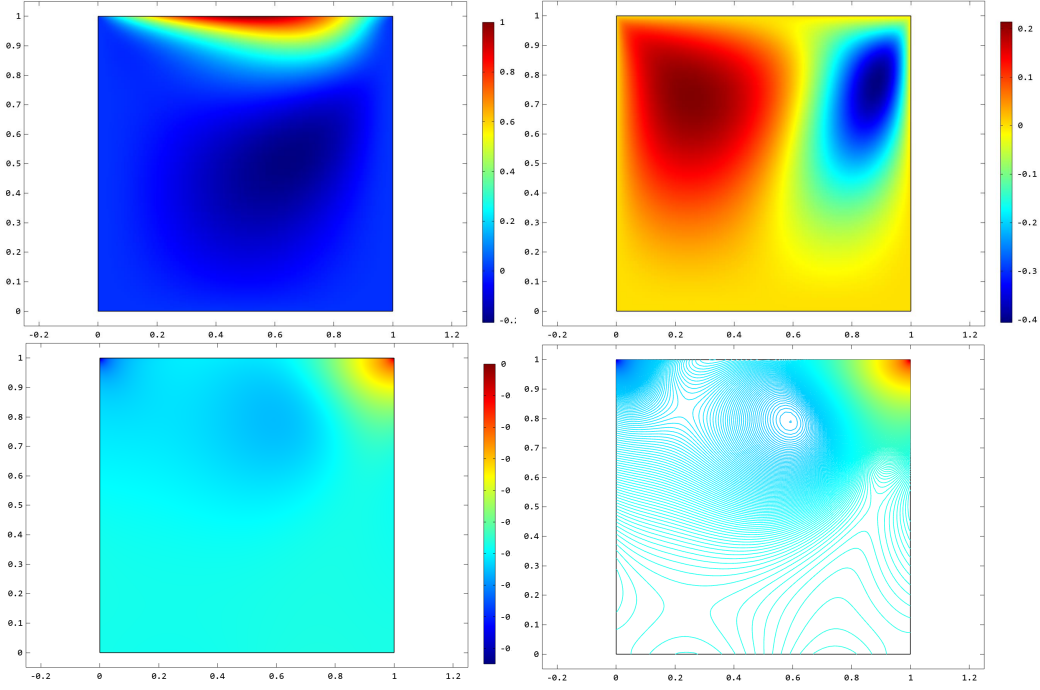


Figure 13: Reference solution of NS2d-Ld by FEM solver.

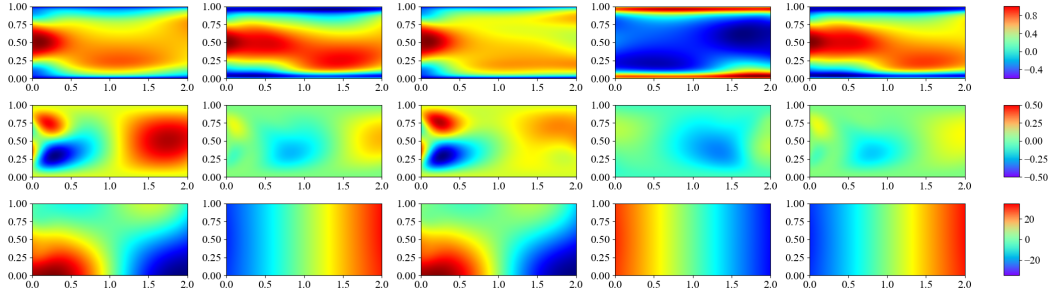


Figure 14: Reference fields u, v, p from top to bottom of NS2d-LT by FEM solver at timesteps $t = 0.5, 1.0, 2.5, 4.0, 5.0$.

613 The boundary conditions are similar to case 12, and the left inlet initial condition can be given as an
614 oscillatory form:

$$u(0, y, t) = \sin(\pi y)(A_1 \sin(\pi t) + A_2 \sin(3\pi t) + A_3 \sin(5\pi t)). \quad (71)$$

615 where $A_1 = 1, A_2 = 1, A_3 = 1$.

616 The initial condition in the domain is

$$u(x, y, 0) = 0. \quad (72)$$

617 14. Basic 1D Wave Equation (Wave1d-C)

618 The governing PDE is

$$u_{tt} - 4u_{xx} = 0 \quad (73)$$

619 The domain is $\Omega \times T = [0, 1] \times [0, 1]$. The boundary conditions are

$$u(0, t) = u(1, t) = 0 \quad (74)$$

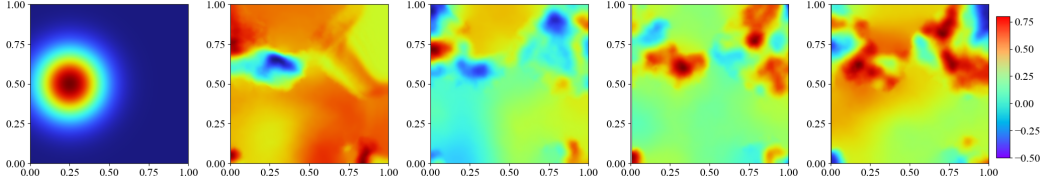


Figure 15: Reference solution of Wave2d-CG by FEM solver at timesteps $t = 0, 0.5, 2.0, 4.0, 5.0$.

620 The initial condition:

$$u(x, 0) = \sin(\pi x) + \frac{1}{2} \sin(4\pi x) \quad (75)$$

$$u_t(x, 0) = 0 \quad (76)$$

621 The analytical solution of this problem is

$$u(x, t) = \sin(\pi x) \cos(2\pi t) + \frac{1}{2} \sin(4\pi x) \cos(8\pi t). \quad (77)$$

622 15. 2D Wave Equation in Heterogeneous Medium (Wave2d-CG)

623 The governing PDE is given by

$$\left[\nabla^2 - \frac{1}{c(x)} \frac{\partial^2}{\partial t^2} \right] u(x, t) = 0 \quad (78)$$

624 The Domain is $\Omega = [-1, 1] \times [-1, 1]$ and the initial condition is

$$u(x, 0) = \exp\left(-\frac{\|x - \mu\|^2}{2\sigma^2}\right), x \in \Omega \quad (79)$$

$$\frac{\partial u}{\partial t}(x, 0) = 0, x \in \Omega \quad (80)$$

625 The boundary conditions are

$$\frac{\partial u}{\partial n} = 0, x \in \partial\Omega \quad (81)$$

626 The parameters are

$$\mu = (-0.5, 0), \sigma = 0.3, \quad (82)$$

627 and $c(x)$ are generated by a Gaussian random field.

628

629 16. 2D Multi-Scale Long Time Wave Equation (Wave2d-MS)

630 The governing PDE is

$$u_{tt} - (u_{xx} + a^2 u_{yy}) = 0 \quad (83)$$

631 The domain is defined as $\Omega = [0, 1]^2 \times [0, 100]$ and the boundary and initial conditions are

$$u(x, y, t) = c_1 \sinh(m_1 \pi x) \sinh(n_1 \pi y) \cos(p_1 \pi t), (x, y) \in \partial\Omega. \quad (84)$$

$$\frac{\partial u}{\partial t}(x, y, 0) = 0 \quad (85)$$

632 The exact solution to this problem is

$$u(x, y, t) = c_1 \sinh(m_1 \pi x) \sinh(n_1 \pi y) \cos(p_1 \pi t), \quad (86)$$

633 where $a = \sqrt{2}, m_1 = 1, n_1 = 1, p_1 = \sqrt{3}$ and $c_1 = 1$.

634 17. 2D Diffusion-Reaction Gray-Scott Model (GS)

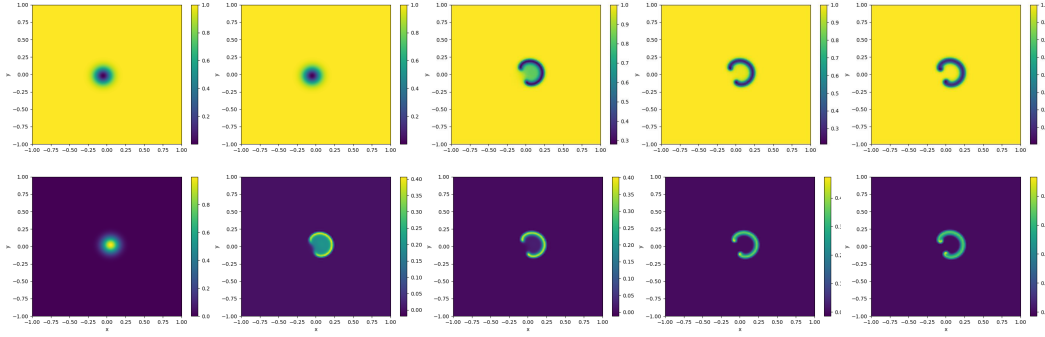


Figure 16: Reference solution of GS equation at timestep $t = 0.0, 2.5, 5.0, 7.5, 10.0$.

635 The governing PDE is

$$u_t = \varepsilon_1 \Delta u + b(1 - u) - uv^2 \quad (87)$$

$$v_t = \varepsilon_2 \Delta v - dv + uv^2 \quad (88)$$

636 The domain is $\Omega \times T = [-1, 1]^2 \times [0, 200]$ and parameters are

$$b = 0.04, d = 0.1, \varepsilon_1 = 1 \times 10^{-5}, \varepsilon_2 = 5 \times 10^{-6} \quad (89)$$

637 The initial conditions are

$$u(x, y, 0) = 1 - \exp(-80((x + 0.05)^2 + (y + 0.02)^2)) \quad (90)$$

$$v(x, y, 0) = \exp(-80((x - 0.05)^2 + (y - 0.02)^2)) \quad (91)$$

638 The visualization of the reference solution of this case is in Figure 16.

639 18. Kuramoto-Sivashinsky Equation (KS)

640 The governing PDE is

$$u_t + \alpha uu_x + \beta u_{xx} + \gamma u_{xxx} = 0 \quad (92)$$

641 The domain is $\Omega \times T = [0, 2\pi] \times [0, 1]$. (Note: Error may increase rapidly in chaotic problems.)

$$\alpha = \frac{100}{16}, \beta = \frac{100}{16^2}, \gamma = \frac{100}{16^4} \quad (93)$$

642 The initial condition is

$$u(x, 0) = \cos(x)(1 + \sin(x)) \quad (94)$$

643 The reference solution of KS equation is shown in Figure B.1.

644 19. N-Dimensional Poisson equation (PNd)

645 The governing PDE is

$$-\Delta u = \frac{\pi^2}{4} \sum_{i=1}^n \sin\left(\frac{\pi}{2} x_i\right) \quad (95)$$

646 The domain is defined by $\Omega = [0, 1]^n$. The exact solution is

$$u = \sum_{i=1}^n \sin\left(\frac{\pi}{2} x_i\right) \quad (96)$$

647 We choose $n = 5$ in our code.

648 20. N-Dimensional Heat Equation (HNd)

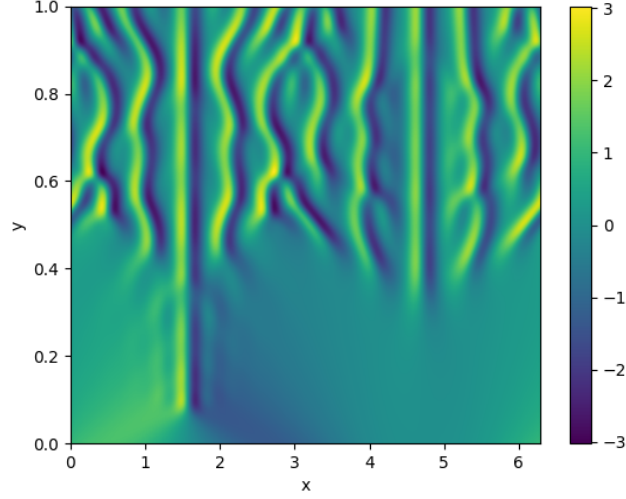


Figure 17: Reference solution of KS equation.

649 The governing PDE is

$$\frac{\partial u}{\partial t} = k\Delta u + f(x, t), x \in \Omega \times [0, 1] \quad (97)$$

$$\mathbf{n} \cdot \nabla u = g(x, t), x \in \partial\Omega \times [0, 1] \quad (98)$$

$$u(x, 0) = g(x, 0), x \in \Omega \quad (99)$$

650 The geometric domain $\Omega = \{x : |x|_2 \leq 1\}$ is a unit sphere in d -dimensional space. We choose
 651 dimension $d = 5$.

$$k = \frac{1}{d} \quad (100)$$

652 The two functions are

$$f(x, t) = -\frac{1}{d}|x|_2^2 \exp\left(\frac{1}{2}|x|_2^2 + t\right) \quad (101)$$

$$g(x, t) = \exp\left(\frac{1}{2}|x|_2^2 + t\right) \quad (102)$$

653 We can see that the exact solution of the equation is $g(x, t)$.

654 **21. Poisson inverse problem (PInv)**

655 The governing PDE is

$$-\nabla(a\nabla u) = f \quad (103)$$

656 The geometric domain is $\Omega = [0, 1]^2$, and

$$u = \sin \pi x \sin \pi y. \quad (104)$$

657 The source term f is

$$f = \frac{2\pi^2 \sin \pi x \sin \pi y}{1 + x^2 + y^2 + (x-1)^2 + (y-1)^2} + \frac{2\pi((2x-1)\cos \pi x \sin \pi y + (2y-1)\sin \pi x \cos \pi y)}{(1 + x^2 + y^2 + (x-1)^2 + (y-1)^2)^2}. \quad (105)$$

658 To ensure the uniqueness of the solution, we impose a boundary condition of $a(x, y)$, i.e.,

$$a(x, y) = \frac{1}{1 + x^2 + y^2 + (x-1)^2 + (y-1)^2}, x \in \partial\Omega \quad (106)$$

659 We sample data of $u(x, y)$ with 2500 uniformly distributed 50×50 points and add Gaussian noise
 660 $\mathcal{N}(0, 0.1)$ to it. The goal is to reconstruct the diffusion coefficients. We see that the ground truth of
 661 $a(x, y)$ is

$$a(x, y) = \frac{1}{1 + x^2 + y^2 + (x - 1)^2 + (y - 1)^2}, x \in \Omega. \quad (107)$$

662 **22. Heat (Diffusion) inverse problem (HInv)**

663 The governing PDE of this inverse problem is

$$u_t - \nabla(a\nabla u) = f \quad (108)$$

664 The geometric domain is $\Omega \times T = [-1, 1]^2 \times [0, 1]$, and

$$u = e^{-t} \sin \pi x \sin \pi y \quad (109)$$

665 Similarly, we impose a boundary condition for the diffusion coefficient field:

$$a(x, y) = 2, \partial x \in \Omega. \quad (110)$$

666 Then the source function f is

$$f = ((4\pi^2 - 1) \sin \pi x \sin \pi y + \pi^2(2 \sin^2 \pi x \sin^2 \pi y - \cos^2 \pi x \sin^2 \pi y - \sin^2 \pi x \cos^2 \pi y))e^{-t} \quad (111)$$

667 We sample data of $u(x, y, t)$ randomly with 2500 points from the temporal domain $\Omega \times T$ and add
 668 Gaussian noise $\mathcal{N}(0, 0.1)$ to it. The goal is to reconstruct the diffusion coefficients. We see that the
 669 ground truth is

$$a(x, y) = 2 + \sin \pi x \sin \pi y, x \in \Omega. \quad (112)$$

670 **B.2 Definitions and design choices for parametric PDEs**

671 We design a set of parametric PDEs and evaluate the average performance of PINN variants on cases
 672 with different parameters. We choose Burgers2d-C, Poisson2d-C, Heat2d-MS, NS2d-C, Wave2d-C,
 673 and Heat-Nd to design these parametric cases.

674 **1. 2D Coupled Burgers equation (Burgers2d-C) with different initial values.**

675 The initial values of this case are shown in Eq 16 where \mathbf{a} and \mathbf{b} are sampled from Gaussian Random
 676 Field. Here the initial values are used as parameters and we sample 5 different \mathbf{a} and \mathbf{b} from GRF
 677 and test the performance of PINN variants on all 5 cases. Each parametrized PDE is solved using
 678 COMSOL. In PDEBench, the authors similarly tested the average effect of PDEs sampled multiple
 679 times from the GRF with the same equation. Since the GRF has not changed, there is not much
 680 variation in the magnitude and frequency of the initial flow velocity, but there may be significant
 681 differences in their spatial distribution. This can also lead to differences in difficulty when solving
 682 with the PINN method. From the 4, we see that the error of the best method increased from 26% to
 683 41%, indicating a significant influence of the flow distribution on the solution.

684 **2. Poisson 2d Classic (Poisson2d-C)**

685 This PDE is defined on $\Omega = [-L, L]^2$. We parametrize this case by using different domain scales L
 686 from $\{1, 2, 4, 8, 16\}$. Since this PDE is linear, we could compute the ground truth solution by linearly
 687 scaling the original PDE where $L = 0.5$. Some papers [58] pointed out that the effect of PINN is
 688 influenced by the size of the domain. This is because scaling the domain directly to $[0, 1]^d$ may be
 689 suboptimal and can lead to an imbalanced ratio of PDE loss to boundary loss. This is because PINNs
 690 are sensitive to initialization, so different domain scales might lead to different results. Here the real
 691 solution of this linear PDE can be obtained through a linear transformation from a solution of another
 692 domain scale L . The condition number does not differ when we change L , making it suitable to
 693 study the influence of domain scale on PINN's performance. We observed from the results that some
 694 methods (PINN-NTK, MultiAdam, FBPINN) are relatively robust to domain scale.

695 **3. 2D Heat Multi-Scale (Heat2d-MS)**

696 We parameterize this case using different initial conditions in Eq 53,

$$u(x, y, 0) = \sin(a\pi x) \sin(\pi y). \quad (113)$$

697 Here we choose (a, b) from $\{(20, 1), (1, 20), (10, 2), (2, 10), (5, 4)\}$. The reference solutions for
698 different parameters are solved using COMSOL. Changes in the frequency of the initial condition
699 will lead to changes in the frequency of the solution, which allows us to study the influence of the
700 initial condition frequency on PINN. Comparing the results of several experiments, we found that the
701 loss reweighting strategy of PINN-NTK and the adaptive activation function of LAAF perform well
702 for multi-scale problems overall. However, when the frequency variation range is more significant,
703 both their performances decline, suggesting room for improvement.

704 4. 2D NS lid-driven flow (NS2d-C)

705 We parametrize NS2d-C by setting different speeds at the top boundary in Eq 65,

$$\mathbf{u}(\mathbf{x}) = (ax(1-x), 0), x \in \Gamma_1, \quad (114)$$

706 where a is chosen from $\{2, 4, 8, 16, 32\}$. The reference solutions for different parameters are solved
707 using COMSOL. Different flow rates imply different Reynolds numbers, thus altering the difficulty
708 of solving the equation. As the Reynolds number increases, the condition number of the equation
709 will also increase. Generally, the higher the Reynolds number, the more likely turbulence or some
710 small-scale complex flow states will occur. Testing different Reynolds numbers is a natural idea.
711 Specifically, we chose a velocity $u = ax(1-x)$, where a ranges between 2 and 32. Compared to the
712 main experiment with $a = 4$, the Reynolds number increased eightfold when $a = 32$.

713 5. 1D Wave Equation

714 We parametrize this case with different initial conditions in Eq 76,

$$u(x, 0) = \sin(\pi x) + \frac{1}{2} \sin(a\pi x), \quad (115)$$

715 where a is chosen from $\{2, 4, 6, 8, 10\}$. The ground truth solution is given by,

$$u(x, t) = \sin(\pi x) \cos(2\pi t) + \frac{1}{2} \sin(\pi a x) \cos(2a\pi t). \quad (116)$$

716 6. N-Dimensional Heat Equation

717 We parametrize this case by choosing a different number of dimensions n from $\{4, 5, 6, 8, 10\}$.
718 The solutions are given by Eq 102. Although neural networks are theoretically universal function
719 approximators, the ability to fit the solution of high-dimensional PDEs still needs to be studied. So,
720 we chose heat equations of different dimensions to compare the effects of various PINN methods.
721 We observed that for high-dimensional heat equations, the improved optimizer MultiAdam is very
722 helpful in solving high-dimensional problems.

723 B.3 Relationship with PDEBench and PDEArena

724 Here we compare the PDEs we used with PDEs in PDEBench [50] and PDEArena [15]. The selection
725 of PDEs for our study was carefully curated to align with the objectives of comparing PINN methods,
726 which differs from the approach taken in PDEBench or PDEArena. While PDEBench and PDEArena
727 are oriented towards time-dependent PDEs, such as the compressible Navier-Stokes and Diffusion
728 Reaction equations, and provide extensive datasets for neural operator research, our focus was
729 distinct. We chose a range of PDEs specifically for their relevance to PINN research, where datasets
730 are not typically provided, emphasizing the direct application of PINNs to the PDEs themselves.
731 We select a diverse range of PDE types and complexities from existing PINN literature. Among
732 these, we included widely applicable and representative PDEs like the incompressible Navier-Stokes
733 equation and the Poisson equation (Darcy flow), which are fundamental to a multitude of disciplines.
734 Our choice thus facilitates a more targeted and appropriate comparison of PINN methodologies,
735 underscoring the unique aspects of our research approach.

736 **B.4 Overview of methods**

737 The baselines we selected could be roughly divided into several categories, i.e., loss reweighting/re-
738 sampling, novel optimizer, novel loss functions, and novel activation/architectures. As shown in Eq
739 117, the general formulation of PINNs is to optimize a mixture of PDE residual loss, boundary loss,
740 and available data loss,

$$\mathcal{L}(\theta) = \frac{w_c}{N_c} \sum_{i=1}^{N_c} \|\mathcal{F}(u_\theta(x_c^i); x_c^i)\|^2 + \frac{w_b}{N_b} \sum_{i=1}^{N_b} \|\mathcal{B}(u_\theta(x_b^i); x_b^i)\|^2 + \frac{w_d}{N_d} \sum_{i=1}^{N_d} \|u_\theta(x_d^i) - u(x_d^i)\|^2. \tag{117}$$

741 Under this formulation, we could explain different variants of PINNs.

- 742 • Loss reweighting methods dynamically modify the weights w_c, w_b, w_d to enable a better
743 convergence rate. Resampling methods allocate new collocation points x_c, x_b or adjust their
744 sampling probability. These methods alleviate the imbalance between PINN optimization.
745 Results show that they achieve remarkable results on many cases of Poisson, Heat, and
746 Wave equations.
- 747 • Novel loss functions. It modifies the form of $\mathcal{L}(\theta)$ or adds new regularization terms for
748 higher convergence accuracy. Results show that vPINNs are excellent at solving inverse
749 problems.
- 750 • Novel optimizer. An example of novel optimizer is Multi-Adam which is more suitable for
751 dealing with multiple conflict loss terms especially when they have a different scale. Results
752 show that it works for several problems with multi-scale problems.
- 753 • Novel activations/architectures. It modifies the form of surrogate neural networks u_θ for
754 better model capacity. We see that these modifications are effective for some problems with
755 complex geometries and nonlinear NS equations.

756 **C Model Configuration and Hyperparameters**

757 **C.1 Model architecture**

758 Our research employs a specific model structure: a Multilayer Perceptron (MLP) with 5 layers, each
759 of which has a width of 100 neurons.

760 The model was trained for a total of 20,000 iterations or epochs. This number of training rounds was
761 found to be sufficient for the model to learn the underlying patterns in the data, while also avoiding
762 potential overfitting that might occur with too many epochs.

763 As for the number of collocation points, for 2-dimensional problems, we used 8192 points. These
764 collocation points provide dense coverage of the problem space while it does not consume too much
765 GPU memory. In addition to these, we utilized 2048 boundary/initial points.

766 For 3-dimensional problems, the number of collocation points and boundary/initial points were
767 increased to 32768 and 8192, respectively. This increase corresponds to the added complexity of
768 3-dimensional problems, requiring a more comprehensive representation of the problem space to
769 achieve reliable and accurate results.

770 **C.2 Optimization hyperparameters**

771 In our primary experiment, we use Adam optimizer with momentum (0.9, 0.999). We set the learning
772 rate at 1e-3. This learning rate was selected after carefully considering the trade-off between the
773 speed of convergence and the stability of learning, which we discussed previously. We found that this
774 learning rate provides a good balance, enabling robust learning without the issues associated with
775 excessively high or low rates. For vanilla PINNs, the loss weights are set to 1.

776 In summary, our model structure and parameters were carefully selected to balance the need for
777 accuracy and computational efficiency, providing a fair and effective comparison in our study. Detailed
778 ablation studies about these hyperparameters are reported in Appendix E.

779 C.3 Other method-specific hyperparameters

780 Here we present the hyperparameters of the methods we tested.

- 781 • **PINN.** There are no special hyperparameters for the baseline PINN. Please refer to the
782 section above for the network structure and optimization hyperparameters.
- 783 • **PINN-w.** We assign larger weights to boundary conditions for PINN-w. Specifically, the
784 weight for PDE loss is set at 1, while those for initial and boundary conditions are increased
785 to 100. These losses are then aggregated as the target loss.
- 786 • **PINN-LRA.** We set $\alpha = 0.1$ for updating loss weights, which is the recommended value in
787 the original paper.
- 788 • **PINN-NTK.** No special hyperparameter is needed for this method.
- 789 • **RAR.** For residual-based adaptive refinement, we add new points where the residual is
790 greatest into the training set every 2000 epochs.
- 791 • **MultiAdam.** Although there is no manual weighting for MultiAdam, the loss grouping
792 criteria can affect its performance. Due to time constraints, we only tuned the grouping
793 criteria for the Wave1d-C case, where losses were divided into Dirichlet boundary losses and
794 non-Dirichlet losses and trained for 10,000 epochs. For all other cases, we simply categorize
795 the losses into PDE and boundary losses.
- 796 • **gPINN.** For simplicity, we assign a weight of 0.01 to the gradient terms and a weight of 1 to
797 all others. However, these weights are delicate and require further fine-tuning.

798 D High-level Structure of Toolbox

799 In Figure 18, we provide a high-level overview of the usage and modules of the benchmark. We
800 provide several encapsulated classes upon DeepXDE. Specifically, we have a PDE class for building
801 PDE problems conveniently. Then we warp the model class by passing neural network architecture,
802 optimizer, and custom callbacks. After that, the model is compiled by DeepXDE. Finally, we invoke
803 the multi-GPU parallel training and evaluation framework to allocate the training tasks to different
804 GPUs. We support convenient one-button parallel training and testing on all PDE cases using all
805 methods. An example code snippet is shown here.

```
806 import deepxde as dde
807 from trainer import Trainer
808 from src.pde import PDE1, ..., PDEn
809 from src.utils.callbacks import TesterCallback
810
811 trainer = Trainer('experiment-name', device)
812 for pde_class in [PDE1, ..., PDEn]:
813     def get_model():
814         pde = pde_class()
815         net = dde.nn.FNN([pde.input_dim] + n_layers * [n_hidden] + [pde.output_dim])
816         opt = torch.optim.Adam(net.parameters(), lr=learning_rate)
817         model = pde.create_model(net)
818         model.compile(opt)
819         return model
820
821     trainer.add_task(
822         get_model, {'iterations': num_iterations, 'callbacks': [TesterCallback()]}
823     )
824 trainer.train_all_parallel()
```

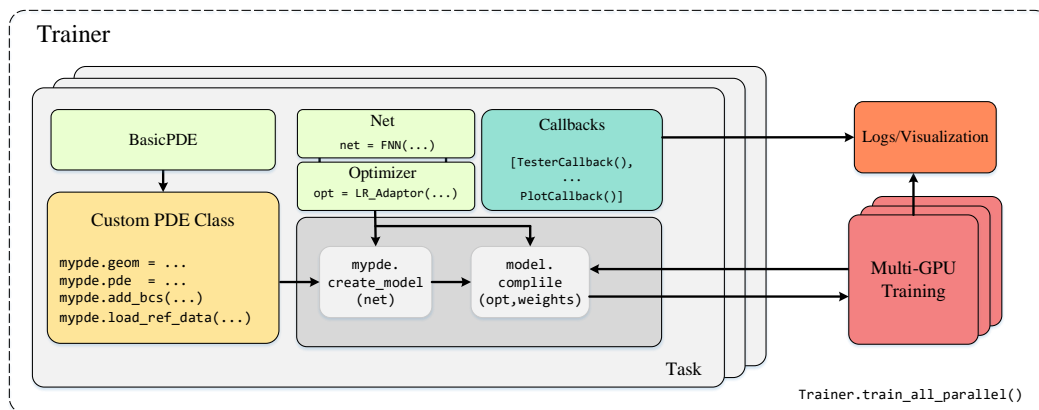


Figure 18: A high-level illustration of PINNacle code structure.

825 E Detailed Experimental Results

826 E.1 Detailed results of main experiments.

827 The detailed results of the main experiments in listed in the subsection. In Table 7, we provide the
 828 mean and std of L2RE for all baselines on all PDEs. In Table 6, we provide the mean and std of
 829 L1RE for all baselines on all PDEs. In Table 9, Table 10, and Table 11, we provide the low-frequency,
 830 medium-frequency, and high-frequency Fourier errors, respectively. In Table 8, we provide the mean
 831 and std of MSE for all baselines on all PDEs. In Table 12, we provide the average runtime (seconds)
 832 for all baselines trained with 20000 epochs on all PDEs averaged by three runs. In Table E.2, we
 833 show the results of all baselines on parametric PDEs. **We run all experiments on a Linux server with**
 834 **20 Intel(R) Xeon(R) Silver 4210 CPUs @ 2.20GHz and eight NVIDIA GeForce RTX 2080 Ti each**
 835 **with 12 GB GPU memory.**

836 Here we provide an analysis of these results. Since the results of the main experiments have been
 837 described in the main text, we won't go over them again. For different metrics of the same PDE, the
 838 best-performing methods often differ. This is because different errors reflect different mismatches
 839 between the predicted solution and the true solution.

- 840 • From the results, we can see that for most cases, methods that perform well in L2RE error
 841 also perform well in L1RE. This shows that L1RE and L2RE are generally similar. Although
 842 the absolute values differ, they can mostly be used interchangeably, or one can be chosen for
 843 calculation.
- 844 • Max error measures the worst-case error, significantly different from the average loss
 845 measured by L1RE/L2RE. From the results, we can see that hp-VPINN performs very
 846 well on this metric, followed by the adaptive activation function LAAF. PINN-LRA and
 847 PINN-NTK are optimal for some equations, but their effects are not as stable.
- 848 • Fourier error allows for the convergence of different frequency components, so it's an
 849 essential reference indicator. Since functions defined in irregular geometric areas are not
 850 suitable for calculating Fourier error, we ignored these equations. Looking at ****Table 9,**
 851 **Table 10, and Table 11**** comprehensively, for mid-low frequency functions, FBPINN is the
 852 best performing in most instances. Loss reweighting methods like PINN-LRA and ordinary
 853 PINN are better for low and high-frequency components, respectively. We speculate that
 854 reweighting the loss to some extent changes the convergence order of different function
 855 components.
- 856 • Regarding the runtime metric, hp-VPINN is the fastest in most problems. This might be due
 857 to the optimization inherent in hp-VPINN's implementation and its fewer required differ-
 858 entiations than vanilla PINN. All other methods introduced varying degrees of additional

859 computational overhead compared to vanilla PINN, with some methods like gPINN even
860 requiring about twice the computational time. We list all training and inference Flops in
861 Table 13 and Table 16. The flops metric also shows that vanilla PINNs and hp-VPINNs are
862 the most efficient PINN variants.

L2RE	Name	Vanilla		Loss Reweighting/Sampling			Optimizer	Loss functions		Architecture		
		PINN	PINN-w	LRA	NTK	RAR	MultiAdam	gPINN	vPINN	LAAF	GAAF	FBPINN
Burgers	1d-C	1.45E-2(1.59E-3)	2.63E-2(4.68E-3)	2.61E-2(1.18E-2)	1.84E-2(3.66E-3)	3.32E-2(2.14E-2)	4.85E-2(1.61E-2)	2.16E-1(3.34E-2)	3.47E-1(3.49E-2)	1.43E-2(1.44E-3)	5.20E-2(2.08E-2)	2.32E-1(9.14E-2)
	2d-C	3.24E-1(7.54E-4)	2.70E-1(3.93E-3)	2.60E-1(5.78E-3)	2.75E-1(4.78E-3)	3.45E-1(4.56E-5)	3.33E-1(8.65E-3)	3.27E-1(1.25E-4)	6.38E-1(1.47E-2)	2.77E-1(1.39E-2)	2.95E-1(1.17E-2)	–
Poisson	2d-C	6.94E-1(8.78E-3)	3.49E-2(6.91E-3)	1.17E-1(1.26E-1)	1.23E-2(7.37E-3)	6.99E-1(7.46E-3)	2.63E-2(6.57E-3)	6.87E-1(1.87E-2)	4.91E-1(1.55E-2)	7.68E-1(4.70E-2)	6.04E-1(7.52E-2)	4.49E-2(7.91E-3)
	2d-CG	6.36E-1(2.57E-3)	6.08E-2(4.88E-3)	4.34E-2(7.95E-3)	1.43E-2(4.31E-3)	6.48E-1(7.87E-3)	2.76E-1(1.03E-1)	7.92E-1(4.56E-3)	2.86E-1(2.00E-3)	4.80E-1(1.43E-2)	8.71E-1(2.67E-1)	2.90E-2(3.92E-3)
	3d-CG	5.60E-1(2.84E-2)	3.74E-1(3.23E-2)	1.02E-1(3.16E-2)	9.47E-1(4.94E-4)	5.76E-1(5.40E-2)	3.63E-1(7.81E-2)	4.85E-1(5.70E-2)	7.38E-1(6.47E-4)	5.79E-1(2.65E-2)	5.02E-1(7.47E-2)	7.39E-1(7.24E-2)
	2d-MS	6.30E-1(1.07E-2)	7.60E-1(6.96E-3)	7.94E-1(6.51E-2)	7.48E-1(9.94E-3)	6.44E-1(2.13E-2)	5.90E-1(4.06E-2)	6.16E-1(1.74E-2)	9.72E-1(2.23E-2)	5.93E-1(1.18E-1)	9.31E-1(7.12E-2)	1.04E+0(6.13E-5)
Heat	2d-VC	1.01E+0(6.34E-2)	2.35E-1(1.70E-2)	2.12E-1(8.61E-4)	2.14E-1(5.82E-3)	9.66E-1(1.86E-2)	4.75E-1(8.44E-2)	2.12E+0(5.51E-1)	9.40E-1(1.73E-1)	6.42E-1(6.32E-2)	8.49E-1(1.06E-1)	9.52E-1(2.29E-3)
	2d-MS	6.21E-2(1.38E-2)	2.42E-1(2.67E-2)	8.79E-2(2.56E-2)	4.40E-2(4.81E-3)	7.49E-2(1.05E-2)	2.18E-1(9.26E-2)	1.13E-1(3.08E-3)	9.30E-1(2.06E-2)	7.40E-2(1.92E-2)	9.85E-1(1.04E-1)	8.20E-2(4.87E-3)
	2d-CG	3.64E-2(8.82E-3)	1.45E-1(4.77E-3)	1.25E-1(4.30E-3)	1.16E-1(1.21E-2)	2.72E-2(3.22E-3)	7.12E-2(1.30E-2)	9.38E-2(1.45E-2)	1.67E+0(3.62E-3)	2.39E-2(1.39E-3)	4.61E-1(2.63E-1)	9.16E-2(3.29E-2)
	2d-LT	9.99E-1(1.05E-5)	9.99E-1(8.01E-5)	9.99E-1(7.37E-5)	1.00E+0(2.82E-4)	9.99E-1(1.56E-4)	1.00E+0(3.85E-5)	1.00E+0(9.82E-5)	1.00E+0(0.00E+0)	9.99E-1(4.49E-4)	9.99E-1(2.20E-4)	1.01E+0(1.23E-4)
NS	2d-C	4.70E-2(1.12E-3)	1.45E-1(1.21E-2)	NaN(NaN)	1.98E-1(2.60E-2)	4.69E-1(1.16E-2)	7.27E-1(1.95E-1)	7.70E-2(2.99E-3)	2.92E-1(8.24E-2)	3.60E-2(3.87E-3)	3.79E-2(4.32E-3)	8.45E-2(2.26E-2)
	2d-CG	1.19E-1(5.46E-3)	3.26E-1(7.69E-3)	3.32E-1(7.60E-3)	2.93E-1(2.02E-2)	3.34E-1(6.52E-4)	4.31E-1(6.95E-2)	1.54E-1(5.89E-3)	9.94E-1(3.80E-3)	8.24E-2(8.21E-3)	1.74E-1(7.00E-2)	8.27E+0(3.68E-5)
	2d-LT	9.96E-1(1.19E-3)	1.00E+0(3.34E-4)	1.00E+0(4.05E-4)	9.99E-1(6.04E-4)	1.00E+0(3.35E-4)	1.00E+0(2.19E-4)	9.95E-1(7.19E-4)	1.73E+0(1.00E-5)	9.98E-1(3.42E-3)	9.99E-1(1.10E-3)	1.00E+0(2.07E-3)
Wave	1d-C	5.88E-1(9.63E-2)	2.85E-1(8.97E-3)	3.61E-1(1.95E-2)	9.79E-2(7.72E-3)	5.39E-1(1.77E-2)	1.21E-1(1.76E-2)	5.56E-1(1.67E-2)	8.39E-1(5.94E-2)	4.54E-1(1.08E-2)	6.77E-1(1.05E-1)	5.91E-1(4.74E-2)
	2d-CG	1.84E+0(3.40E-1)	1.66E+0(7.39E-2)	1.48E+0(1.03E-1)	2.16E+0(1.01E-1)	1.15E+0(1.06E-1)	1.09E+0(1.24E-1)	8.14E-1(1.18E-2)	7.99E-1(4.31E-2)	8.19E-1(2.67E-2)	7.94E-1(9.33E-3)	1.06E+0(7.54E-2)
	2d-MS	1.34E+0(2.34E-1)	1.02E+0(1.16E-2)	1.02E+0(1.36E-2)	1.04E+0(3.11E-2)	1.35E+0(2.43E-1)	1.01E+0(5.64E-3)	1.02E+0(4.00E-3)	9.82E-1(1.23E-3)	1.06E+0(1.71E-2)	1.06E+0(5.35E-2)	1.03E+0(6.68E-3)
Chaotic	GS	3.19E-1(3.18E-1)	1.58E-1(9.10E-2)	9.37E-2(4.42E-5)	2.16E-1(7.73E-2)	9.46E-2(9.46E-4)	9.37E-2(1.21E-5)	2.48E-1(1.10E-1)	1.16E+0(1.43E-1)	9.47E-2(7.07E-5)	9.46E-2(1.15E-4)	7.99E-2(1.69E-2)
	KS	1.01E+0(1.28E-3)	9.86E-1(2.24E-2)	9.57E-1(2.85E-3)	9.64E-1(4.94E-3)	1.01E+0(8.63E-4)	9.61E-1(4.77E-3)	9.94E-1(3.83E-3)	9.72E-1(5.80E-4)	1.01E+0(2.12E-3)	1.00E+0(1.24E-2)	1.02E+0(2.31E-2)
High dim	PNd	3.04E-3(5.62E-4)	2.58E-3(1.31E-3)	4.58E-4(1.89E-5)	4.64E-3(4.36E-3)	3.59E-3(1.25E-3)	3.98E-3(1.11E-3)	5.05E-3(6.07E-4)	–	4.14E-3(5.59E-4)	7.75E-3(1.41E-3)	–
	HNd	3.61E-1(4.40E-3)	4.59E-1(4.34E-3)	3.94E-1(1.28E-2)	3.97E-1(1.26E-2)	3.57E-1(3.69E-3)	3.02E-1(4.07E-2)	3.17E-1(6.66E-3)	–	5.22E-1(3.12E-3)	5.21E-1(7.79E-4)	–
Inverse	PInv	9.42E-2(1.58E-3)	1.66E-1(5.45E-3)	1.54E-1(3.32E-3)	1.93E-1(1.39E-2)	9.35E-2(1.12E-2)	1.30E-1(1.55E-2)	8.03E-2(2.79E-3)	2.45E-2(1.03E-2)	1.30E-1(1.07E-2)	2.54E-1(1.53E-1)	8.44E-1(1.37E-1)
	HInv	1.57E+0(7.21E-2)	5.26E-2(3.31E-3)	5.09E-2(4.34E-3)	7.52E-2(5.42E-3)	1.52E+0(6.46E-2)	8.04E-2(1.20E-2)	4.84E+0(2.07E+0)	4.56E-1(1.30E-2)	5.59E-1(5.24E-1)	2.12E-1(4.89E-2)	9.27E-1(1.20E-1)

Table 5: Mean (Std) of L2RE for main experiments.

L1RE	Name	Vanilla		Loss Reweighting/Sampling			Optimizer	Loss functions		Architecture		
		PINN	PINN-w	LRA	NTK	RAR	MultiAdam	gPINN	vPINN	LAAF	GAAF	FBPINN
Burgers	1d-C	9.55E-3(6.42E-4)	1.88E-2(4.05E-3)	1.35E-2(2.57E-3)	1.30E-2(1.73E-3)	1.35E-2(4.66E-3)	2.64E-2(5.69E-3)	1.42E-1(1.98E-2)	4.02E-2(6.41E-3)	1.40E-2(3.68E-3)	1.95E-2(8.30E-3)	3.75E-2(9.70E-3)
	2d-C	2.96E-1(7.40E-4)	2.43E-1(2.98E-3)	2.31E-1(7.16E-3)	2.48E-1(5.33E-3)	3.27E-1(3.73E-5)	3.12E-1(1.15E-2)	3.01E-1(3.55E-4)	6.56E-1(3.01E-2)	2.57E-1(2.06E-2)	2.67E-1(1.22E-2)	–
Poisson	2d-C	7.40E-1(5.49E-3)	3.08E-2(5.13E-3)	7.82E-2(7.47E-2)	1.30E-2(8.23E-3)	7.48E-1(1.01E-2)	2.47E-2(6.38E-3)	7.35E-1(2.08E-2)	4.60E-1(1.39E-2)	7.67E-1(1.36E-2)	6.57E-1(3.99E-2)	5.01E-2(4.71E-3)
	2d-CG	5.45E-1(4.71E-3)	4.54E-2(6.42E-3)	2.63E-2(5.50E-3)	1.33E-2(4.96E-3)	5.60E-1(8.19E-3)	2.46E-1(1.07E-1)	7.31E-1(2.77E-3)	2.45E-1(5.14E-3)	4.04E-1(1.03E-2)	7.09E-1(2.12E-1)	3.21E-2(6.23E-3)
	3d-CG	4.51E-1(3.35E-2)	3.33E-1(2.64E-2)	7.76E-2(1.63E-2)	9.93E-1(2.91E-4)	4.61E-1(4.46E-2)	3.55E-1(7.75E-2)	4.57E-1(5.07E-2)	7.96E-1(3.57E-4)	4.60E-1(1.13E-2)	3.82E-1(4.89E-2)	6.91E-1(7.52E-2)
	2d-MS	7.60E-1(1.06E-2)	7.49E-1(1.12E-2)	7.93E-1(7.62E-2)	7.26E-1(1.46E-2)	7.84E-1(2.42E-2)	6.94E-1(5.61E-2)	7.41E-1(2.01E-2)	9.61E-1(5.67E-2)	6.31E-1(5.42E-2)	9.04E-1(1.01E-1)	9.94E-1(9.67E-5)
Heat	2d-VC	1.12E+0(5.79E-2)	2.41E-1(1.73E-2)	2.07E-1(1.04E-3)	2.03E-1(1.12E-2)	1.06E+0(5.13E-2)	5.45E-1(1.07E-1)	2.41E+0(5.27E-1)	8.79E-1(2.57E-1)	7.49E-1(8.54E-2)	9.91E-1(1.37E-1)	9.44E-1(1.75E-3)
	2d-MS	9.30E-2(2.27E-2)	2.90E-1(2.43E-2)	1.13E-1(3.57E-2)	6.69E-2(8.24E-3)	1.19E-1(2.16E-2)	3.00E-1(1.14E-1)	1.80E-1(1.12E-2)	9.25E-1(3.90E-2)	1.14E-1(4.98E-2)	1.08E+0(2.02E-1)	5.33E-2(3.92E-3)
	2d-CG	3.05E-2(8.47E-3)	1.37E-1(7.70E-3)	1.12E-1(2.57E-3)	1.07E-1(1.44E-2)	2.21E-2(3.42E-3)	5.88E-2(1.02E-2)	8.20E-2(1.32E-2)	3.09E+0(1.86E-2)	1.94E-2(1.98E-3)	3.77E-1(2.17E-1)	6.77E-1(3.93E-2)
	2d-LT	9.98E-1(6.00E-5)	9.98E-1(1.42E-4)	9.98E-1(1.47E-4)	9.99E-1(1.01E-3)	9.98E-1(2.28E-4)	9.99E-1(5.69E-5)	9.98E-1(8.62E-4)	9.98E-1(0.00E+0)	9.98E-1(1.27E-4)	9.98E-1(8.58E-5)	1.01E+0(7.75E-4)
NS	2d-C	5.08E-2(3.06E-3)	1.84E-1(1.52E-2)	NaN	2.44E-1(3.05E-2)	5.54E-1(1.24E-2)	9.86E-1(3.16E-1)	9.43E-2(3.24E-3)	1.98E-1(7.81E-2)	4.42E-2(7.38E-3)	3.78E-2(8.71E-3)	1.18E-1(3.10E-2)
	2d-CG	1.77E-1(1.00E-2)	4.22E-1(8.72E-3)	4.12E-1(6.93E-3)	3.69E-1(2.46E-2)	4.65E-1(4.44E-3)	6.23E-1(8.86E-2)	2.36E-1(1.15E-2)	9.95E-1(3.50E-4)	1.25E-1(1.42E-2)	2.40E-1(8.01E-2)	5.92E+0(5.65E-4)
	2d-LT	9.88E-1(1.86E-3)	9.98E-1(4.68E-4)	9.97E-1(3.64E-4)	9.95E-1(6.66E-4)	1.00E+0(2.46E-4)	9.99E-1(9.27E-4)	9.90E-1(3.60E-4)	1.00E+0(1.40E-4)	9.90E-1(3.78E-3)	9.96E-1(2.68E-3)	1.00E+0(1.38E-3)
Wave	1d-C	5.87E-1(9.20E-2)	2.78E-1(8.86E-3)	3.49E-1(2.02E-2)	9.42E-2(9.13E-3)	5.40E-1(1.74E-2)	1.15E-1(1.91E-2)	5.60E-1(1.69E-2)	1.41E+0(1.30E-1)	4.38E-1(1.40E-2)	6.82E-1(1.08E-1)	6.55E-1(4.86E-2)
	2d-CG	1.96E+0(3.83E-1)	1.78E+0(8.89E-2)	1.58E+0(1.15E-1)	2.34E+0(1.14E-1)	1.16E+0(1.16E-1)	1.09E+0(1.54E-1)	7.22E-1(1.63E-2)	1.08E+0(1.25E-1)	7.45E-1(2.15E-2)	7.08E-1(9.13E-3)	1.15E+0(1.03E-1)
	2d-MS	2.04E+0(7.38E-1)	1.10E+0(4.25E-2)	1.08E+0(6.01E-2)	1.13E+0(4.91E-2)	2.08E+0(7.45E-1)	1.07E+0(1.40E-2)	1.11E+0(1.91E-2)	1.05E+0(1.00E-2)	1.17E+0(4.66E-2)	1.12E+0(8.62E-2)	1.29E+0(2.81E-2)
Chaotic	GS	3.45E-1(4.57E-1)	1.29E-1(1.54E-1)	2.01E-2(5.99E-5)	1.11E-1(4.79E-2)	2.98E-2(6.44E-3)	2.00E-2(6.12E-5)	2.72E-1(1.79E-1)	1.04E+0(3.04E-1)	2.07E-2(9.19E-4)	1.16E-1(1.31E-1)	5.06E-2(1.87E-2)
	KS	9.44E-1(8.57E-4)	8.95E-1(2.99E-2)	8.60E-1(3.48E-3)	8.64E-1(3.31E-3)	9.42E-1(8.75E-4)	8.73E-1(8.40E-3)	9.36E-1(6.12E-3)	8.88E-1(9.92E-3)	9.39E-1(3.25E-3)	9.44E-1(9.86E-3)	9.85E-1(3.35E-2)
High dim	PNd	2.40E-3(3.44E-4)	2.34E-3(1.27E-3)	3.17E-4(9.16E-6)	4.58E-3(4.56E-3)	2.98E-3(1.24E-3)	3.40E-3(8.71E-4)	4.43E-3(8.45E-4)	–	4.33E-3(1.88E-3)	5.72E-3(1.57E-3)	–
	HNd	2.25E-1(3.87E-3)	3.27E-1(5.13E-3)	2.63E-1(1.30E-2)	2.64E-1(1.59E-2)	2.24E-1(2.56E-3)	1.58E-1(2.71E-2)	1.83E-1(5.99E-3)	–	3.42E-1(3.32E-3)	3.40E-1(5.24E-3)	–
Inverse	PInv	8.30E-2(6.88E-4)	1.14E-1(3.56E-3)	1.14E-1(6.95E-3)	1.33E-1(1.01E-2)	8.35E-2(9.53E-3)	1.13E-1(1.64E-2)	7.33E-2(2.49E-3)	1.96E-2(7.75E-3)	8.12E-1(1.01E+0)	2.18E-1(1.20E-1)	8.39E-1(1.39E-1)
	HInv	1.06E+0(5.39E-2)	4.16E-2(3.18E-3)	3.94E-2(1.52E-3)	5.96E-2(2.54E-3)	1.01E+0(5.68E-2)	6.29E-2(8.58E-3)	3.51E+0(1.59E+0)	4.59E-1(1.22E-3)	3.93E-1(3.32E-1)	1.89E-1(6.30E-2)	8.46E-1(7.18E-2)

Table 6: Mean (Std) of L1RE for main experiments.

mERR	Name	Vanilla	Loss Reweighting/Sampling			Optimizer	Loss functions		Architecture		
		PINN	LRA	NTK	RAR	MultiAdam	gPINN	vPINN	LAAF	GAAF	FBPINN
Burgers	1d-C	9.03E-02(6.76E-03)	1.53E-01(5.64E-02)	1.33E-01(7.85E-02)	3.38E-01(2.82E-01)	4.02E-01(2.04E-01)	9.47E-01(1.88E-02)	1.84E+00(1.53E-02)	2.58E-01(2.96E-01)	1.88E-01(6.02E-02)	1.34E+00(4.98E-1)
	2d-C	4.32E+00(8.01E-02)	3.84E+00(1.96E-01)	4.07E+00(6.99E-02)	4.47E+00(1.32E-01)	3.99E+00(1.33E-01)	3.83E+00(6.03E-03)	9.12E+00(3.83E+00)	4.11E+00(1.99E-01)	4.14E+00(1.11E-01)	-
Poisson	2d-C	9.41E-01(9.40E-02)	5.93E-01(3.87E-01)	2.94E-02(1.37E-02)	9.27E-01(9.67E-02)	3.99E-01(3.67E-01)	7.99E-01(2.80E-02)	2.09E-01(1.30E-02)	8.26E-01(2.78E-02)	5.02E-01(2.37E-03)	1.71E-1(1.52E-2)
	2d-CG	1.63E+00(1.76E-02)	3.49E-01(2.49E-01)	6.81E-02(3.06E-02)	1.65E+00(1.32E-02)	5.84E-01(7.86E-02)	1.67E+00(5.90E-03)	1.62E+00(3.37E-03)	1.61E+00(2.51E-02)	1.49E+00(1.45E-01)	1.98E-1(3.14E-2)
	3d-CG	1.04E+00(5.37E-02)	3.91E-01(1.40E-01)	1.12E+00(7.37E-04)	1.09E+00(1.11E-01)	6.88E-01(1.51E-01)	7.87E-01(1.34E-01)	1.59E-1(7.13E-5)	1.14E+00(3.77E-02)	1.21E+00(2.49E-01)	1.07E+00(2.63E-02)
	2d-MS	4.87E+00(2.10E-01)	9.58E+00(2.05E-01)	9.66E+00(1.86E-02)	4.96E+00(2.90E-01)	5.88E+00(6.69E-01)	5.01E+00(2.61E-01)	9.87E+00(1.20E-03)	4.40E+00(4.58E-01)	8.77E+00(2.15E+00)	9.87E+00(5.44E-4)
Heat	2d-VC	9.93E-01(7.20E-02)	2.63E-01(8.90E-03)	2.67E-01(1.74E-02)	1.03E+00(7.73E-02)	4.73E-01(1.07E-01)	4.46E+00(1.05E+00)	8.83E-01(3.35E-01)	7.79E-01(8.19E-02)	7.85E-01(2.12E-01)	7.78E-1(1.11E-3)
	2d-MS	9.10E-02(3.20E-02)	1.60E-01(5.65E-02)	6.65E-02(2.50E-02)	4.36E-02(1.28E-02)	1.58E-01(8.85E-02)	7.10E-01(3.05E-01)	3.69E-01(1.00E-03)	5.53E-02(1.20E-02)	8.35E-02(4.70E-02)	1.81E-1(4.94E-3)
	2d-CG	9.40E-01(7.48E-02)	6.40E-01(3.70E-02)	1.14E+00(1.21E-01)	9.00E-01(1.47E-01)	1.39E+00(2.32E-01)	2.20E+00(2.95E-01)	4.38E+00(3.48E-01)	9.59E-01(5.39E-02)	3.18E+00(4.99E-01)	2.83E+00(3.63E-1)
	2d-LT	2.18E+00(6.95E-01)	1.82E+00(1.60E-02)	1.83E+00(1.40E-02)	1.85E+00(1.16E-02)	1.82E+00(2.40E-02)	5.46E+00(6.13E+00)	3.09E+00(3.46E-01)	1.84E+00(1.51E-02)	1.81E+00(7.94E-03)	3.32E+00(6.15E-2)
NS	2d-C	2.26E-01(6.33E-03)	nan(nan)	2.65E-01(3.05E-02)	2.22E-01(1.42E-02)	5.67E-01(6.28E-02)	4.73E-01(3.17E-02)	1.80E-01(1.64E-02)	1.84E-01(5.41E-03)	1.99E-01(9.09E-03)	2.00E-1(4.73E-2)
	2d-CG	2.06E-01(6.69E-03)	4.97E-01(9.10E-02)	3.33E-01(3.92E-02)	2.11E-01(4.38E-03)	6.23E-01(1.87E-01)	2.94E-01(9.84E-03)	4.31E+00(1.47E-02)	1.68E-01(2.34E-03)	1.80E-01(7.47E-03)	8.00E+00(0.00E+00)
	2d-LT	1.17E+02(5.00E-01)	1.21E+02(2.00E-01)	1.21E+02(6.51E-01)	1.18E+02(7.69E-01)	1.21E+02(2.40E-01)	1.21E+02(5.69E-01)	1.23E+02(5.54E-01)	1.18E+02(6.76E-01)	1.19E+02(5.28E-01)	1.24E+02(7.76E-1)
Wave	1d-C	9.34E-01(1.16E-01)	5.17E-01(6.11E-02)	2.75E-01(2.22E-02)	8.16E-01(6.80E-02)	1.26E+00(1.89E-01)	1.28E+00(6.21E-02)	6.17E-01(5.41E-02)	7.40E-01(7.71E-02)	1.18E+00(3.23E-01)	8.51E-1(1.11E-1)
	2d-CG	2.00E+00(9.89E-02)	1.95E+00(1.26E-01)	2.00E+00(1.80E-02)	1.93E+00(8.80E-02)	1.71E+00(5.74E-02)	1.73E+00(2.81E-03)	1.66E+00(2.19E-02)	1.93E+00(1.48E-01)	1.88E+00(1.13E-01)	1.65E+00(2.44E-2)
	2d-MS	1.44E+03(2.92E+02)	1.95E+03(3.91E+02)	1.74E+03(2.15E+02)	1.30E+03(2.72E+02)	1.05E+03(4.29E+01)	1.09E+03(4.19E+01)	4.43E+02(4.24E+00)	1.80E+03(8.80E+01)	1.45E+03(4.66E+02)	5.59E+03(1.55E+02)
Chaotic	GS	3.66E+00(1.00E-01)	3.48E+00(8.97E-02)	3.61E+00(6.38E-02)	3.60E+00(6.85E-02)	3.41E+00(1.27E-01)	3.41E+00(3.54E-02)	8.93E-01(6.51E-02)	3.76E+00(5.27E-02)	3.41E+00(1.28E-01)	8.36E-1(8.16E-2)
	KS	9.84E-01(1.64E-03)	9.83E-01(3.76E-04)	8.76E-01(1.72E-01)	9.83E-01(7.11E-04)	9.82E-01(1.42E-04)	9.84E-01(4.09E-03)	3.33E+00(7.80E-02)	9.83E-01(6.72E-04)	9.83E-01(3.76E-04)	3.30E+00(4.74E-2)
High dim	PNd	2.96E-02(1.57E-02)	4.05E-03(9.49E-04)	4.99E-03(4.48E-03)	2.72E-02(1.17E-02)	3.96E-02(2.29E-02)	3.16E-02(1.21E-02)	-	5.90E-02(4.88E-02)	1.76E+00(8.43E-01)	-
	HNd	5.18E-02(2.21E-02)	1.29E-01(1.94E-01)	6.32E-02(3.49E-02)	4.64E-02(1.59E-02)	7.92E-03(3.01E-03)	5.02E-02(5.95E-03)	-	2.04E-02(1.22E-02)	1.27E+00(1.45E+00)	-

Table 7: Mean (Std) of max error for main experiments.

MSE	Name	Vanilla		Loss Reweighting/Sampling			Optimizer	Loss functions		Architecture		
		PINN	PINN-w	LRA	NTK	RAR	MultiAdam	gPINN	vPINN	LAAF	GAAF	FBPINN
Burgers	1d-C	7.90E-5(1.78E-5)	2.64E-4(8.69E-5)	3.03E-4(2.62E-4)	1.30E-4(5.19E-5)	5.78E-4(6.31E-4)	9.68E-4(5.51E-4)	1.77E-2(5.58E-3)	5.13E-3(1.90E-3)	1.80E-4(1.35E-4)	3.00E-4(1.56E-4)	1.53E-2(1.03E-2)
	2d-C	1.69E-1(7.86E-4)	1.17E-1(3.41E-3)	1.09E-1(4.84E-3)	1.22E-1(4.22E-3)	1.92E-1(5.07E-5)	1.79E-1(9.36E-3)	1.72E-1(1.31E-4)	7.08E-1(5.16E-2)	1.26E-1(1.54E-2)	1.41E-1(1.12E-2)	–
Poisson	2d-C	1.17E-1(2.98E-3)	3.09E-4(1.25E-4)	7.24E-3(9.95E-3)	5.00E-5(5.33E-5)	1.19E-1(2.55E-3)	1.79E-4(8.84E-5)	1.15E-1(6.22E-3)	4.86E-2(4.43E-3)	1.39E-1(5.67E-3)	9.38E-2(1.91E-2)	7.89E-4(2.17E-4)
	2d-CG	1.28E-1(1.03E-3)	1.17E-3(1.83E-4)	6.13E-4(2.31E-4)	6.99E-5(3.50E-5)	1.32E-1(3.23E-3)	2.73E-2(1.92E-2)	1.98E-1(2.28E-3)	2.50E-2(3.80E-4)	7.67E-2(2.73E-3)	1.77E-1(8.70E-2)	4.84E-4(9.87E-5)
	3d-CG	2.64E-2(2.67E-3)	1.18E-2(1.97E-3)	9.51E-4(6.51E-4)	7.54E-2(7.86E-5)	2.81E-2(5.15E-3)	1.16E-2(4.42E-3)	2.01E-2(4.93E-3)	4.58E-2(8.04E-5)	2.82E-2(2.62E-3)	2.16E-2(5.87E-3)	4.63E-2(9.28E-3)
	2d-MS	2.67E+0(9.04E-2)	3.90E+0(7.16E-2)	4.28E+0(6.83E-1)	3.77E+0(9.98E-2)	2.80E+0(1.87E-1)	2.36E+0(3.15E-1)	2.56E+0(1.43E-1)	6.09E+0(5.46E-1)	1.83E+0(3.00E-1)	5.87E+0(8.72E-1)	6.68E+0(8.23E-4)
Heat	2d-VC	4.00E-2(4.94E-3)	2.19E-3(3.21E-4)	1.76E-3(1.43E-5)	1.79E-3(9.80E-5)	3.67E-2(1.42E-3)	9.14E-3(3.13E-3)	1.89E-1(9.44E-2)	3.23E-2(2.26E-2)	1.74E-2(4.35E-3)	2.93E-2(7.12E-3)	3.56E-2(1.71E-4)
	2d-MS	1.09E-4(4.94E-5)	1.60E-3(3.35E-4)	2.25E-4(1.22E-4)	5.27E-5(1.18E-5)	1.54E-4(4.17E-5)	1.51E-3(1.25E-3)	3.43E-4(1.87E-5)	2.57E-2(2.22E-3)	1.57E-4(8.06E-5)	3.10E-2(1.15E-2)	2.17E-4(2.47E-5)
	2d-CG	2.09E-3(9.69E-4)	3.15E-2(2.08E-3)	2.32E-2(1.59E-3)	2.02E-2(4.15E-3)	1.12E-3(2.65E-4)	7.79E-3(2.63E-3)	1.34E-2(4.13E-3)	1.16E+1(9.04E-2)	8.53E-4(9.74E-5)	3.94E-1(2.71E-1)	5.61E-1(5.96E-2)
	2d-LT	1.14E+0(2.38E-5)	1.13E+0(1.82E-4)	1.14E+0(1.67E-4)	1.14E+0(6.41E-4)	1.14E+0(3.55E-4)	1.14E+0(8.74E-5)	1.14E+0(2.23E-4)	1.14E+0(0.00E+0)	1.14E+0(2.20E-4)	1.14E+0(3.27E-4)	1.16E+0(2.83E-4)
NS	2d-C	4.19E-5(2.00E-6)	4.03E-4(6.45E-5)	NaN	7.56E-4(1.90E-4)	4.18E-3(2.05E-4)	1.07E-2(5.67E-3)	1.13E-4(8.77E-6)	5.30E-4(3.50E-4)	2.33E-5(4.71E-6)	2.67E-5(4.71E-6)	1.37E-4(7.24E-5)
	2d-CG	6.94E-4(6.45E-5)	5.19E-3(2.43E-4)	5.40E-3(2.49E-4)	4.22E-3(5.82E-4)	5.45E-3(2.13E-5)	9.32E-3(3.09E-3)	1.16E-3(8.97E-5)	1.06E+0(1.61E-2)	3.37E-4(6.60E-5)	1.72E-3(1.33E-3)	3.34E+0(2.97E-5)
	2d-LT	5.06E+2(1.21E+0)	5.10E+2(3.40E-1)	5.10E+2(4.13E-1)	5.09E+2(6.15E-1)	5.10E+2(3.42E-1)	5.10E+2(2.23E-1)	5.05E+2(7.30E-1)	5.11E+2(1.76E-2)	5.06E+2(1.82E+0)	5.11E+2(2.99E+0)	5.15E+2(1.77E+0)
Wave	1d-C	1.11E-1(3.66E-2)	2.54E-2(1.61E-3)	4.08E-2(4.31E-3)	3.01E-3(4.82E-4)	9.07E-2(6.02E-3)	4.68E-3(1.28E-3)	9.66E-2(5.85E-3)	6.17E-1(1.19E-1)	6.03E-2(2.87E-3)	1.48E-1(4.44E-2)	1.39E-1(1.97E-2)
	2d-CG	1.64E-1(6.13E-2)	1.28E-1(1.13E-2)	1.03E-1(1.46E-2)	2.17E-1(2.05E-2)	6.25E-2(1.17E-2)	5.59E-2(1.29E-2)	3.09E-2(8.98E-4)	5.24E-2(9.01E-3)	3.49E-2(3.38E-3)	2.99E-2(4.68E-4)	5.78E-2(7.99E-3)
	2d-MS	1.30E+5(4.25E+4)	7.35E+4(1.68E+3)	7.34E+4(1.97E+3)	7.69E+4(4.55E+3)	1.33E+5(4.47E+4)	7.15E+4(8.04E+2)	7.27E+4(5.47E+2)	1.13E+2(1.46E+2)	7.91E+4(2.55E+3)	7.98E+4(8.00E+3)	8.95E+5(1.15E+4)
Chaotic	GS	1.00E-1(1.35E-1)	1.64E-2(1.70E-2)	4.32E-3(4.07E-6)	2.59E-2(1.44E-2)	4.40E-3(8.83E-5)	4.32E-3(1.11E-6)	3.62E-2(2.28E-2)	4.00E-1(2.33E-1)	4.32E-3(4.71E-6)	1.69E-2(1.79E-2)	5.16E-3(1.64E-3)
	KS	1.16E+0(2.95E-3)	1.11E+0(5.07E-2)	1.04E+0(6.20E-3)	1.06E+0(1.09E-2)	1.16E+0(1.98E-3)	1.05E+0(1.04E-2)	1.12E+0(8.67E-3)	1.05E+0(2.50E-3)	1.16E+0(4.50E-3)	1.14E+0(2.33E-2)	1.16E+0(5.28E-2)
High dim	PNd	9.47E-5(3.47E-5)	8.30E-5(5.53E-5)	2.09E-6(1.69E-7)	4.02E-4(5.23E-4)	1.43E-4(9.92E-5)	1.70E-4(9.61E-5)	2.57E-4(6.31E-5)	–	3.03E-4(2.25E-4)	4.80E-4(2.81E-4)	–
	HNd	1.19E+1(2.92E-1)	1.93E+1(3.65E-1)	1.42E+1(9.23E-1)	1.44E+1(9.14E-1)	1.17E+1(2.41E-1)	8.52E+0(2.34E+0)	9.21E+0(3.90E-1)	–	2.49E+1(2.99E-1)	2.50E+1(2.76E-1)	–
Inverse	PInv	1.89E-3(6.31E-5)	5.89E-3(3.88E-4)	5.08E-3(2.18E-4)	7.94E-3(1.16E-3)	1.89E-3(4.49E-4)	3.64E-3(8.28E-4)	1.37E-3(9.45E-5)	1.23E-4(9.50E-5)	6.25E-1(8.80E-1)	1.87E-2(1.98E-2)	3.98E+0(1.33E+0)
	HInv	5.36E+0(4.86E-1)	6.02E-3(7.71E-4)	5.66E-3(9.88E-4)	1.23E-2(1.75E-3)	5.01E+0(4.22E-1)	1.43E-2(4.35E-3)	6.01E+1(3.72E+1)	8.83E-1(6.52E-2)	1.27E+0(1.69E+0)	1.03E-1(4.73E-2)	2.23E+2(5.54E+1)

Table 8: Mean (Std) of MSE for main experiments.

fmSE-L	Name	Vanilla	Loss Reweighting/Sampling			Optimizer	Loss functions		Architecture		
		PINN	LRA	NTK	RAR	MultiAdam	gPINN	vPINN	LAAF	GAAF	FBPINN
Burgers	1d-C	2.21E-02(1.02E-02)	1.46E-02(1.77E-02)	1.75E-01(2.76E-01)	5.02E-01(6.21E-01)	1.19E-01(2.00E-01)	1.79E+00(1.99E+00)	1.40E+01(1.06E+00)	1.32E-01(2.50E-01)	9.38E-02(1.47E-01)	2.10E+00(1.50E+00)
	2d-C	4.85E+01(9.27E+00)	8.18E+01(1.24E+01)	8.36E+01(1.07E+01)	4.77E+01(6.85E+00)	1.39E+02(5.63E+01)	8.89E+01(3.98E+00)	4.54E+03(5.57E+03)	8.34E+01(7.63E+00)	9.27E+01(7.53E+00)	–
Poisson	2d-C	–	–	–	–	–	–	–	–	–	–
	2d-CG	–	–	–	–	–	–	–	–	–	–
	3d-CG	–	–	–	–	–	–	–	–	–	–
	2d-MS	1.74E+03(6.29E+01)	8.62E+03(1.10E+03)	8.62E+03(6.08E+02)	2.99E+03(2.59E+02)	3.46E+03(1.93E+03)	7.41E+03(5.99E+02)	1.13E+04(4.70E+01)	2.61E+03(5.60E+02)	1.24E+04(5.71E+03)	5.90E+03(6.03E+00)
Heat	2d-VC	4.78E+00(5.53E-01)	3.66E-02(8.92E-03)	3.58E-01(2.81E-01)	2.00E+00(1.49E+00)	2.78E+00(3.95E+00)	2.91E+03(1.84E+03)	1.74E+00(1.04E+00)	1.43E+00(1.87E+00)	1.28E+01(2.08E+01)	4.34E+00(2.13E-2)
	2d-MS	1.56E-01(2.33E-01)	1.12E-01(1.76E-01)	1.46E+00(1.60E+00)	3.55E-01(3.96E-01)	3.48E-01(3.43E-01)	1.37E+01(1.38E+01)	–	3.50E-01(2.74E-01)	1.11E+00(1.01E+00)	–
	2d-CG	–	–	–	–	–	–	–	–	–	–
	2d-LT	3.90E+02(6.18E+02)	2.71E+01(3.42E-02)	2.75E+01(5.86E-01)	2.70E+01(1.36E-01)	2.70E+01(9.84E-02)	3.34E+05(6.48E+05)	2.63E+01(7.51E-01)	2.70E+01(1.56E-01)	2.71E+01(3.78E-02)	8.47E+01(7.99E-1)
NS	2d-C	4.29E-02(3.76E-02)	–	3.74E-01(1.26E-01)	2.35E-02(1.24E-02)	2.20E+01(2.96E+01)	6.97E-01(4.72E-01)	5.38E-01(1.29E-01)	1.34E-02(1.03E-02)	1.73E-02(8.42E-03)	2.47E-2(2.70E-3)
	2d-CG	–	–	–	–	–	–	–	–	–	–
	2d-LT	2.07E+05(9.61E+02)	2.05E+05(2.37E+02)	2.07E+05(5.52E+02)	2.06E+05(4.53E+02)	2.05E+05(2.78E+02)	2.05E+05(2.96E+02)	4.87E+04(1.64E+02)	2.07E+05(7.29E+02)	2.06E+05(7.01E+02)	–
Wave	1d-C	5.38E+01(1.52E+01)	4.81E-01(5.90E-01)	4.65E-01(4.37E-01)	1.10E+02(7.79E+01)	3.57E+02(1.97E+02)	3.00E+02(8.28E+01)	2.85E+01(8.07E+00)	1.98E+01(1.48E+01)	3.89E+02(3.79E+02)	6.01E+01(1.46E+01)
	2d-CG	2.42E+01(1.08E+01)	3.47E+02(2.09E+02)	5.26E+02(5.40E+01)	1.75E+02(1.90E+02)	1.25E+02(9.42E+01)	8.10E+01(6.42E+00)	1.25E+01(4.98E+00)	4.36E+02(4.69E+02)	7.19E+01(6.05E+01)	1.49E+01(3.22E+00)
	2d-MS	3.72E+08(3.03E+08)	8.91E+05(1.18E+06)	7.01E+05(3.95E+05)	3.93E+08(3.18E+08)	2.39E+06(2.83E+06)	1.85E+06(1.89E+06)	1.13E+02(9.57E-01)	3.08E+06(2.04E+06)	4.33E+06(8.23E+06)	1.10E+07(1.93E+06)
Chaotic	GS	1.45E+02(4.99E+00)	1.44E+01(1.09E+01)	7.79E+00(4.79E+00)	2.96E+02(7.67E+01)	6.51E+00(9.23E+00)	5.26E+01(2.87E+01)	2.79E+01(2.09E+01)	2.69E+02(1.34E+01)	4.89E+01(5.30E+01)	3.49E+00(2.45E+00)
	KS	1.65E+01(3.09E+01)	1.06E+00(5.77E-03)	3.81E+02(2.09E+02)	1.03E+00(6.13E-02)	1.07E+00(6.48E-03)	1.38E+02(6.24E+00)	1.24E+02(1.76E+01)	1.08E+00(1.41E-02)	1.04E+00(2.96E-02)	–
High dim	PNd	–	–	–	–	–	–	–	–	–	–
	HNd	–	–	–	–	–	–	–	–	–	–

Table 9: Mean (Std) of low-frequency Fourier error for main experiments.

fMSE-M	Name	Vanilla	Loss Reweighting/Sampling			Optimizer	Loss functions		Architecture		
		PINN	LRA	NTK	RAR	MultiAdam	gPINN	vPINN	LAAF	GAAF	FBPINN
Burgers	1d-C	1.43E-03(1.93E-04)	2.94E-05(2.03E-05)	9.34E-05(7.38E-05)	7.51E-05(6.01E-05)	6.18E-04(5.93E-04)	6.69E-03(1.40E-03)	3.00E+00(2.22E-01)	3.53E-05(5.77E-05)	1.72E-05(1.72E-05)	4.88E-1(3.65E-1)
	2d-C	3.28E-01(4.31E-03)	2.23E-01(3.59E-02)	2.11E-01(2.04E-02)	3.32E-01(4.83E-03)	3.25E-01(1.15E-03)	3.03E+00(3.63E+00)	3.23E-01(2.30E-04)	3.25E-01(2.89E-02)	2.95E-01(1.71E-02)	–
Poisson	2d-C	–	–	–	–	–	–	–	–	–	–
	2d-CG	–	–	–	–	–	–	–	–	–	–
	3d-CG	–	–	–	–	–	–	–	–	–	–
	2d-MS	6.57E+00(3.70E-02)	1.70E+01(4.14E+00)	1.47E+01(1.54E+00)	1.18E+01(2.32E+00)	5.61E+00(3.18E+00)	8.26E+00(5.99E-01)	2.88E+01(2.37E-01)	1.26E+01(3.53E+00)	9.87E+00(2.25E+00)	2.03E+01(2.50E-3)
Heat	2d-VC	2.75E-02(2.11E-03)	1.46E-03(4.26E-04)	7.99E-03(1.17E-02)	1.01E-01(7.00E-02)	1.54E-02(1.23E-02)	6.91E+01(1.07E+02)	9.26E-03(3.06E-03)	3.58E-02(2.86E-02)	8.90E-01(1.27E+00)	1.56E-2(2.62E-4)
	2d-MS	7.35E-04(7.70E-04)	4.55E-05(5.24E-05)	1.26E-04(3.07E-05)	2.07E-05(1.15E-05)	3.13E-03(3.56E-03)	2.65E-03(1.55E-03)	7.57E-02(2.40E-03)	6.19E-05(1.89E-05)	1.05E-04(1.25E-04)	Nan
	2d-CG	–	–	–	–	–	–	–	–	–	–
	2d-LT	2.11E+00(3.00E+00)	1.59E+02(1.37E-01)	1.59E+02(1.97E-01)	1.59E+02(2.12E-01)	1.59E+02(3.85E-02)	1.59E+02(1.81E-01)	4.57E-01(2.67E-02)	1.59E+02(2.20E-01)	1.59E+02(1.36E-01)	8.91E-1(4.84E-2)
NS	2d-C	1.72E-04(9.81E-05)	–	3.96E-03(3.45E-03)	1.48E-04(6.28E-05)	1.48E-01(2.31E-01)	5.84E-03(9.82E-04)	2.86E-03(1.58E-03)	1.05E-04(8.46E-05)	4.46E-05(3.38E-05)	2.18E-5(2.47E-6)
	2d-CG	–	–	–	–	–	–	–	–	–	–
	2d-LT	1.00E-02(9.51E-04)	2.63E-02(2.55E-03)	1.49E-02(3.02E-03)	1.06E-02(9.30E-04)	2.52E-02(4.51E-03)	2.12E-02(2.08E-03)	–	1.05E-02(1.37E-03)	1.26E-02(2.12E-03)	4.53E+00(1.83E-2)
Wave	1d-C	1.61E-01(3.55E-02)	7.58E-03(8.03E-03)	3.62E-02(8.80E-03)	8.55E-01(3.57E-01)	2.63E+00(2.04E+00)	2.50E+00(9.12E-01)	5.93E-01(6.18E-02)	1.96E-01(1.46E-01)	1.48E+00(9.12E-01)	8.48E-2(2.36E-2)
	2d-CG	8.29E-02(6.50E-03)	1.06E-03(1.01E-03)	8.18E-04(2.57E-04)	8.27E-04(3.83E-04)	3.12E-03(2.43E-03)	1.36E-03(3.20E-04)	4.73E-02(3.85E-03)	4.73E-02(3.85E-03)	1.53E-03(5.15E-04)	1.49E-03(5.58E-04)
	2d-MS	1.47E+04(1.73E+04)	1.31E+05(1.66E+05)	1.78E+05(9.50E+04)	2.39E+04(4.63E+04)	2.39E+05(1.80E+05)	1.82E+04(2.13E+04)	4.75E+01(2.01E+00)	1.62E+05(1.72E+05)	3.15E+05(4.71E+05)	6.18E+04(3.16E+04)
Chaotic	GS	5.39E+01(2.19E-01)	7.94E-02(5.38E-02)	3.37E-02(9.80E-03)	6.27E-02(1.76E-02)	8.88E-02(8.20E-02)	1.72E-01(3.91E-02)	2.36E-02(1.40E-02)	4.62E-02(6.99E-03)	1.35E-01(1.17E-01)	5.08E-2(3.92E-2)
	KS	5.54E-01(1.46E-02)	5.45E-01(2.42E-03)	5.60E-01(2.11E-02)	5.47E-01(3.82E-03)	5.46E-01(6.98E-05)	5.48E-01(1.06E-02)	–	5.46E-01(3.93E-04)	5.46E-01(1.23E-03)	–
High dim	PNd	–	–	–	–	–	–	–	–	–	–
	HNd	–	–	–	–	–	–	–	–	–	–

Table 10: Mean (Std) of medium-frequency Fourier error for main experiments.

fmSE-H	Name	Vanilla	Loss Reweighting/Sampling			Optimizer	Loss functions		Architecture		
		PINN	LRA	NTK	RAR	MultiAdam	gPINN	vPINN	LAAF	GAAF	FBPINN
Burgers	1d-C	2.96E-05(9.65E-06)	1.85E-04(8.34E-05)	1.48E-04(1.36E-04)	2.39E-03(2.55E-03)	6.16E-04(4.21E-04)	1.09E-01(8.12E-03)	1.40E-02(1.26E-03)	7.15E-04(1.24E-03)	1.93E-04(7.30E-05)	6.87E-3(4.12E-3)
	2d-C	6.78E-02(1.23E-03)	5.33E-02(1.37E-03)	5.43E-02(1.56E-03)	6.78E-02(1.08E-03)	7.07E-02(7.45E-04)	6.80E-02(2.95E-04)	2.31E-01(2.46E-01)	5.84E-02(1.19E-03)	5.98E-02(1.01E-03)	–
Poisson	2d-C	–	–	–	–	–	–	–	–	–	–
	2d-CG	–	–	–	–	–	–	–	–	–	–
	3d-CG	–	–	–	–	–	–	–	–	–	–
	2d-MS	1.68E-02(4.05E-04)	2.07E+00(3.81E-01)	2.23E+00(1.14E-01)	1.89E+00(2.11E-01)	2.30E+00(5.97E-01)	8.62E-01(3.40E-02)	5.44E-02(4.98E-03)	1.27E+00(2.34E-01)	3.07E+00(1.14E+00)	7.17E-2(8.16E-6)
Heat	2d-VC	4.22E-04(2.39E-04)	1.88E-03(1.07E-04)	1.90E-03(7.60E-05)	3.02E-02(3.49E-03)	1.15E-02(8.98E-03)	1.99E+00(9.14E-01)	5.11E-04(3.47E-04)	2.43E-02(2.66E-03)	2.63E-02(1.52E-02)	6.39E-5(3.77E-6)
	2d-MS	6.81E-06(5.66E-06)	7.12E-05(4.00E-05)	9.24E-05(6.51E-05)	9.91E-05(1.35E-04)	5.69E-04(3.34E-04)	1.03E-02(3.68E-03)	1.99E-03(1.45E-04)	8.63E-05(3.67E-05)	1.62E-04(1.36E-04)	–
	2d-CG	–	–	–	–	–	–	–	–	–	–
	2d-LT	2.10E-01(1.45E-02)	7.73E-01(2.31E-04)	7.72E-01(2.41E-04)	7.72E-01(9.35E-05)	7.73E-01(2.03E-04)	7.95E-01(4.27E-02)	2.70E-01(2.79E-02)	7.73E-01(1.59E-04)	7.72E-01(8.87E-05)	2.05E-1(4.46E-4)
NS	2d-C	4.89E-06(1.01E-06)	–	2.05E-04(4.41E-05)	3.80E-06(3.71E-07)	2.16E-03(5.85E-04)	1.32E-03(3.12E-04)	6.98E-06(4.41E-06)	1.18E-06(2.56E-07)	2.05E-06(7.23E-07)	6.48E-8(1.75E-8)
	2d-CG	–	–	–	–	–	–	–	–	–	–
	2d-LT	1.09E+02(1.92E-01)	1.11E+02(3.51E-02)	1.10E+02(1.61E-01)	1.09E+02(1.16E-01)	1.10E+02(2.72E-01)	1.10E+02(1.00E-01)	4.51E+02(3.00E+00)	1.09E+02(1.30E-01)	1.09E+02(4.04E-01)	–
Wave	1d-C	1.25E-03(3.43E-04)	3.43E-02(9.35E-03)	4.28E-03(6.00E-04)	7.06E-02(7.51E-03)	8.96E-02(1.06E-02)	8.64E-02(5.08E-03)	6.15E-04(7.67E-05)	5.34E-02(2.92E-03)	8.45E-02(1.85E-02)	–
	2d-CG	6.39E-03(1.09E-03)	3.93E-02(1.01E-02)	4.80E-02(3.17E-03)	3.31E-02(9.96E-03)	2.70E-02(4.96E-03)	3.09E-02(5.50E-04)	3.03E-03(2.29E-04)	4.91E-02(3.19E-02)	2.54E-02(2.53E-03)	5.11E-3(1.86E-4)
	2d-MS	7.61E+04(4.06E+03)	7.51E+04(1.67E+03)	7.90E+04(4.65E+03)	7.62E+04(5.81E+03)	7.35E+04(3.05E+02)	7.49E+04(5.94E+02)	–	8.09E+04(2.45E+03)	8.09E+04(6.69E+03)	–
Chaotic	GS	5.30E-01(1.48E-03)	1.04E+00(7.44E-03)	1.05E+00(4.11E-03)	1.12E+00(2.99E-03)	1.04E+00(5.34E-03)	1.10E+00(2.14E-03)	1.70E-03(1.01E-03)	1.12E+00(2.14E-03)	1.09E+00(7.71E-03)	–
	KS	1.27E-03(2.94E-04)	1.11E-03(1.32E-06)	2.17E-03(2.09E-03)	1.12E-03(2.36E-05)	1.11E-03(7.08E-09)	7.28E-03(1.16E-03)	4.48E-01(1.76E-03)	1.11E-03(1.45E-07)	1.11E-03(7.82E-07)	–
High dim	PNd	–	–	–	–	–	–	–	–	–	–
	HNd	–	–	–	–	–	–	–	–	–	–

Table 11: Mean (Std) of high-frequency Fourier error for main experiments.

Avg Runtime	Name	Vanilla		Loss Reweighting/Sampling		Optimizer	Loss functions		Architecture		
		PINN	PINN-w	LRA	NTK	MultiAdam	gPINN	vPINN	LAAF	GAAF	FBPINN
–	1d-C	2.84E+2	2.78E+2	7.64E+2	6.70E+2	5.06E+2	6.28E+2	2.85E+2	3.61E+2	3.56E+2	1.11E+3
	2d-C	3.11E+3	3.11E+3	1.84E+4	4.35E+3	2.72E+3	4.03E+3	8.95E+2	4.08E+3	4.07E+3	–
Burgers	2d-C	3.39E+2	3.33E+2	9.01E+2	8.09E+2	6.13E+2	7.66E+2	3.29E+2	5.72E+2	4.20E+2	4.12E+3
	2d-CG	3.69E+2	3.59E+2	9.36E+2	8.80E+2	6.57E+2	8.06E+2	3.55E+2	6.05E+2	4.34E+2	4.17E+3
	3d-CG	1.45E+3	2.32E+3	4.06E+3	4.40E+3	2.41E+3	5.01E+3	1.94E+3	2.01E+3	1.68E+3	2.18E+3
	2d-MS	3.83E+2	3.74E+2	7.47E+2	8.74E+2	6.67E+2	7.92E+2	1.81E+3	6.62E+2	4.57E+2	4.22E+3
Heat	2d-VC	1.16E+3	1.16E+3	3.52E+3	1.69E+3	1.91E+3	1.34E+3	3.03E+3	1.52E+3	1.52E+3	3.92E+3
	2d-MS	1.13E+3	1.14E+3	3.48E+3	1.61E+3	1.89E+3	1.30E+3	1.69E+3	1.51E+3	1.50E+3	5.84E+3
	2d-CG	1.16E+3	1.17E+3	5.14E+3	1.64E+3	1.90E+3	1.31E+3	3.05E+3	1.52E+3	1.51E+3	5.28E+3
	2d-LT	1.15E+3	1.18E+3	3.52E+3	1.65E+3	1.90E+3	1.32E+3	2.12E+3	1.51E+3	1.50E+3	3.93E+3
NS	2d-C	7.52E+2	7.64E+2	2.24E+3	1.84E+3	1.25E+3	2.03E+3	5.68E+2	9.49E+2	9.43E+2	7.16E+3
	2d-CG	7.56E+2	7.58E+2	3.26E+3	1.84E+3	1.22E+3	1.97E+3	6.79E+2	9.35E+2	9.31E+2	5.48E+3
	2d-LT	3.05E+3	3.05E+3	2.25E+4	4.29E+3	3.73E+3	4.42E+3	1.38E+3	3.99E+3	3.99E+3	4.10E+3
Wave	1d-C	3.50E+2	3.52E+2	1.12E+3	8.40E+2	2.72E+2	7.75E+2	2.22E+2	6.01E+2	4.36E+2	3.09E+3
	2d-CG	1.21E+3	1.24E+3	4.50E+3	1.77E+3	2.01E+3	1.27E+3	5.99E+2	2.35E+3	1.57E+3	3.01E+3
	2d-MS	2.19E+3	2.19E+3	6.76E+3	5.02E+3	4.12E+3	6.18E+3	2.11E+3	2.63E+3	2.25E+3	3.67E+3
Chaotic	GS	2.55E+3	2.55E+3	7.57E+3	3.17E+3	4.22E+3	2.59E+3	6.12E+2	3.23E+3	3.22E+3	5.47E+3
	KS	1.40E+3	1.40E+3	3.17E+3	3.59E+3	2.29E+3	3.83E+3	7.14E+2	1.62E+3	1.63E+3	8.83E+3
High dim	PNd	1.78E+3	1.83E+3	4.30E+3	4.75E+3	3.02E+3	1.91E+3	–	3.50E+3	2.33E+3	–
	HNd	2.35E+3	2.45E+3	7.42E+3	6.28E+3	4.00E+3	2.74E+3	–	3.09E+3	3.08E+3	–
Inverse	PInv	4.53E+2	4.88E+2	1.25E+3	1.71E+3	7.46E+2	1.50E+3	4.90E+2	5.75E+2	5.88E+2	3.63E+3
	HInv	1.09E+3	1.12E+3	3.39E+3	1.68E+3	1.77E+3	1.56E+3	1.86E+3	1.44E+3	1.44E+3	3.93E+3

Table 12: Average running time (seconds) for main experiments, we run all methods three times with 20000 epochs.

Training Flops	Name	Vanilla		Loss Reweighting/Sampling		Optimizer	Loss functions		Architecture		
		PINN	PINN-w	LRA	NTK	MultiAdam	gPINN	vPINN	LAAF	GAAF	FBPINN
–	1d-C	1.87E+11	1.87E+11	5.12E+11	4.29E+11	3.39E+11	4.11E+11	1.81E+11	2.22E+11	2.29E+11	7.34E+11
	2d-C	2.72E+12	2.72E+12	1.23E+13	2.61E+12	1.82E+12	2.79E+12	6.23E+11	2.53E+12	2.73E+12	–
Poisson	2d-C	2.55E+11	2.55E+11	6.04E+11	5.32E+11	4.15E+11	5.03E+11	2.21E+11	3.83E+11	2.81E+11	2.46E+12
	2d-CG	2.37E+11	2.37E+11	6.17E+11	5.82E+11	4.4E+11	5.29E+11	2.38E+11	4.05E+11	2.91E+11	2.79E+12
	3d-CG	9.03E+11	9.03E+11	2.72E+12	2.95E+12	1.61E+12	3.36E+12	1.3E+12	1.35E+12	1.13E+12	1.46E+12
	2d-MS	2.75E+11	2.75E+11	5.02E+11	5.66E+11	4.47E+11	5.31E+11	1.21E+12	4.44E+11	3.06E+11	2.83E+12
Heat	2d-VC	7.10E+11	7.10E+11	2.26E+12	1.03E+12	1.28E+12	8.98E+11	2.03E+12	1.02E+12	1.02E+12	2.63E+12
	2d-MS	7.15E+11	7.15E+11	2.23E+12	1.01E+12	1.27E+12	8.71E+11	1.13E+12	1.05E+12	1.01E+12	3.71E+12
	2d-CG	6.91E+11	6.91E+11	3.34E+12	1.07E+12	1.27E+12	8.78E+11	2.04E+12	1.08E+12	1.01E+12	3.54E+12
	2d-LT	7.62E+11	7.62E+11	2.26E+12	1.11E+12	1.27E+12	8.84E+11	1.42E+12	1.01E+12	1.01E+12	2.63E+12
NS	2d-C	5.05E+11	5.05E+11	1.39E+12	1.23E+12	8.38E+11	1.36E+12	3.81E+11	6.36E+11	6.32E+11	4.85E+12
	2d-CG	4.85E+11	4.85E+11	2.14E+12	1.23E+12	8.17E+11	1.32E+12	4.55E+11	6.26E+11	6.24E+11	3.67E+12
	2d-LT	1.87E+12	1.87E+12	1.51E+13	2.87E+12	2.5E+12	2.96E+12	9.25E+11	2.77E+12	2.67E+12	2.75E+12
Wave	1d-C	2.15E+11	2.15E+11	7.51E+11	5.63E+11	1.82E+11	5.19E+11	1.49E+11	4.13E+11	2.92E+11	2.07E+12
	2d-CG	7.11E+11	7.11E+11	3.02E+12	1.19E+12	1.35E+12	8.51E+11	4.01E+11	1.75E+12	1.08E+12	2.02E+12
	2d-MS	1.47E+12	1.47E+12	4.53E+12	3.36E+12	2.76E+12	4.14E+12	1.41E+12	1.74E+12	1.51E+12	2.46E+12
Chaotic	GS	1.68E+12	1.68E+12	5.07E+12	2.12E+12	2.83E+12	1.74E+12	4.07E+11	2.16E+12	2.16E+12	3.66E+12
	KS	9.12E+11	9.12E+11	2.12E+12	2.41E+12	1.53E+12	2.57E+12	4.78E+11	1.09E+12	1.09E+12	5.92E+12
High dim	PNd	1.19E+12	1.19E+12	2.88E+12	3.18E+12	2.02E+12	1.28E+12	–	2.35E+12	1.56E+12	–
	HNd	1.57E+12	1.57E+12	4.97E+12	4.21E+12	2.68E+12	1.84E+12	–	2.07E+12	2.06E+12	–
Inverse	PInv	3.04E+11	3.27E+11	8.38E+11	1.15E+12	5.24E+11	1.01E+12	3.28E+11	3.85E+11	3.94E+11	2.43E+12
	HInv	7.34E+11	7.34E+11	2.27E+12	1.13E+12	1.19E+12	1.05E+12	1.25E+12	9.65E+11	9.65E+11	2.63E+12

Table 13: Average Flops every epoch for main experiments, we run all methods three times.

L2RE		Burgers1d	GS	Heat2d-CG	Poisson2d-C
PINN	1e-5	2.35E-2(1.90E-3)	9.39E-2(3.60E-4)	1.20E-1(2.40E-3)	1.08E+0(1.08E-1)
	1e-4	1.99E-2(4.30E-3)	1.79E-1(1.20E-1)	1.35E-1(2.00E-2)	2.81E-2(2.44E-3)
	1e-3	1.93E-2(4.00E-3)	9.35E-2(2.30E-4)	8.51E-2(8.90E-3)	2.32E-2(1.52E-3)
	1e-2	3.79E-1(1.40E-1)	1.91E-1(1.30E-1)	1.73E-1(7.10E-2)	3.26E-2(1.51E-3)
	decay	1.69E-2(4.10E-3)	1.81E-1(1.20E-1)	1.59E-1(2.00E-2)	2.41E-2(9.33E-4)
PINN-LRA	1e-5	3.44E-2(1.40E-2)	1.79E-1(1.20E-1)	1.18E-1(7.60E-4)	2.91E-2(3.19E-3)
	1e-4	2.12E-2(5.30E-3)	9.36E-2(4.50E-4)	1.37E-1(8.50E-3)	2.49E-2(3.88E-3)
	1e-3	1.49E-2(9.60E-4)	9.37E-2(3.63E-5)	1.31E-1(9.60E-3)	2.26E-2(1.93E-3)
	1e-2	6.23E-1(7.40E-2)	1.29E-1(5.10E-2)	8.99E-2(7.00E-3)	1.00E+0(5.62E-7)
	decay	1.37E-2(5.00E-4)	1.81E-1(1.20E-1)	1.19E-1(1.30E-2)	2.61E-2(7.64E-4)
PINN-NTK	1e-5	1.08E-1(2.70E-2)	4.09E-1(1.20E-3)	1.21E-1(2.80E-3)	1.86E-3(1.26E-4)
	1e-4	4.72E-2(8.70E-3)	1.96E-1(1.40E-1)	1.27E-1(5.30E-3)	2.30E-3(9.48E-4)
	1e-3	2.91E-2(7.40E-3)	2.99E-1(1.50E-1)	1.21E-1(9.50E-3)	5.34E-3(1.22E-4)
	1e-2	NaN	1.90E+0(1.63E+0)	NaN	2.39E-1(2.00E-1)
	decay	1.74E-2(2.30E-3)	3.06E-1(1.50E-1)	1.48E-1(9.60E-3)	8.24E-4(1.32E-4)

Table 14: Results of PINN, PINN-NTK, PINN-LRA under different learning rates or learning rate schedules.

L2RE		Burgers1d	GS	Heat2d-CG	Poisson2d-C
PINN	512	4.59E-1(8.36E-2)	2.46E-1(1.09E-1)	4.31E-1(6.57E-2)	3.15E-2(4.04E-3)
	2048	2.60E-1(2.43E-1)	9.37E-2(2.60E-4)	2.02E-1(1.92E-2)	2.62E-2(2.31E-3)
	8192	2.14E-2(1.76E-3)	9.41E-2(6.05E-4)	1.35E-1(1.71E-2)	2.58E-2(6.51E-4)
	32768	1.44E-2(4.91E-4)	9.37E-2(3.89E-5)	3.73E-2(3.23E-3)	2.63E-2(2.32E-3)
PINN-LRA	512	2.80E-1(2.02E-1)	9.39E-2(1.66E-4)	3.66E-1(3.86E-2)	3.00E-2(3.16E-3)
	2048	1.82E-1(1.85E-1)	1.33E-1(5.57E-2)	2.07E-1(4.96E-3)	2.57E-2(1.78E-3)
	8192	1.88E-2(9.45E-4)	9.36E-2(2.14E-4)	1.01E-1(2.18E-2)	2.82E-2(8.12E-4)
	32768	1.49E-2(1.51E-3)	1.17E-1(3.25E-2)	4.44E-2(1.05E-2)	2.49E-2(6.32E-4)

Table 15: Comparison of PINN and PINN-LRA’s performance under different batch sizes (number of collocation points).

863 E.2 Ablation Experiments

864 **Influence of learning rates.** To understand the impact of learning rates We selected three methods,
865 i.e., vanilla Physics-Informed Neural Networks (PINN), PINN-NTK, and PINN-LRA. We conduct
866 experiments on four PDE problems, i.e., Burgers1d-C, GS, Heat2d-CG, and Poisson2d-C. The
867 comparative analysis involved evaluating the performance of these methods using learning rates of
868 1e-5, 1e-4, 1e-3, and 1e-2, along with a step learning rate decay strategy implemented every 1000
869 epochs with a decay factor of 0.75. The results are shown in Table E.2. As stated in the main text, a
870 moderate learning rate like 1e-3, 1e-4, or using a decay strategy is a good choice.

871 **Influence of batch size (Collocation points).** To further understand the impact of the number
872 of collocation points on our model’s performance, we conducted an ablation study. We used four
873 different numbers of collocation points, specifically 512, 2048, 8192, and 32768. The cases tested
874 in this study were burgers1d, GS, Heat2d-CG, and Poisson2d, which is the same as the ablation
875 study on learning rates. We utilized two variants of Physics-Informed Neural Networks: the vanilla
876 PINN and the PINN-LRA. We found that using more batch size leads to a continual improvement in
877 performance. For some cases, 8192 is a enough large batch size and the performance saturates. The
878 conclusions and plots of this experiment are shown in the main text.

879 **Influence of training epochs.** In this ablation study, we examine the impact of varying the number
880 of training epochs on our model’s performance. We selected four different values, specifically 5k,
881 20k, 80k, and 160k epochs. Similar to the previous study, the cases chosen for testing were burgers1d,
882 GS, Heat2d-CG, and Poisson2d. The trend is that training more epochs leads to better performance.
883 However, it is easier to saturate than a larger batch size.

Name		Inference Flops
Burgers	1d-C	5.03E+4
	2d-C	5.05E+4
Poisson	2d-C	5.03E+4
	2d-CG	5.03E+4
	3d-CG	5.03E+4
Heat	2d-MS	5.04E+4
	2d-VC	5.03E+4
	2d-MS	5.04E+4
	2d-CG	5.04E+4
NS	2d-LT	5.04E+4
	2d-C	5.05E+4
	2d-CG	5.05E+4
Wave	2d-LT	5.05E+4
	1d-C	5.06E+4
	2d-CG	5.04E+4
Chaotic	2d-MS	5.04E+4
	GS	5.02E+4
High dim	KS	5.04E+4
	PNd	5.06E+4
Inverse	HNd	5.06E+4
	PInv	5.04E+4
	HInv	5.05E+4

Table 16: Inference flops on a single collocation point for PINNs using network parameters the same with main experiments.

L2RE	Burgers1d-C	GS	Heat2d-CG	Poisson2d-C	
PINN	5k	3.71E-2(1.21E-2)	2.40E-1(1.11E-1)	1.23E-1(3.77E-3)	3.84E-2(1.77E-3)
	20k	1.66E-2(1.87E-3)	1.65E-1(1.01E-1)	8.95E-2(2.29E-2)	2.38E-2(1.43E-3)
	80k	1.42E-2(6.63E-4)	9.36E-2(8.41E-5)	9.64E-2(1.85E-2)	1.86E-2(3.26E-3)
	160k	1.38E-2(5.45E-4)	9.38E-2(5.38E-5)	8.21E-2(7.52E-3)	1.48E-2(1.55E-3)
PINN-LRA	5k	3.60E-2(8.82E-3)	1.64E-1(9.91E-2)	1.18E-1(2.32E-3)	3.87E-2(3.28E-3)
	20k	1.56E-2(8.87E-4)	1.09E-1(2.19E-2)	9.29E-2(1.97E-2)	2.65E-2(1.92E-3)
	80k	1.42E-2(1.23E-3)	9.38E-2(1.63E-4)	1.05E-1(1.48E-2)	1.79E-2(4.19E-4)
	160k	1.35E-2(1.84E-4)	9.38E-2(5.48E-4)	1.19E-1(2.28E-2)	1.66E-2(3.50E-3)

Table 17: Performance of PINNs and PINN-LRA with different numbers of training epochs on 4 cases.

884 **Influence of Adam hyperparameters.** Here we examine the impact of varying the momentum
885 hyperparameters in the Adam optimizer. Despite the learning rate, Adam contains two momentum
886 hyperparameters, i.e., (β_1, β_2) for storing the approximate first and second-order momentum. In
887 experiments, we observe that the momentum parameters not only affect the convergence speed and
888 stability but also influence the final error. Here we list the results in Table E.2. We observe that in
889 average $(\beta_1, \beta_2) = (0.99, 0.99)$ achieves the best results compared with others.

890 **Other method-specific parameters**

L2RE	burgers	GS	HeatComplex	Poisson2d	
PINN	(0.9,0.999)	1.79E-2(2.20E-3)	2.47E-1(1.09E-1)	7.76E-2(8.27E-3)	2.72E-2(2.40E-3)
	(0.9,0.99)	1.52E-2(1.34E-4)	9.38E-2(5.93E-5)	5.10E-2(7.20E-3)	3.00E-2(6.98E-3)
	(0.9,0.9)	1.68E-2(2.45E-3)	9.38E-2(1.98E-4)	4.56E-2(2.55E-3)	2.81E-2(3.95E-3)
	(0.99,0.99)	1.35E-2(1.03E-4)	9.37E-2(1.38E-5)	2.98E-2(5.24E-3)	9.18E-3(4.90E-4)
PINN-NTK	(0.9,0.999)	1.60E-2(5.50E-4)	1.79E-1(1.20E-1)	7.37E-2(1.59E-2)	1.40E-2(4.06E-3)
	(0.9,0.99)	1.57E-2(1.34E-4)	9.37E-2(5.93E-5)	6.65E-2(7.20E-3)	1.57E-2(3.03E-3)
	(0.9,0.9)	1.74E-2(1.40E-3)	9.37E-2(2.11E-4)	8.12E-2(3.33E-2)	2.45E-2(3.64E-3)
	(0.99,0.99)	1.35E-2(2.27E-4)	9.37E-2(1.54E-5)	3.62E-2(1.60E-3)	2.85E-3(1.68E-4)

Table 18: Performance comparison of PINN and PINN-NTK under different momentum parameters of Adam optimizer.

α	Burgers1d	GS	Heat2d-CG	Poisson2d-C
0.01	2.45E-2(1.75E-3)	9.37E-2(4.25E-5)	1.18E-1(4.72E-3)	2.51E-2(8.40E-3)
0.05	5.20E-2(2.14E-2)	9.37E-2(3.48E-5)	1.25E-1(7.62E-3)	2.63E-2(1.10E-2)
0.1	1.99E-2(5.61E-3)	9.37E-2(1.70E-5)	1.28E-1(4.66E-3)	2.62E-1(3.00E-1)
0.2	2.04E-2(3.66E-3)	9.37E-2(1.03E-5)	1.55E-1(3.31E-2)	4.69E-2(1.37E-2)
0.4	3.53E-2(2.47E-2)	1.75E-1(1.15E-1)	1.35E-1(7.37E-3)	1.14E-1(1.23E-1)
0.7	2.00E-2(3.72E-3)	9.37E-2(4.21E-5)	1.90E-1(4.09E-2)	3.50E-1(2.24E-1)

Table 19: Performance comparison of PINN-LRA with different momentum parameters.

weight w	Burgers1d	GS	Heat2d-CG	Poisson2d-C
0.001	6.12E-2(1.36E-2)	1.66E-1(1.01E-1)	4.97E-2(7.10E-4)	6.74E-1(1.71E-2)
0.01	1.95E-1(2.47E-2)	1.79E-1(1.21E-1)	7.78E-2(1.47E-2)	6.89E-1(2.47E-2)
0.1	4.93E-1(1.59E-2)	4.61E-1(1.99E-1)	1.34E-1(1.37E-3)	6.92E-1(7.72E-3)
1	5.53E-1(7.49E-2)	9.38E-2(1.79E-5)	2.19E-1(9.90E-2)	6.96E-1(4.39E-3)

Table 20: Performance comparison of gPINN with different weights.

891 We chose several different method-specific hyperparameters to study their influence.

892 **Influence of momentum parameters for loss reweighting.** Here we choose the momentum update
893 α from $\{0.01, 0.05, 0.2, 0.4, 0.7\}$. We see that the optimal value of α is problem-dependent. However,
894 we observe that relatively small α achieves better performance.

895 **Influence of weight for gPINNs.** Here we choose the weight of gPINNs w from
896 $\{0.001, 0.01, 0.1, 1\}$. We see that the optimal value of w is also problem-dependent and the property
897 is intriguing. We observe that the performance of gPINNs is bad on Poisson2d-C for all values of
898 w . We suggest that adding higher-order PDE residuals might harm the training process in some
899 situations.

900 **Influence of number of grids for hp-VPINNs.** The number of points to compute integral within a
901 domain Q and number of grids N_{grid} are two critical hyperparameters for hp-VPINN. Here we choose
902 Q from $\{5, 10, 15, 20\}$ for 2-dimensional problems and $\{6, 8, 10, 12\}$ for 3-dimensional problems to
903 investigate their influence. We also take N_{grid} into consideration, which varies in $\{4, 8, 16, 32\}$ for
904 2-dimensional problems and 3-dimensional problems. Different parameter selection is applied due to
905 the limit of the VRAM. We can observe a consistent trend that as the Q value rises, the accuracy of the
906 model’s predictions also enhanced. This is attributed to the fact that the Q value dictates the number
907 of integration points; hence, a higher value leads to more precise integration. However, for certain
908 scenarios where hp-VPINN might not be the best fit, a surge in the Q value doesn’t significantly
909 bolster the prediction accuracy. On the other hand, the choice of N_{grid} exhibits a complex influence
910 on accuracy. Generally, as the value of N_{grid} increases, precision tends to improve. However, in
911 regions where the solution has large gradients or discontinuities, a denser grid might amplify these
912 anomalies, leading to larger errors during model training.

913 **Influence of the number of subdomains and overlap factors for FBPINNs.** The number of
914 subdomains for domain decomposition and the overlap ratio α are two important hyperparameters for
915 FBPINNs. The overlap ratio is chosen from $\{0.2, 0.4, 0.6, 0.8\}$.

Q	Burgers1d	Q	GS	Q	Heat2d-CG	Q	Poisson2d-C
5	3.19E-01(2.91E-02)	6	3.88E-01(9.73E-02)	6	7.14E-01(7.14E-01)	5	2.46E-01(1.62E-01)
10	2.88E-01(6.03E-03)	8	4.25E-01(1.51E-01)	8	7.19E-01(4.89E-02)	10	2.43E-01(1.57E-01)
15	1.85E-01(6.97E-02)	10	3.68E-01(2.04E-01)	10	7.19E-01(4.75E-02)	15	2.45E-01(1.61E-01)
20	1.85E-01(4.65E-02)	12	3.58E-01(2.06E-01)	12	7.21E-01(4.95E-02)	20	2.46E-01(2.46E-01)

Table 21: Performance comparison of hp-VPINN with different Q .

N_{grid}	Burgers1d	N_{grid}	GS	N_{grid}	Heat2d-CG	N_{grid}	Poisson2d-C
4	3.67E-01(1.28E-02)	3	1.93E-01(2.06E-02)	3	6.91E-01(2.44E-02)	4	4.95E-01(8.46E-02)
8	2.43E-01(2.39E-03)	4	3.68E-01(2.04E-01)	4	7.19E-01(4.75E-02)	8	4.95E-01(8.63E-02)
16	3.66E-01(3.67E-02)	5	3.59E-01(1.34E-01)	5	7.22E-01(5.14E-02)	16	2.86E-01(1.94E-02)
32	4.59E-01(1.34E-02)	6	2.81E-01(1.96E-01)	6	7.23E-01(5.19E-02)	32	2.43E-01(1.57E-01)

Table 22: Performance comparison of hp-VPINN with different number of grids N_{grid} .

Burgers1d		GS	
(1,1)	2.12E-1(1.19E-1)	(1,1,1)	7.98E-2(3.59E-3)
(2,1)	1.75E-1(7.97E-2)	(1,1,3)	8.15E-2(1.73E-3)
(3,1)	1.61E-1(9.77E-2)	(1,1,5)	7.90E-2(1.28E-3)
(1,2)	1.98E-1(7.34E-2)	(2,2,1)	8.15E-2(3.56E-3)
Heat2d-CG		Poisson2d-C	
(1,1,1)	3.30E-1(1.04E-1)	(1,1)	5.01E-2(2.80E-3)
(1,1,3)	6.80E-1(1.18E-1)	(1,2)	3.51E-1(1.26E-1)
(1,1,5)	7.48E-1(3.39E-2)	(2,1)	4.38E-1(5.30E-2)
(2,2,1)	2.89E-1(2.30E-2)	(2,2)	5.54E-2(1.23E-3)

Table 23: Performance (L2RE) comparison of FBPINN with different domain decomposition types.

916 **Results on different domain scale** Here we study the influence of domain scales. While numerical
917 methods are usually resistant to domain scales, PINN methods are not invariant to domain scale
918 changes. Moreover, normalizing the domain to $[0, 1]$ might be suboptimal for PINNs. Here we
919 take the domain scale L of Poisson2d-C as an example to study the performance under different
920 settings. We see that Multi-Adam is the most stable under domain scale changes and achieves the
921 best performance when L is small.

922 **Comparison between MultiAdam and L-BFGS** . Here we compare the new MultiAdam optimizer
923 for PINNs with L-BFGS, which is a frequently used optimizer in PINN variants. The L2Re result is
924 listed in the Table E.2. We see that L-BFGS does not converge in many cases as it is unstable while
925 MultiAdam has a better convergence property. However, L-BFGS achieves better accuracy on some
926 of the problems like high dimensional PDEs.

927 **Temporal error analysis** For time-dependent problems, an important metric is the generalization
928 ability along the time dimension. We selected Heat2d-CG, Heat2d-MS, and Wave1d-C with two
929 different parameters (domain scale is 2 and 8) to observe how the error evolves over time. We found
930 that the error accumulation over time varies depending on the specific PDE problem. For instance,
931 in the case of Heat2d-CG, its final state is a relatively easy steady state, which results in a gradual
932 reduction of error over time. On the other hand, for Heat2d-MS, the solution continuously oscillates,
933 leading to an increasing error as time progresses. In the case of Wave1d-C, due to the periodic nature
934 of the wave equation and the presence of a ground truth solution that is entirely zero, we observed
935 the L2 Relative Error (L2RE) also increases with fluctuations. In summary, error accumulation in
936 time-dependent problems remains challenging for PINNs, necessitating deeper analysis and improved
937 optimization methods in future research.

938 **Runtime analysis** The runtime results for different methods are shown in Table 12. We have
939 analyzed the results in the previous section.

α	Burgers1d	GS	Heat2d-CG	Poisson2d-C
0.2	9.88E-2(1.75E-2)	8.57E-2(3.14E-3)	1.05E+0(1.68E-1)	5.81E-1(1.01E-3)
0.4	9.01E-2(1.43E-2)	8.09E-2(7.63E-4)	7.36E-1(7.23E-2)	2.85E-1(9.30E-2)
0.6	1.75E-1(7.97E-2)	7.95E-2(6.30E-4)	6.79E-1(1.17E-1)	5.54E-2(1.23E-3)
0.8	1.61E-1(1.08E-1)	8.04E-2(1.03E-3)	6.96E-1(1.50E-1)	4.19E-2(4.71E-3)

Table 24: Performance (L2RE) comparison of FBPINN with different overlap ratios α .

Scale L	Adam	MultiAdam	LRA	GePinn
0.5	6.94E-1(1.76E-2)	5.71E-1(6.11E-2)	6.93E-1(1.48E-2)	7.06E-1(2.94E-3)
1	6.92E-1(1.79E-2)	3.56E-2(1.25E-2)	3.88E-1(2.61E-1)	6.89E-1(1.41E-2)
2	4.41E-1(9.57E-2)	3.81E-2(9.38E-3)	1.68E-1(6.78E-2)	6.76E-1(3.86E-2)
4	1.77E-2(4.66E-3)	3.38E-2(9.71E-3)	1.11E-1(1.43E-1)	3.13E-2(2.85E-3)
8	2.39E-2(7.26E-3)	4.40E-2(3.07E-2)	1.41E-1(7.10E-2)	1.95E-2(6.42E-3)
16	1.83E-2(8.19E-3)	3.62E-2(1.10E-2)	9.45E-2(2.05E-2)	1.59E-2(6.03E-3)

Table 25: Performance comparison of vanilla PINNs, Multi-Adam, PINN-LRA, and gPINN on Poisson2d-C different domain scales.

	L2RE	MultiAdam	L-BFGS
Burgers	1d-C	4.85E-2(1.61E-2)	1.33E-2(5.30E-5)
	2d-C	3.33E-1(8.65E-3)	4.65E-1(4.69E-3)
Poisson	2d-C	2.63E-2(6.57E-3)	NaN
	2d-CG	2.76E-1(1.03E-1)	2.96E-1(4.77E-1)
	3d-CG	3.64E+0(2.74E-2)	3.51E+0(9.33E-2)
	2d-MS	5.90E-1(4.06E-2)	1.45E+0(4.75E-3)
Heat	2d-VC	4.75E-1(8.44E-2)	2.32E-1(5.29E-3)
	2d-MS	2.18E-1(9.26E-2)	1.73E-2(4.74E-3)
	2d-CG	7.12E-2(1.30E-2)	8.57E-1(6.69E-4)
	2d-LT	1.00E+0(3.85E-5)	1.00E+0(6.69E-5)
NS	2d-C	7.27E-1(1.95E-1)	2.14E-1(1.07E-3)
	2d-CG	4.31E-1(6.95E-2)	NaN
	2d-LT	1.00E+0(2.19E-4)	9.70E-1(3.66E-4)
Wave	1d-C	1.21E-1(1.76E-2)	NaN
	2d-CG	1.09E+0(1.24E-1)	1.33E+0(2.34E-1)
	2d-MS	9.33E-1(1.26E-2)	NaN
Chaotic	GS	9.37E-2(1.21E-5)	NaN
	KS	9.61E-1(4.77E-3)	NaN
High dim	PNd	3.98E-3(1.11E-3)	4.67E-4(7.12E-5)
	HNd	3.02E-1(4.07E-2)	1.19E-4(4.01E-6)

Table 26: Mean L2RE comparison between MultiAdam and L-BFGS.

L2RE Name		Burgers-P 2d-C	Poisson-P 2d-C	Heat-P 2d-MS	NS-P 2d-C	Wave-P 1d-C	High dim-P HNd
Vanilla	PINN	4.74E-1(1.93E-1)	1.73E-1(2.40E-1)	7.66E-3(3.61E-3)	3.89E-1(4.40E-1)	2.24E-1(3.03E-1)	5.22E-1(3.56E-2)
Reweighting	LRA	4.36E-1(1.99E-1)	1.23E-1(1.56E-1)	6.53E-3(6.12E-3)	0.00E+0(0.00E+0)	7.07E-2(1.14E-1)	3.44E-1(1.81E-1)
	NTK	4.13E-1(1.82E-1)	1.50E-1(1.86E-1)	9.04E-3(6.52E-3)	4.52E-1(3.01E-1)	1.66E-2(4.52E-3)	2.69E-1(1.88E-1)
Sampling	RAR	4.71E-1(1.98E-1)	1.53E-1(2.11E-1)	8.07E-3(1.75E-3)	3.91E-1(4.46E-1)	2.33E-1(3.10E-1)	5.05E-1(6.10E-2)
Optimizer	MultiAdam	4.93E-1(1.94E-1)	4.00E-1(3.20E-1)	2.22E-3(1.55E-3)	9.33E-1(4.32E-2)	8.24E-2(9.22E-2)	6.89E-1(8.46E-2)
Loss functions	gPINN	4.91E-1(2.01E-1)	4.59E-1(4.57E-1)	7.87E-3(2.82E-3)	7.19E-1(2.89E-1)	4.03E-1(3.44E-1)	7.66E-1(3.30E-2)
	vPINN	2.82E+0(1.79E+0)	5.12E-1(2.43E-1)	-	3.76E-1(6.90E-2)	5.51E-1(6.09E-1)	-
Architecture	LAAF	4.37E-1(1.77E-1)	6.27E-2(4.65E-2)	6.97E-3(5.23E-3)	3.63E-1(4.38E-1)	1.84E-1(2.91E-1)	4.03E-1(1.27E-1)
	GAAF	4.34E-1(1.85E-1)	1.89E-1(2.54E-1)	1.94E-1(8.63E-2)	4.85E-1(4.09E-1)	2.97E-1(2.38E-1)	9.00E-1(1.68E-1)
	FBPINN	-	2.46E-1(4.50E-1)	-	3.99E-1(2.97E-1)	2.87E-2(2.81E-2)	1.15E+0(1.06E+0)

Table 27: L2RE (mean/std) of different methods on parametric experiments.

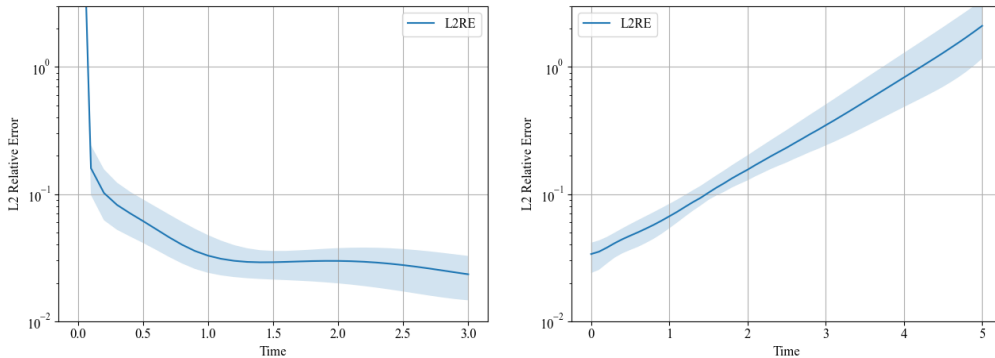


Figure 19: L2RE varying with time for PINNs on Heat2d-CG, Heat2d-MS.

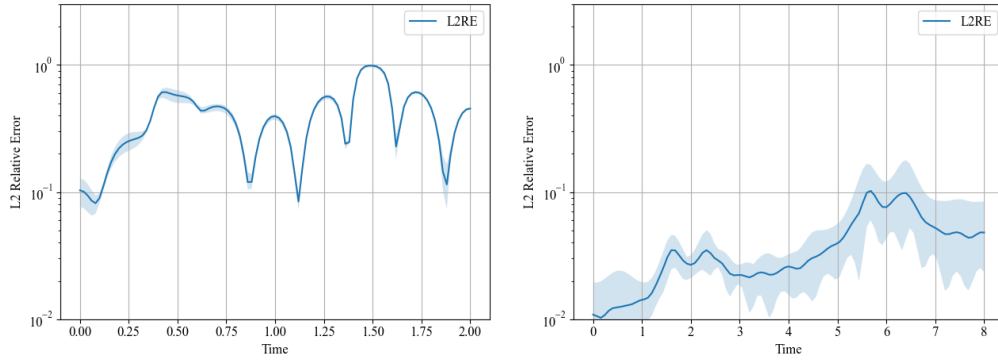


Figure 20: L2RE varying with time for PINNs on Wave1d-C-scale2 and Wave1d-C-Scale8.

940 **F Other visualization results and analysis**

941 Here we list some visualization results of these experiments. We see that Burgers1d, Poisson2d-C,
 942 Poisson2d-CG, and NS2d-C could be solved with a relatively low error. Other problems are difficult
 943 to learn, even the approximate shape of the solution. Here we only visualize two-dimensional cases,
 944 which are easier to display in the paper. Note that we also support different forms of three-dimensional
 945 plot functionals in our code.

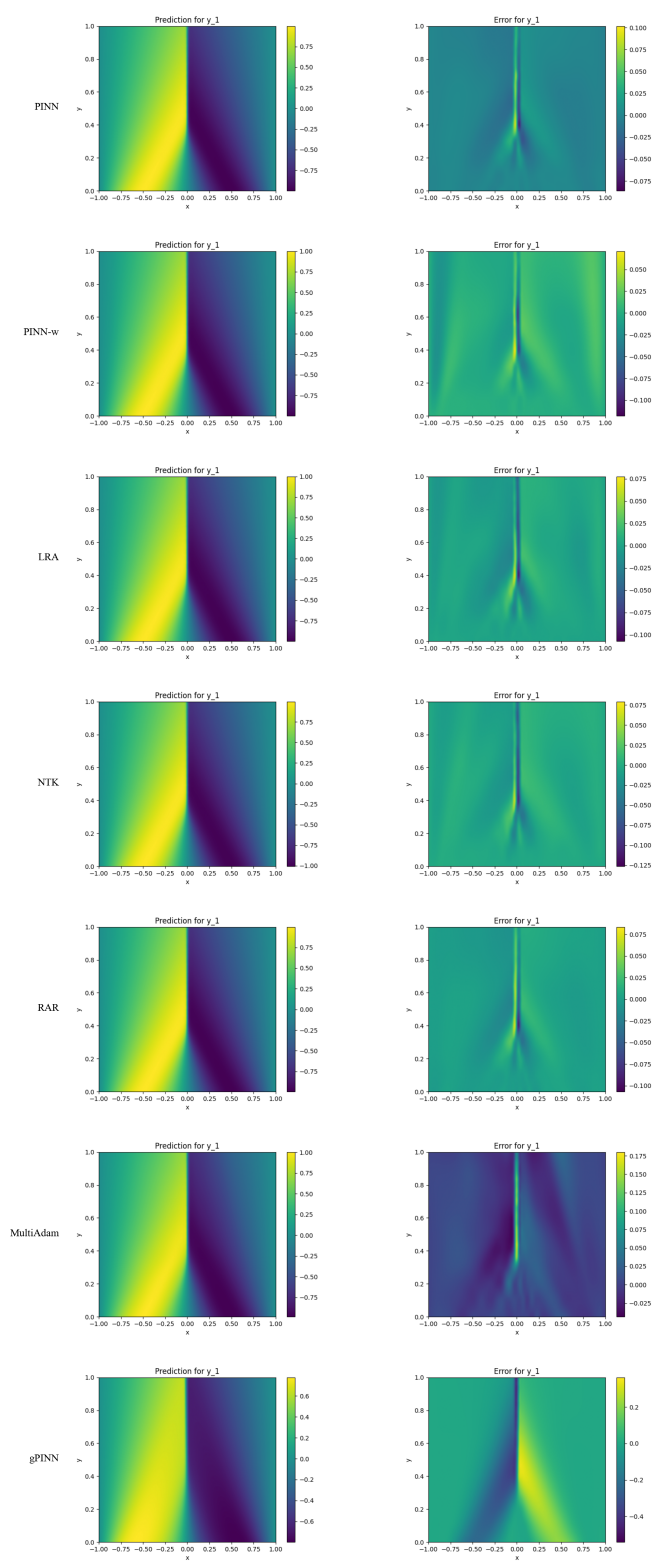


Figure 21: Visualization of Burgers1d. The left pictures are the prediction of PINN methods. The right pictures show the error between the prediction and the ground truth.

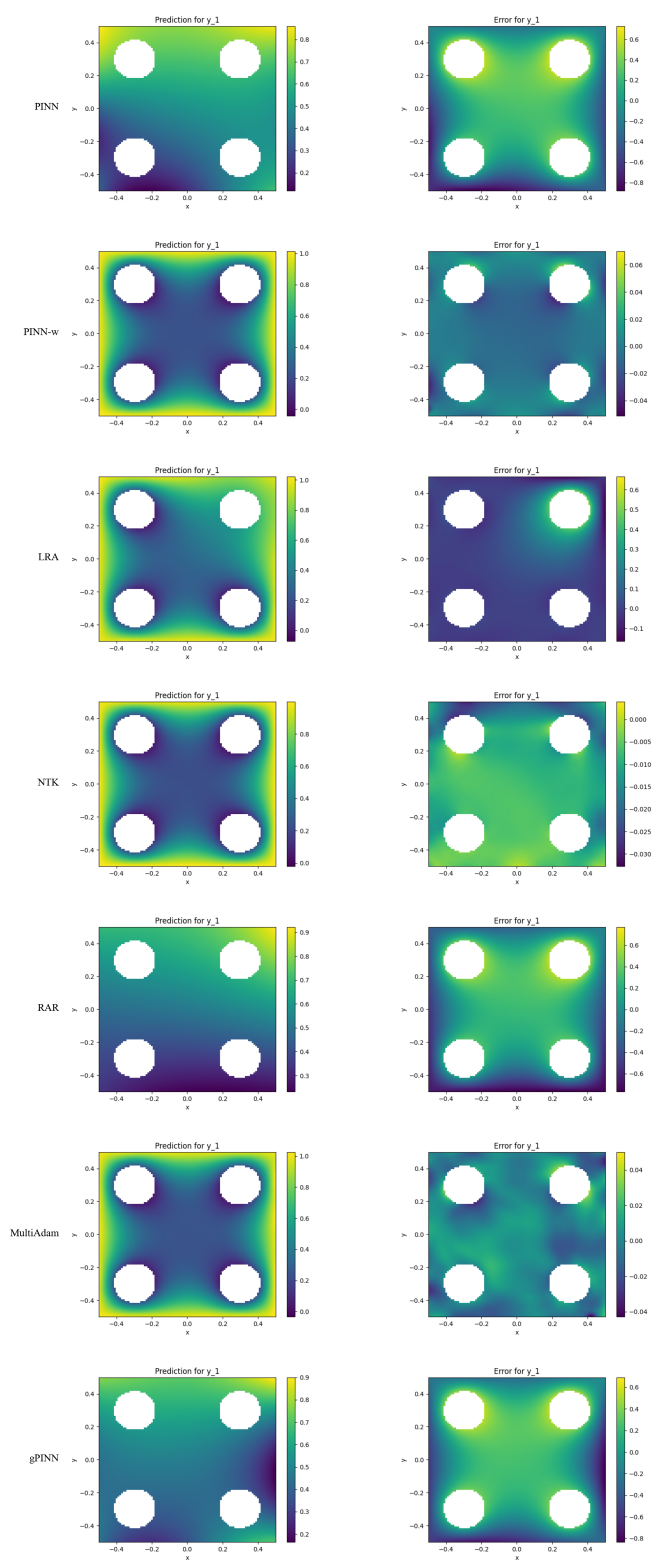


Figure 22: Visualization of Poisson2d-C. The left pictures are the prediction of PINN methods. The right pictures show the error between the prediction and the ground truth.

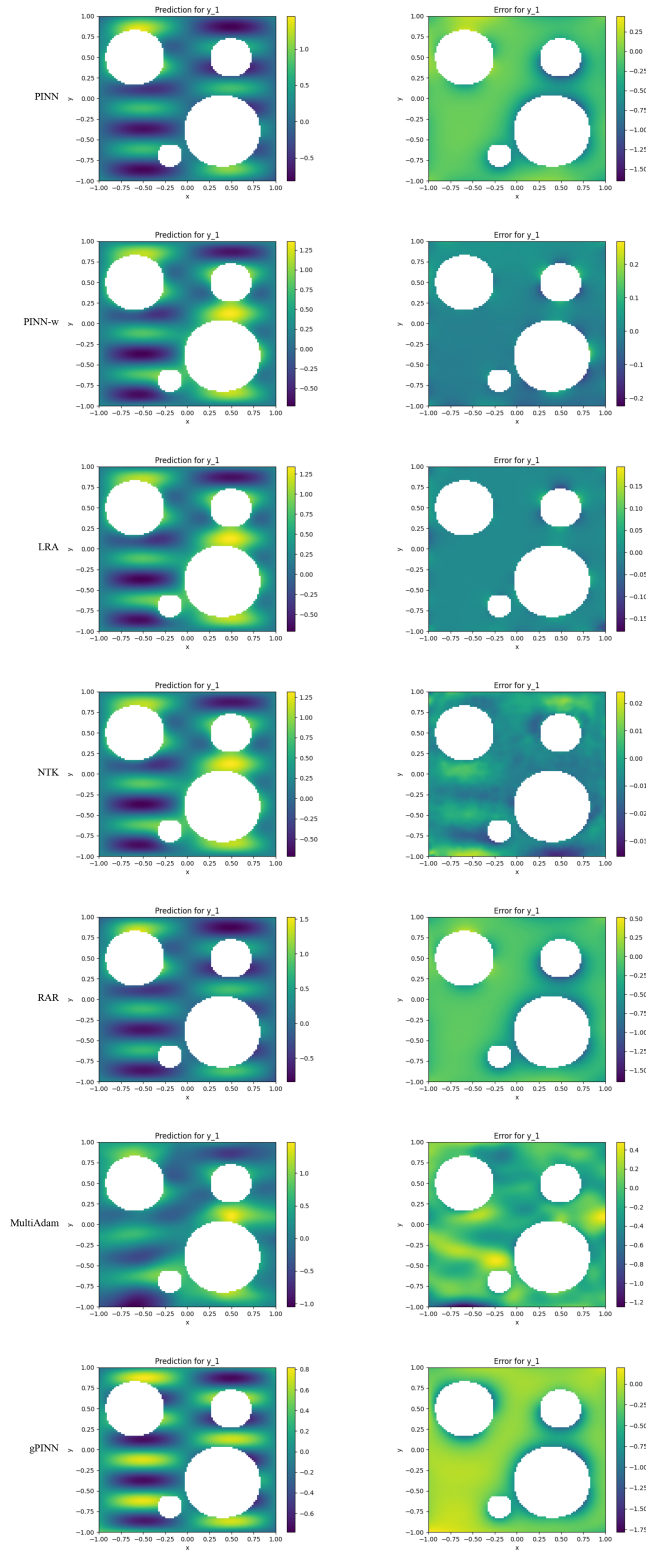


Figure 23: Visualization of Poisson2d-CG. The left pictures are the prediction of PINN methods. The right pictures show the error between the prediction and the ground truth.

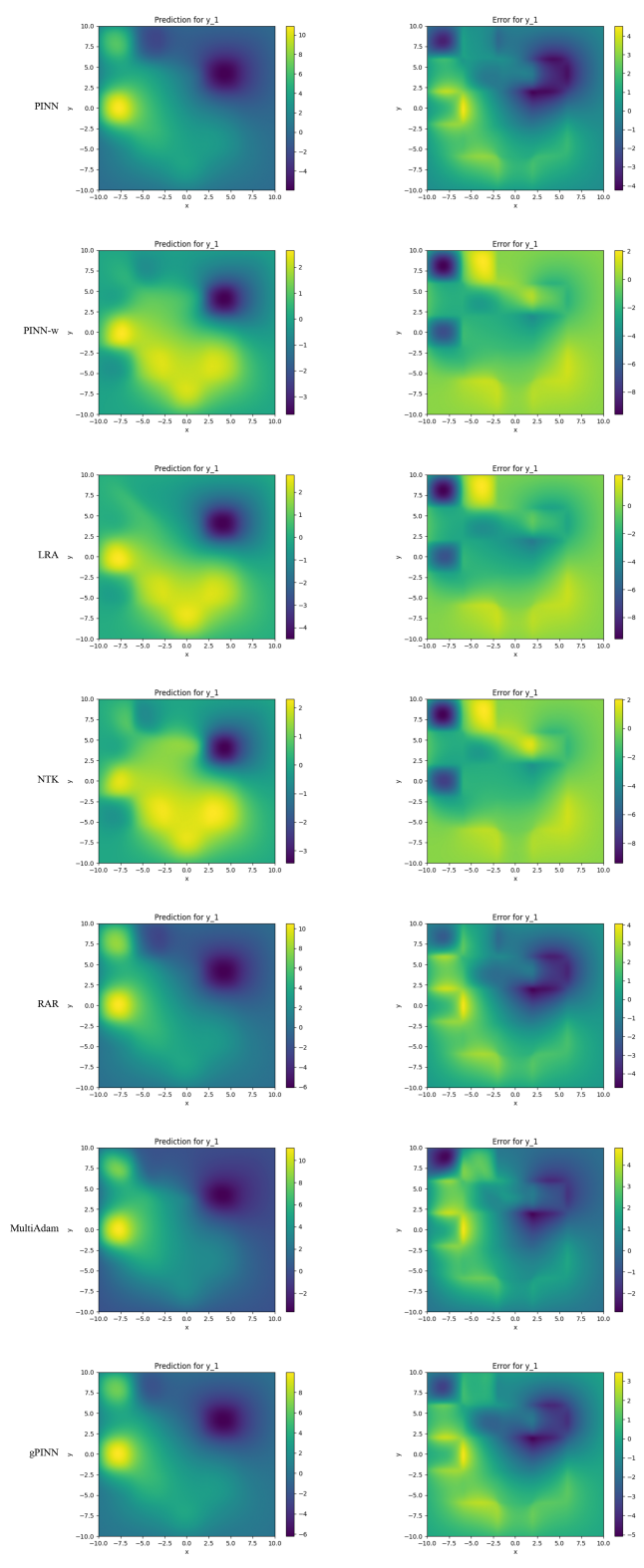


Figure 24: Visualization of Poisson2d-MS. The left pictures are the prediction of PINN methods. The right pictures show the error between the prediction and the ground truth.

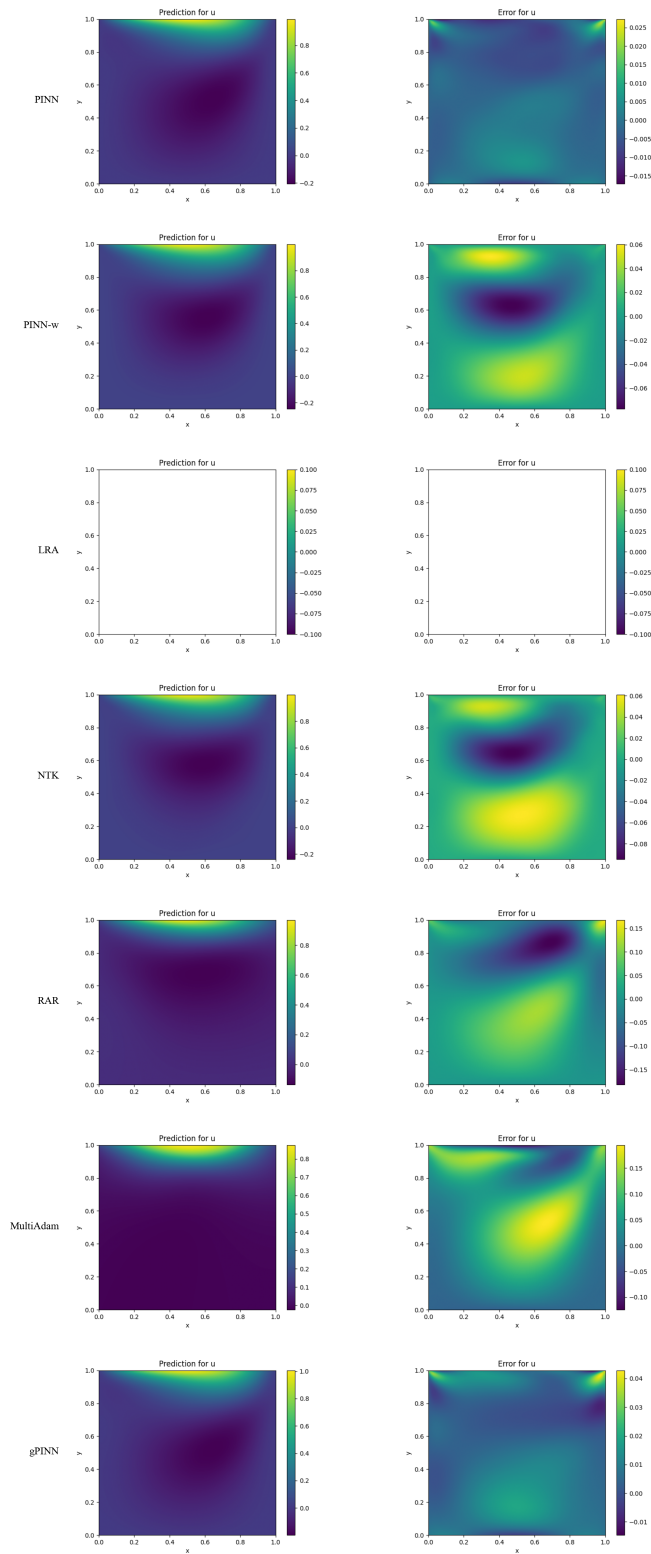


Figure 25: Visualization of NS2d-C. The left pictures are the prediction of PINN methods. The right pictures show the error between the prediction and the ground truth. Note that PINN-LRA diverged in this case.

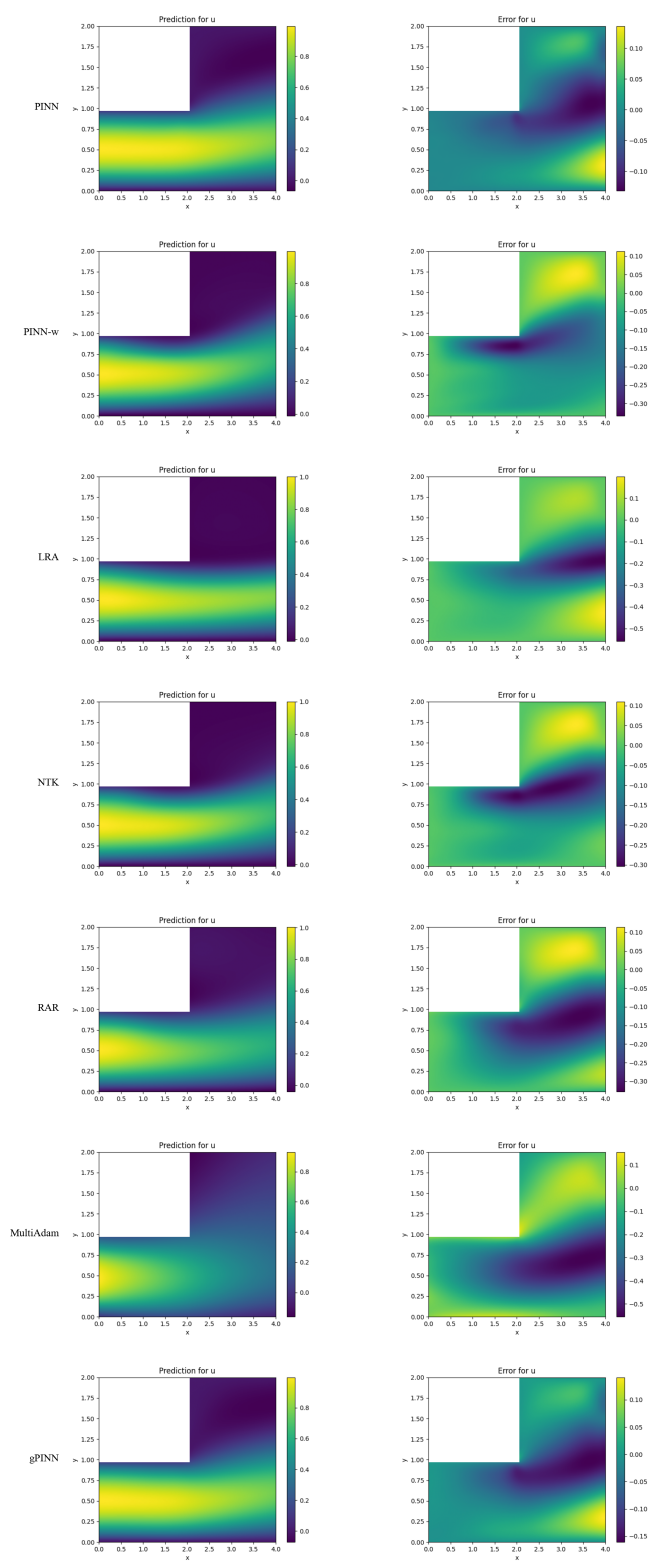


Figure 26: Visualization of NS2d-CG. The left pictures are the prediction of PINN methods. The right pictures show the error between the prediction and the ground truth.

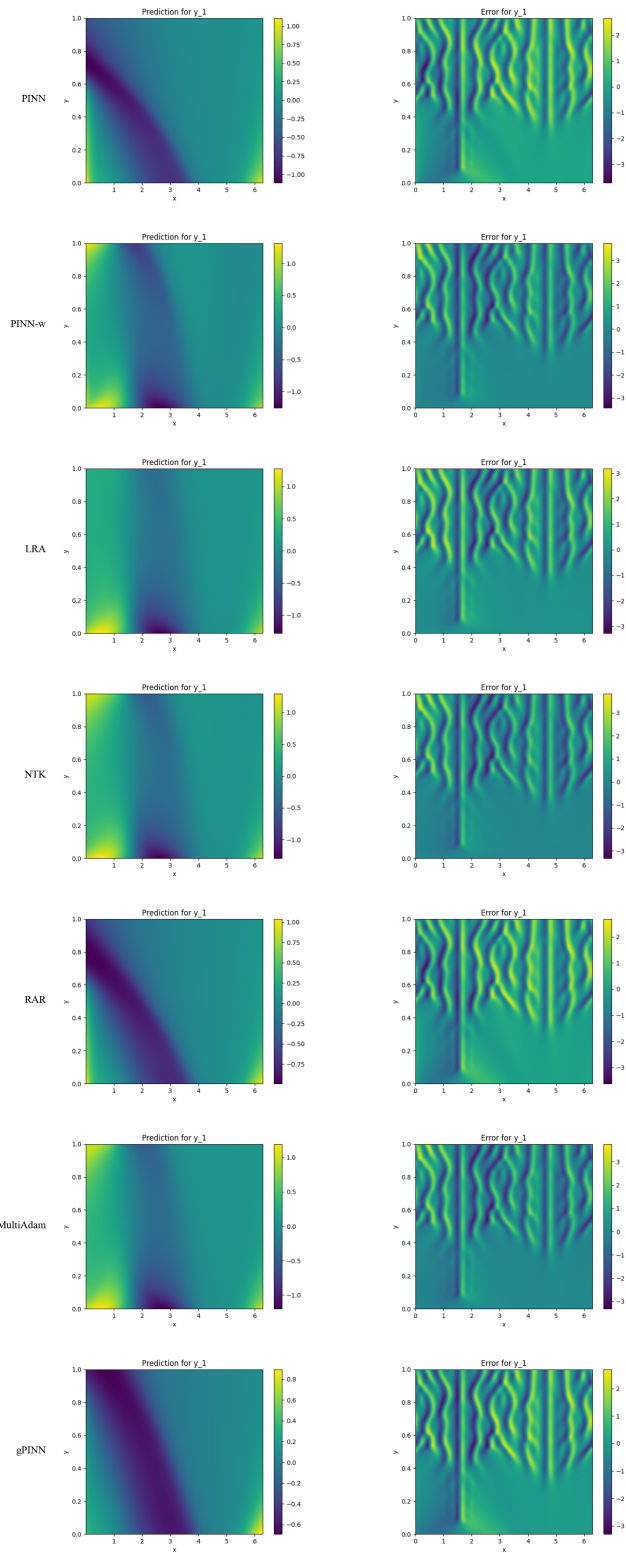


Figure 27: Visualization of KS. The left pictures are the prediction of PINN methods. The right pictures show the error between the prediction and the ground truth.